Development of High-performing Polydimethylsiloxane-based Membranes for Carbon Dioxide Separation

A Dissertation Presented for the
Doctor of Philosophy
Degree
The University of Tennessee, Knoxville

Tao Hong
December 2017

Copyright © 2017 by Tao Hong
All rights reserved.

DEDICATION

To my beloved wife, Yan.

To my parents.

To my family.

ACKNOWLEDGEMENTS

First and foremost, I want to thank my advisor, Prof. Alexei P. Sokolov for his guidance, encouragement, and support throughout my Ph.D. study, giving me the opportunity to learn the cutting-edge science, professional experimental skills and the collaborative spirit. His kindness to students and passion for scientific research have influenced me in the past five years and will keep inspiring me in my future life.

I would like to thank my doctoral committee members: Prof. Jimmy W. Mays, Prof. Charles S. Feigerle and Prof. Jaan Mannik, for their suggestions and efforts in my candidacy exams and dissertation review process.

I would also like to thank Dr. Tomonori Saito (ORNL), who taught me in detail the material synthesis, data interpretation and article writing. I really appreciate his efforts for training me to be a qualified polymer scientist and membrane scientist.

My thanks go to our collaborators for their contributions and helps in all the projects: Dr. Shannon M. Mahurin (ORNL) who first trained me the preparation and measurement of gas permeation; Prof. Brian K. Long, Dr. Nam-Goo Kang, Kevin Gmernicki for all the fruitful discussion; Prof. De-en Jiang (UC, Riverside) and Prof. Konstantinos D. Vogiatzis for performing the simulation work; Dr. Xunxiang Hu (ORNL) for all the PALS measurements.

I want to thank Dr. Alexander L. Agapov for teaching me the fundamental knowledge and experimental operation when I first joined the group; thank Dr. Alexander Kisliuk for setting up the permeation and sorption instrument; thank Dr. Zhenbin Niu for teaching me the membrane synthesis and characterization when I started the project; thank Dr. Shiwang

Cheng, Dr. Yangyang Wang and Dr. Fei Fan for teaching me so many polymer characterization techniques; thank Dr. Pengfei Cao for teaching me synthetic skills of various polymer materials.

I would also like to acknowledge the collaborative efforts and many discussions with member in the group: Dr. Vladimir Novikov, Dr. Vera Bocharova, Dr. Dmitry N. Voylov, Dr. Martin Tress, Dr. Zaneta Wojnarowska, Dr. Sabornie Chatterjee, Dr. J. Casey Johnson, Dr. Adam P. Holt, Danna Sharp, Eunice Hong, Kunyue Xing, Bingrui Li, Sheng Zhao, Bobby Carroll and all former group members. It has been a great pleasure to work with all of you.

I want to thank all my friends, with whom I traveled together, played basketball together and enjoyed my spare time together. Special thanks go to my roommates, Dr. Weiyu Wang and Dr. Hongbo Feng. I want to thank them for all the help in my study and daily life.

Last part is reserved for my family. I want to thank my father, Guohu Hong and my mother, Wene Zhang, for all their unconditional and selfless love throughout my life. I want to thank my father-in-law, Anning Zhou and mother-in-law, Heqing Zhang, for all the understanding and support. I want to thank my grandparents, my uncles, my aunts and my cousins, for all the help in my life. Finally, to my wife, Yan Zhou, thank you for all the love and I'm so lucky to have you for the rest of my life.

Tao Hong

ABSTRACT

Membrane separation is highlighted as one of the most promising approaches to mitigate the excessive CO_2 [carbon dioxide] emission, due to its significant reduction of energy cost compared with many conventional separation techniques. Unfortunately, the separation performance of current membranes does not meet the practical CO_2/N_2 [nitrogen] separation requirements. And due to the huge volume of industrial flue gas, membranes with exceptionally high permeability are needed for practical reasons.

Currently, the separation mechanism of most polymeric membranes is based on size-sieving. However, this method is not sufficient for CO_2/N_2 separations due to the similar kinetic diameters of CO_2 (3.30 Å [angstrom]) and N_2 (3.64 Å). Thus, developing a new method based on a non-size sieving mechanism could offer a solution to the improvement of CO_2/N_2 separation efficiency.

In this dissertation, (bicycloheptenyl) ethyl terminated polydimethylsiloxane (PDMSPNB) membranes were firstly studied. The developed polymer membranes show higher permeability and better selectivity than those of conventional PDMS [polydimethylsiloxane] membrane. The achieved performance (P_{CO2} [CO_2 permeability] 6800 Barrer and $\alpha[_{CO2/N2}]$ [CO_2/N_2 selectivity] 14) is very promising for practical applications. The key to achieving this high performance is the use of an *in-situ* cross-linking method of the difunctional PDMS macromonomers, which provides lightly cross-linked membranes. By combining positron annihilation lifetime spectroscopy, broadband dielectric spectroscopy and gas sorption measurements, we have elucidated the key parameters for achieving their excellent performance.

In the following work, two CO_2-philic groups, amidoxime (AO) and polyethylene oxide (PEO), were successfully incorporated into the rubbery PDMS and glassy poly(1-trimethylsilyl-1-propyne) (PTMSP) systems. By the careful tuning of functional group composition, the membranes showed controlled CO_2/N_2 solubility selectivity. The combination of CO_2-philic groups and highly permeable polymer matrix showed one of the highest CO_2/N_2 separation performance among all polymeric membranes. The overall gas separation performance (P_{CO_2} 6800 Barrer and $\alpha[_{CO_2/N_2}]$ 19 for AO-PDMSPNB; P_{CO_2} 3400 Barrer and $\alpha[_{CO_2/N_2}]$ 19 for PEO-PDMSPNB; P_{CO_2} 6000 Barrer and $\alpha[_{CO_2/N_2}]$ 17 for AO-PTMSP) of the highest performing membranes have exceeded/achieved the Robeson upper bound line. These studies provide a roadmap to enhancing gas separation performance in rubbery and glassy polymers by tuning gas solubility selectivity.

TABLE OF CONTENTS

LIST OF TABLES

LIST OF FIGURES

INTRODUCTION

The climate change over the last decades has been widely discussed and the excessive carbon dioxide (CO_2) emission is considered as one of the key contributors. Various technologies are under exploration to mitigate the emission, and among which the membrane separation is highlighted as one of the most promising approaches for sustainable development, due to its significant reduction of energy cost compared with many conventional separation techniques.

Unfortunately, the separation performance of current membranes does not meet the separation efficiency for practical CO_2/N_2 separation. And due to the huge volume of gas flows coming out, membranes with exceptionally high permeability are needed for practical reasons. According to previous cost analysis studies, treatment cost reduction reaches plateau after CO_2/N_2 selectivity around 30 is achieved, while membranes with high permeability could provide continuous cost reduction due to the escalated efficiency treating larger amount of flue gas.

Currently, the separation mechanism of most polymeric membranes is based on size-sieving. For CO_2/N_2 separation, due to their similar size (CO_2~3.30 Å, N_2~ 3.64 Å), the separation efficiency might not improve much if only focus on size-sieving approach. Thus, developing a new method based on a non-size sieving mechanism could potentially offer a solution to the improvement of CO_2/N_2 separation efficiency.

In this dissertation, membranes based on end-cross-linked polydimethylsiloxane-norbornene (PDMSPNB) were studied for the first time. A variety of the characterization techniques were performed to investigate the gas transport mechanism in the polymer

matrix. Later, two CO_2-philic groups, amidoxime (AO) and polyethylene oxide (PEO), were successfully incorporated into the PDMS matrix. By the careful tuning of functional group composition, the membranes showed controlled CO_2 solubility selectivity. The combination of CO_2-philic groups and highly permeable PDMSPNB matrix showed one of the highest CO_2/N_2 separation performance among all polymeric membranes. This dissertation has the following organization.

Introduction gives the organization of this dissertation.

Chapter 1 gives a brief overview of the fundamental background knowledge in membrane separation field.

Chapter 2 describes materials and experimental procedures employed in this work. This chapter includes the gas permeation test, gas sorption test, as well as other characterization techniques.

Chapter 3 presents the detailed study of lightly cross-linked PDMSPNB membranes. The effect of cross-link density and molecular weight between cross-linked were investigates using a combination of gas permeation, gas sorption, positron annihilation lifetime spectroscopy and broadband dielectric spectroscopy measurements. The synthesized membranes showed significant enhancement in gas separation performance compared with conventional PDMS and the faster dynamics was proved to be the key parameter.

Chapter 4 and 5 extend the work from Chapter 3. Two CO_2-philic groups, amidoxime (AO) and polyethylene oxide (PEO) were successfully incorporated into the PDMSPNB matrix. The AO and PEO moiety were proved to enhance CO_2 solubility and

the CO_2/N_2 selectivity was increased by more than 40%. Both AO-PDMSPNB and PEO-PDMSPNB achieved above/on Robeson upper bound at the high permeability side, indicating their great potential to be fabricated onto the CO_2/N_2 separation systems. The CO_2-polymer binding energy was also calculated and provided additional information detailing the gas transport mechanism inside the membranes. In Chapter 4, the amidoxime-functionalized poly (1-trimethylsilyl-1-propyne) (AO-PTMSP) membranes was also described to demonstrate the fundamental study of CO_2-philicity in glassy system. In Chapter 5, a series of urethane-rich PDMS-based polymer networks (U-PDMS-NW) with improved mechanical performance for gas separation was also studied.

Conclusions and Future Work summarizes and gives future insights of the project.

CHAPTER I

HISTORICAL BACKGROUND

1.1.Major parameters of concern: Permeability and Selectivity

In membrane gas separation field, the two major parameters of concern are permeability and selectivity. Permeability (P_A) is written as the product of gas flux and membrane thickness divided by the pressure difference through the membrane[1, 2]:

$$P_A = \frac{N_F}{(P_0 - P_1)/l} \tag{1.1}$$

where P_A is the gas permeability, N_F is steady state flux of gas through the membrane, p_0 is upstream (i.e. high) partial pressures, p_1 is downstream (i.e. low) partial pressures, l is membrane thickness. The gas permeability is typically expressed in a non-SI unit, Barrer, which is defined as[2]:

$$1\ Barrer = 10^{-10}\frac{cm^3_{STP}.cm}{cm^2.s.cmHg} \tag{1.2}$$

Gas selectivity (α_{AB}) is defined as the ratio of permeability coefficients of any two gases.

$$\alpha_{AB} = \frac{P_A}{P_B} \tag{1.3}$$

where P_A and P_B are gas permeabilities of gas A and B. Typically gas A possesses higher permeability than gas B, so $\alpha_{A/B} > 1$.

1.2.Solution-Diffusion model

The transport of gases through a non-porous condensed polymeric membranes is usually described by a solution–diffusion model.[3] The solution–diffusion mechanism is considered to consist of three steps: (1) the adsorption or absorption of gas molecules at the upstream side, (2) diffusion of the gas molecules through the membrane material, and (3) desorption of gas molecules on the downstream side. The driving force of solution-diffusion mechanism is the difference between the thermodynamic activities at the feed (upstream) and permeate (downstream) sides, as well as the intermolecular interaction between the permeants and membrane materials.

Based on solution–diffusion model, permeability is determined by both the gas solubility (S_A) and gas diffusivity (D_A):

$$P_A = S_A \times D_A \tag{1.4}$$

The unit of the diffusion coefficient, D_A is cm^2/sec. The solubility coefficient, S_A, has unit of $cm^3(STP)/(cm^3$ polymer.atm).

In this way, gas selectivity (α_{AB}) can also be separated as solubility selectivity ($\frac{S_A}{S_B}$) and diffusivity selectivity ($\frac{D_A}{D_B}$),

$$\alpha_{AB} = \frac{P_A}{P_B} = \frac{S_A}{S_B} \times \frac{D_A}{D_B} \tag{1.5}$$

1.3. Challenges in membrane gas separation field

1.3.1 Permeability-Selectivity trade-off and Robeson upper bound

Permeability and selectivity are traditionally evaluated using a log-log plot, which is often known as a "Robeson Plot." This empirical tradeoff relation was first described for a large database of polymers by Robeson in 1991 and updated in 2008.[4, 5] From this plot, the inherent trade-off relation between permeability and selectivity of polymeric membranes can be observed in which polymers exhibiting higher permeability often show lower selectivity, and vice versa. Membrane performance is compared to an empirically derived "upper bound", which is graphically represented by a straight line passing through data points corresponding to the best permeabilities and selectivities observed. A representative Robeson plot for CO_2/N_2 separation is demonstrated in Figure 1.1.

A fundamental theory describing the basis for this tradeoff was proposed by Freeman and the upper bound line could be described using the following equation[6]:

$$\alpha_{A/B} = \beta_{A/B} / P_A^{\lambda_{A/B}} \tag{1.6}$$

which indicates that as the gas permeability, P_A, increases, gas selectivity value, $\alpha_{A/B}$, decreases. The values of fitting parameters, $\beta_{A/B}$ and $\lambda_{A/B}$, were reported for many common gas pairs.[4, 7]

According to Freeman and Robeson, the slope of upper bound line, $\lambda_{A/B}$, is directly correlated to the difference between the kinetic diameters of the penetrant gas molecules, ($d_B - d_A$). This indicates that the slope of the upper bound is the consequence of the size-sieving nature of the glassy polymeric materials with stiff chain, whose properties generally

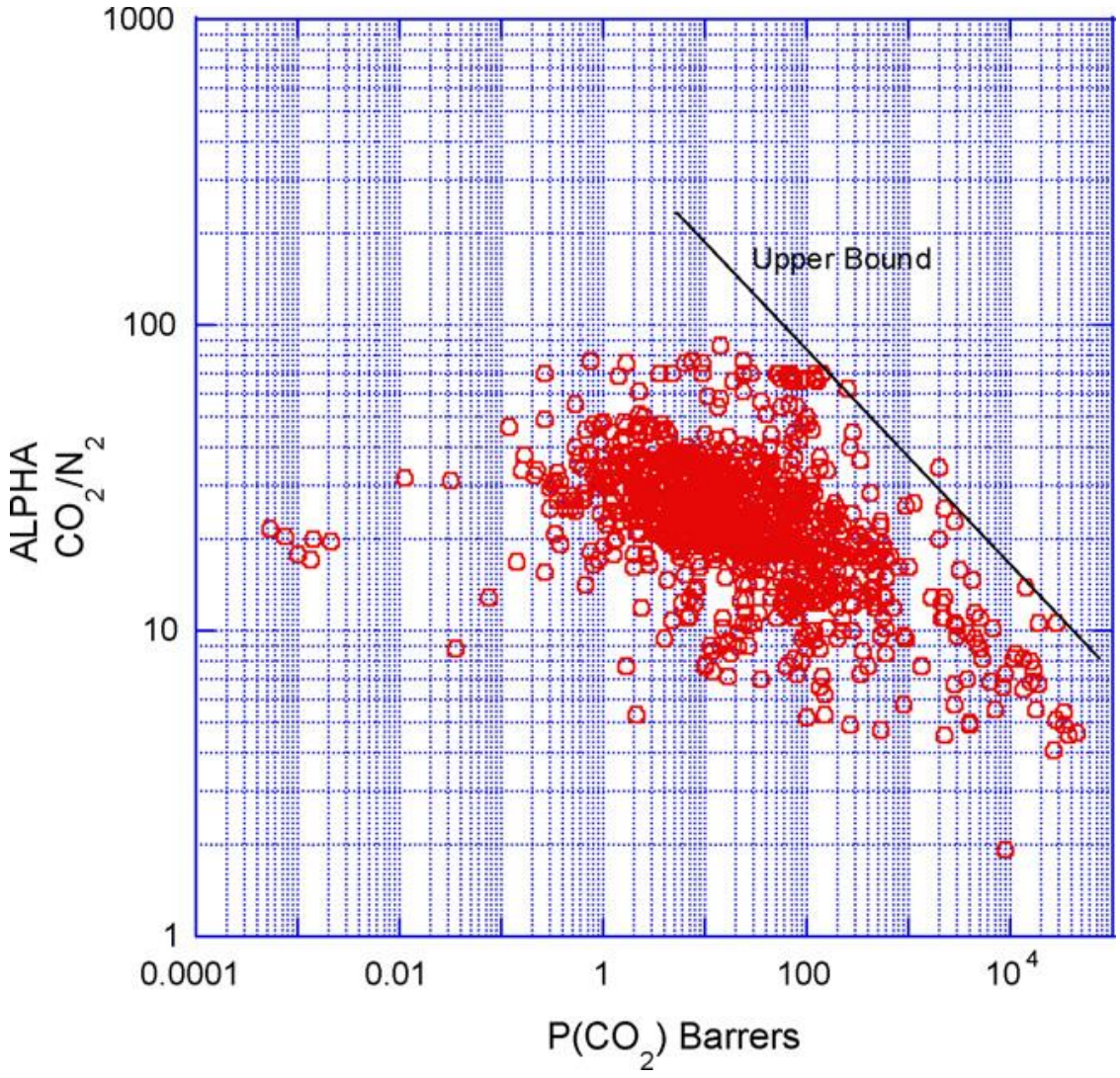

Figure 1.1 The 2008 Robeson upper bound for CO_2/N_2 separation. Reproduced from Robeson.[5]

define the upper bound. The front factor, $\beta_{A/B}$, was found to depend on solubility selectivity and the free volume.

Based on the theoretical prediction, the most efficient way to design polymer materials towards upper bound is to: (1) improve solubility selectivity (2) increases in chain stiffness, while simultaneously increasing fractional free volume, to increase selectivity with minimum loss of gas permeability.

Moreover, since the majority of high-performing gas separation materials are glassy polymers, an upper bound for rubbery polymer was also developed. Most rubbery polymers show lower gas separation performance than that of glassy polymers, leading to a decreased upper bound line.[8]

1.3.2 High permeability

Membranes with both high permeability and selectivity are desired for practical gas separation application. However, as mentioned above, the inherent trade-off relation between permeability and selectivity makes it difficult to obtain high performance at the same time. Predominant amount of current studies focuses on the enhancement of gas selectivity, which works well for fundamental improvement of gas separation materials. However, from practical point of view, the balance of permeability and selectivity should be met to reduce the CO_2 separation/capture cost. In 2010, Merkel et al. reported the effect of gas selectivity and gas permeance on CO_2 capture cost (Figure 1.2).[9, 10] In this report, it was demonstrated that when CO_2/N_2 selectivity is at relatively low level (<30), the capture cost is significantly influenced by the gas selectivity. On the other hand, when the gas selectivity reaches a decent value (>30), its effect on capture cost becomes negligible. This

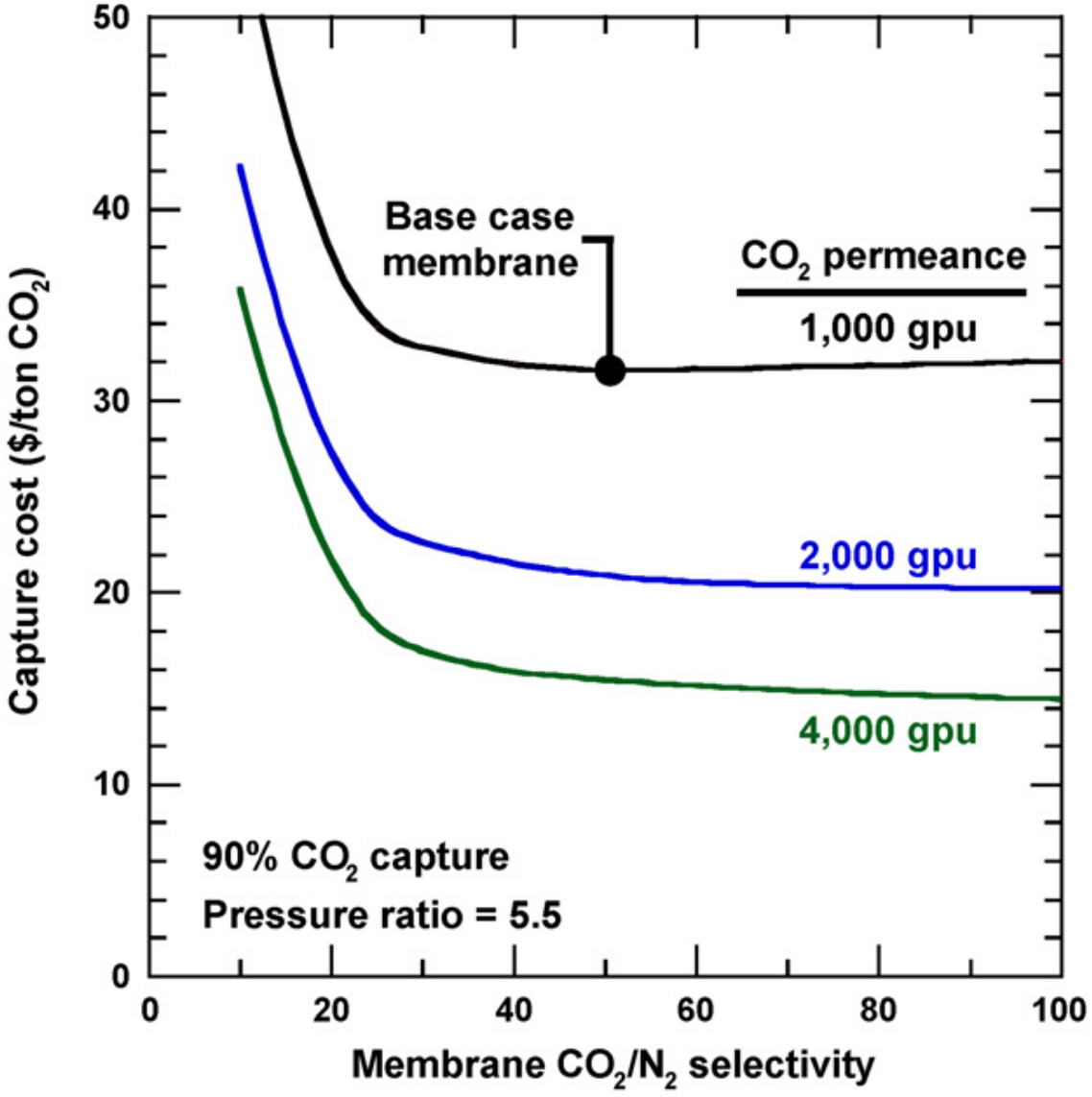

Figure 1.2 Selectivity on the cost of capturing 90% of the CO_2 in flue gas for membranes with a CO_2 permeance of 1000, 2000, and 4000 GPU at a fixed pressure ratio of 5.5. Reproduced from Merkel *et al*.[9]

is due to the limited pressure difference encountered in flue gas treatment. Thus, in practical application, simply pursuing extremely high gas selectivity does not show significant contribution to cost reduction. However, if a membrane exhibits high permeability/permeance, the carbon capture cost is likely to reduce due to the reason that high flux membranes require less area to treat an equal volume of gases. Therefore, the development of high permeability membranes should be targeted and the optimum values of the permeability and selectivity need to be investigated.

1.3.3 Solubility selective *versus* diffusivity selective membranes

According to solution-diffusion model, gas selectivity could be separated as two parts: solubility selectivity and diffusivity selectivity. The overall selectivity could be enhanced from either part. In membrane design, the predominant approach to improve gas selectivity, especially for glassy polymer membranes, is to enhance diffusivity selectivity by tuning the pore size, thereby increasing the membrane's size-sieving capability.[11-14] Among them, a great deal of the studies have been performed on polymers of intrinsic microporosity (PIMs), [15-17] thermally rearranged (TR) polymers, [12, 13, 18] etc. Size-sieving approach works well for gas pairs with strongly different sizes, e.g. CH_4/H_2 ~3.80 Å/2.89 Å, N_2/He ~ 3.64 Å/2.60 Å. However, based on the theoretical prediction by Freeman, this method is not sufficient for CO_2/N_2 separations due to the similar kinetic diameters of CO_2 and N_2 (CO_2~3.30 Å, N_2~ 3.64 Å).[6] Another approach, to which less attention is paid, is to enhance solubility selectivity.[19, 20] For CO_2 separation, researchers reported that the incorporation/blending of CO_2 interactive functionalities could contribute to the enhanced solubility selectivity, therefore overall selectivity. For instance, a number of

studies on Pebax membranes, which exhibits high CO_2 solubility due to the strong affinity of the polar ether linkages (polyethylene oxide functionality) in the structure, have demonstrated the potential of enhancing CO_2 solubility in order to improve the CO_2 separation performance.[21-25] Based on the application of acid-base interaction, some nitrogen-containing groups, like amine,[26, 27] tetrazole[28, 29] and amidoxime,[30-34] are also used to enhance polymer-CO_2 interaction. However, with the incorporation of CO_2-philic groups, the significant loss in gas permeability is generally observed. It still remains a problem how to significantly enhance the gas selectivity with minimum loss of permeability.

1.3.4 Physical aging

One of the most important characteristics of a polymer is glass transition. All polymer materials can be supercooled below their melting temperature without crystallization, and instead, they go through a process called glass transition. The glass transition temperature, T_g, is defined as a temperature at which the material transforms from the liquid state to the solid state without crystallization. Physical aging is defined as physical change in some property of a glassy material as a function of storage time below T_g in the absence of external influences.[35] When temperature is above T_g, the polymer is in the rubbery state and segments of the polymer chains are mobile; when temperature goes below T_g, segmental and chain structure are frozen and remain in a non-equilibrium state, which would lead to the frustration in chain packing and excess free volume (FV) in the structure. The driving towards equilibrium state will cause the decay of FV over time.[36, 37] Since for most glassy polymers, the gas transport property is significantly affected by

FV, the decrease of FV could lead to considerable drop of gas permeability.[38] Much research has been performed to demonstrate the impact of physical aging on gas transport properties of different glassy polymer materials.[39-47] One typical example is poly(1-trimethylsilyl-1-propyne) (PTMSP).[42, 48-51] It has orders of magnitude higher permeability than other polymers (CO_2 permeability ~30000 Barrer), which could be attributed to the exceptionally large FFV and intersegmental gaps in the PTMSP matrix. However, due to the severe physical aging issue, which could cause the substantial collapse of FV, its permeability shows one or two orders of magnitude drop even under ambient environment. Yampolskii et al reported the gas transport property comparisons of initial and aged PTMSP (Figure 1.3). All studied gas permeabilities showed more than one order drop in gas permeability, while some gas selectivities increased due to finer size-sieving capability. The overall gas separation performance reduced significantly. It was also reported by different groups that the aging effect and aging rate were influenced by various membrane parameters, e.g. membrane thickness,[52, 53] aging temperature[54-56] and vacuum.[39, 42]

Much effort has been made to reduce the physical aging issue in glassy membranes, such as the addition of organic/inorganic fillers [57-59], copolymerization[60] and cross-linking,[61] etc. However, the aging effect still cannot be removed completely. Thus, from practical aspect, design and synthesize polymer materials with less or none aging issue are required for the long-term membrane module application.

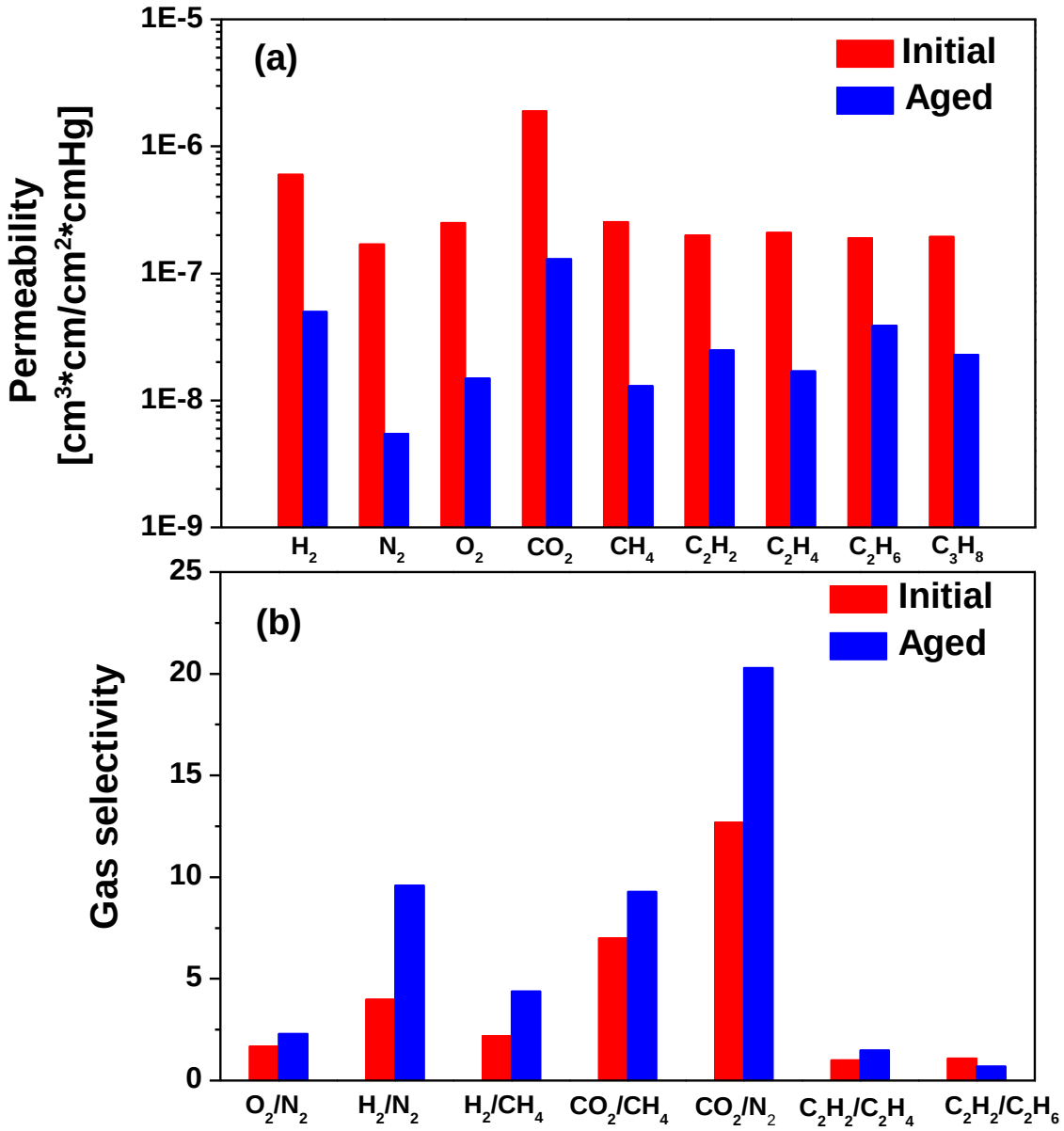

Figure 1.3 (a)Gas permeability and (b) selectivity of initial and aged PTMSP. Data reproduced from Yampolslii et al.[50]

1.4.Polydimethylsiloxane (PDMS)-based membranes

1.4.1 General properties of PDMS

Polydimethylsiloxane (PDMS, CAS number 63148-62-9) is a typical rubbery polymer at room temperature. It has flexible (Si–O) backbones and the repeating unit is($Si(CH_3)_2O$) (Figure 1.4).

Depending on different molecular weight/number of the repeating units, the general viscoelastic properties of the material are varied. Based on practical needs, changes of the viscoelastic properties can be made by several techniques, e.g. cross-linking the polymer,[62] incorporating fillers (e.g. silicon dioxide) to the polymer network[63], etc. PDMS is a non-toxic, translucent and highly hydrophobic polymer that has no bio-accumulation. The glass transition temperature of PDMS is typically around −125 °C.[64, 65] The specific gravity of PDMS generally ranges from 0.91 to 1.00. For PDMS with molecular weight ranged from 10,000 to 60,000 g mol^{-1}, it has very low dielectric constant ranging from 2.72 to 2.75 (implying low refractive index)[66]. Moreover, due to its optically transparency down to 300 nm, PDMS is used in some optical measurements.[67] PDMS is a well-known biocompatible material. In Marois et al's review paper, the authors discussed the hemocompatibility, inflammatory response, *in vitro* biocompatibility, and *in vivo* tissue reactions of PDMS.[68] Although some work still needed to be done, PDMS shows great potential to be used in inflammatory response, *in vitro* biocompatibility, and *in vivo* studies. Moreover, PDMS can be used to treat head lice on the scalp,[69] in over-the-counter drugs as a carminative an antifoaming agent.[70, 71] PDMS is added to many cooking oils as an antifoaming agent. It is

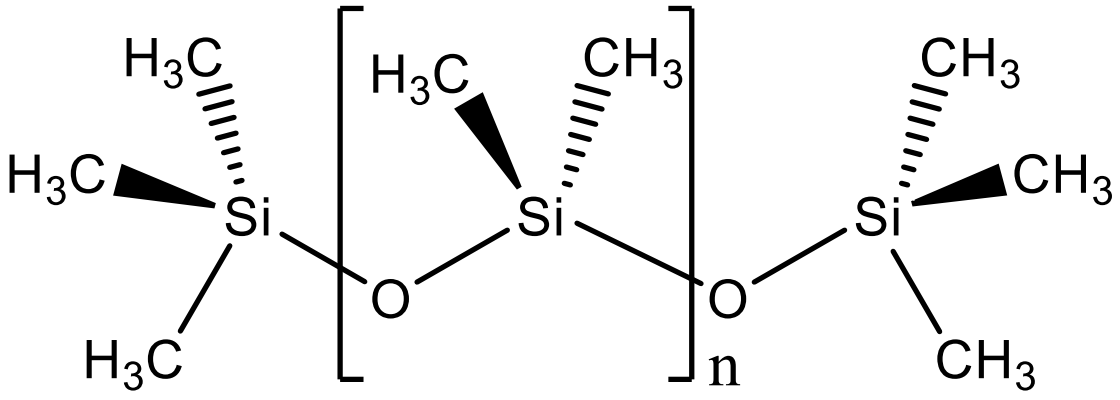

Figure 1.4 Chemical structure of polydimethylsiloxane (PDMS).

used in trace quantities in some fast food processing.[72,73] PDMS possesses good mechanical properties. It has a shear elastic modulus between 0.1 MPa and 3 MPa,[74, 75] small temperature variations of the physical constants,[75] very low loss tangent (tan $\delta << 0.001$[75]), thermal stability and ease of processing,[76-85] together with its relatively low cost makes it a promising candidate for a broad variety of applications.

1.4.2 Gas transport properties of PDMS membranes

Towards the need for high-performing gas separation materials, in recent years, a large number promising polymer material with excellent permeability have been developed, some of which were shown to surpass the upper bound. Among highly permeable polymers, the majority of the studies have been performed on glassy membranes, such as polymers of intrinsic microporosity (PIMs), [15-17] thermally rearranged (TR) polymers, [12, 13, 18] etc., while less studies have been performed on highly permeable rubbery polymers.

PDMS is known to possess some of the highest permeabilities to various gases.[86] Its rubbery nature allows the materials to overcome the aging issue, which is greatly beneficial to the practical applications. A detailed study of gas transport property of conventional PDMS was reported by Merkel and Freeman.[64] The values are summarized in Table 1.1. Compare to other well-known rubbery polymers used for gas separation, e.g. poly(ethylene oxide) with CO_2 permeability about 140 Barrer,[87] PDMS typically possesses one order of magnitude higher CO_2 permeability (3800 Barrer), which primarily originated from its extremely fast segmental motion that leads to high gas diffusion coefficient. However, rubbery polymer membranes, the liquid-like polymer matrix has poor size-sieving ability[88] and the overall selectivity is often determined by different gas solubilities in the membranes[19, 86]. The conventional PDMS has a CO_2/N_2 selectivity around 9.5.[86] If the gas selectivity of PDMS-based membranes can be enhanced while maintaining its high permeability, the developed membrane would readily meet the practical target in separation efficiency and cost.[89]

Much research has been reported on the PDMS membranes in order to obtain higher CO_2/N_2 separation performance. The gas transport property of pure PDMS itself is influenced by various factors, e.g. cross-linking temperature,[85] curing agents, [90-93], thickness,[94] etc. For instance, according to Eq. 1.1, when calculating gas permeability, the thickness is generally normalized. However, researchers reported dependence of permeability on membrane thickness for a variety of materials.[95, 96] Firpo et al reported the detailed study of permeability thickness dependence of PDMS membranes.[94] The SEM/Focused Ion Beams (FIB) was used to determine the membrane thickness.

Table 1.1 Summary of Permeability, Solubility, and Diffusivity Parameters in PDMS at 35 °C. Data from Merkel *et al*.[86]

Penetrant	Permeability [Barrer]	S^{∞} [cm^3(STP)/cm^3.atm]	$D_0 \times 10^6$ [cm^2/s]
H_2	890 ± 30	0.05 ± 0.008	140 ± 5
O_2	800 ± 20	0.18 ± 0.01	34 ± 1
N_2	400 ± 10	0.09 ± 0.008	34 ± 1
CO_2	3800 ± 70	1.29 ± 0.01	22 ± 1
CH_4	1200 ± 40	0.42 ± 0.01	22 ± 1
C_2H_6	3300 ± 100	2.2 ± 0.02	11.3 ± 0.3
C_3H_8	4100 ± 300	5.0 ± 0.07	5.1 ± 0.3
CF_4	200 ± 10	0.19 ± 0.01	8.0 ± 0.2
C_2F_6	190 ± 10	0.33 ± 0.01	4.4 ± 0.1
C_3F_8	280 ± 10	0.85 ± 0.02	2.5 ± 0.1

As shown in Figure 1.5, the authors claimed that gas permeability shows thickness dependence below tens of micrometers, while gas selectivity remains unaffected. In our work, in order to avoid undesired thickness effect on gas transport properties, thick membranes (100-200 μm) were used in all studies.

1.4.3 Modifications of PDMS membranes

To improve PDMS gas separation performance, various methods are reported. One simple method is by mixing/blending PDMS with other CO_2 separation polymers. For instance, Reijerkerk et al reported the blending of PDMS–PEG with Pebax.[97] With the PDMS-PEG composition ranging from 10 wt%-50 wt%, the CO_2/N_2 selectivity changes from 48-36. However, the CO_2 permeability still shows about one order of magnitude decrease.

The copolymerization also offers another route to introduce improved selectivity into PDMS matrix. Park et al reported the copolymerization of PDMS with polyurethanes and polyurethane ureas and achieved improved CO_2/N_2 selectivity up to 25.[98] However, a huge drop in CO_2 permeability was observed (all below 100 Barrer for high selective membranes). Other PDMS-based copolymer membranes were also reported by different groups but the performance was below upper bound.[99-102]

Nowadays, much attention is paid to PDMS-based composite membranes, which typically consist of a polymer matrix as the bulk phase and inorganic fillers, e.g. carbon molecular sieves, zeolite, or nano-size particles, as the dispersed phase.[103, 104] Since the composite membranes could combine the strengths of both polymer matrix and fillers, many of them were shown to surpass the upper bound. For example, Hussain et al synthesized PDMS-

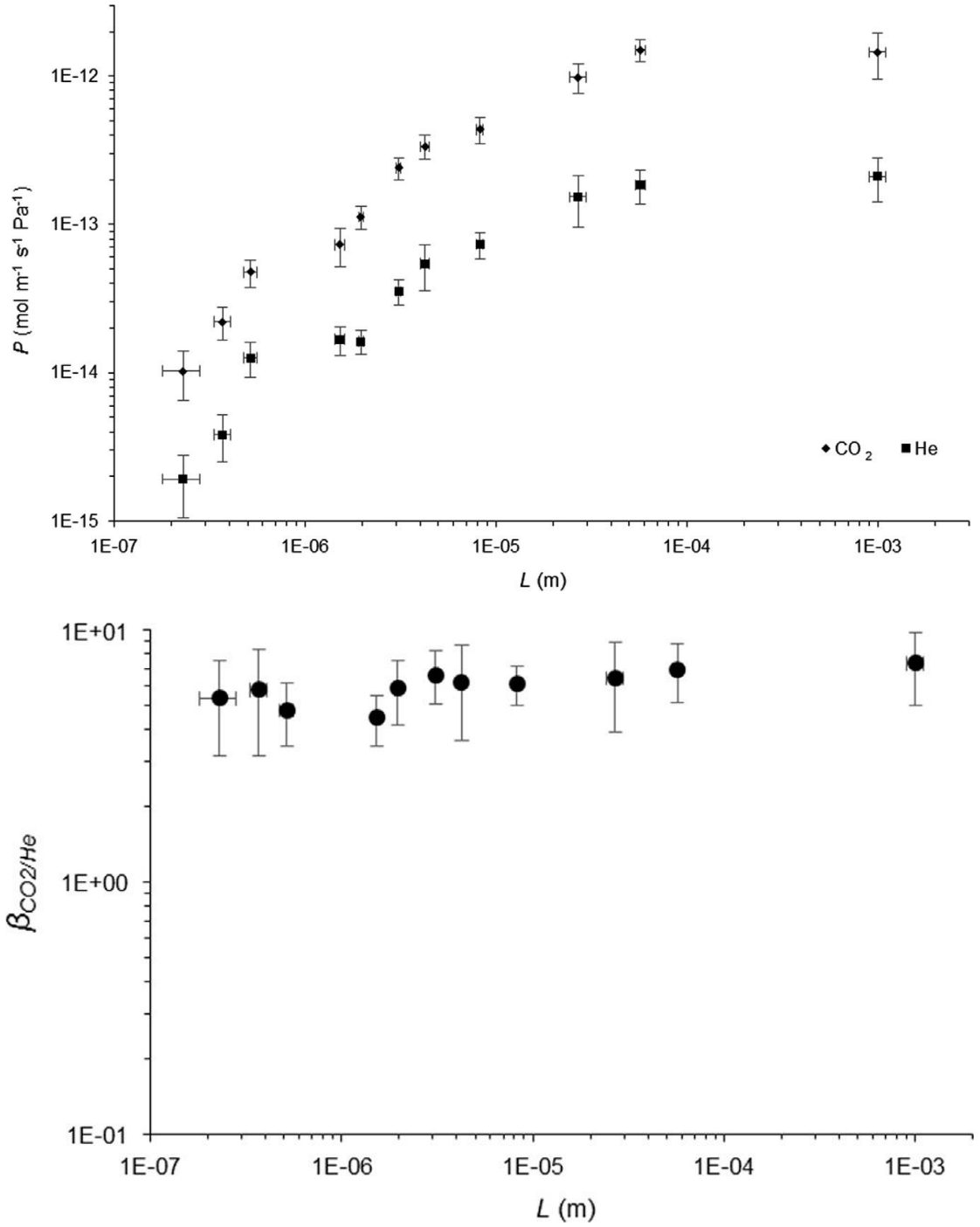

Figure 1.5 Gas permeability and CO_2/He selectivity as a function of membrane thickness L. Reproduced from Firpo et al.[94]

zeolite membrane and obtained a huge increase in gas permeability and moderate increase in gas selectivity.[105] Gurr et al reported polyimide-PDMS copolymer composite membranes and reached CO_2/N_2 selectivity ~20.[106] Other PDMS-based composite membrane used for different types of gas separation are also reported.[107, 108]

While the development of mixed matrix membranes could help overcome the permeability/selectivity trade-off, the advancement of purely polymeric membranes, which serve as a selective layer, is also crucial for fundamentally cultivating the material potential. Thus, in this work, we target purely polymeric membranes with high permeability and good selectivity.

1.5. CO_2-philic functional groups

As mentioned above, all rubbery polymers show poor diffusivity selectivity, due to their low FFV and little size-sieving capability. Thus, the most efficient method to escalate PDMS gas selectivity is to focus on higher solubility selectivity. By introducing CO_2-philic groups, the polymer-CO_2 interaction could be enhanced and the dissolution of CO_2 molecules into the polymer matrix is increased. This could lead to higher CO_2/N_2 selectivity in polymer materials. Since CO_2 is a polar, acidic gas, the application of either polar and/or basic functionalities could contribute to CO_2-philicity.

Theoretical work of CO_2 interaction with a variety of functional groups was done by different groups. For instance, Vogiatzis *et al.* studied the interactions between CO_2 and N-containing organic heterocycles.[109] The authors claimed that interactions occurred at two functional sites and *via* different mechanisms, which are: (a) Lewis acid–Lewis base interactions and (b) hydrogen bonding. Jiang *et al.* reported the ab initio calculations on

over 55 neutral molecules for CO_2 affinity via binding energy (BE) CO_2-philic groups.[110] Some N-containing groups, e.g. piperidine, pyrrolidine, triazole showed good BE with CO_2 molecules. More interestingly, it was found that poly(ethylene oxide)s (PEO) oligomers with more than three repeating units shows excellent CO_2-philicity, which agreed well with the good performance of PEO-based membranes for CO_2/N_2 separation. Other simulation studies were also performed and some functionalities, e.g. N,N,N' TMEDA-EO,[111] piperazine,[112] monoethanolamine,[112] amidoxime,[30, 31, 34]were highlighted as promising CO_2-philic functionalities for further experimental studies. Some representative functionalities and their BE values are summarized in Table 1.2.

With the help of theoretical predictions, more research is focused on those N-containing and PEO-based materials for higher CO_2 interaction. Du et al reported the successful incorporation of tetrazole(TZ) groups into the highly-permeable PIM-1 polymer.[28] The CO_2/N_2 selectivity showed a factor of 2 improvement and reached ~30, while the CO_2 permeability was still around 300 Barrer. Later, thioamide-PIM-1[113] and AO-PIM-1[32] were also reported to significantly enhance CO_2/N_2 selectivity. When using AO modification as an example, Swaidan et al reported the AO-PIM-1 showed more than 40% increase in CO_2/N_2 selectivity (24 to 35).[32] Mahurin et al studied the CO_2/N_2 adsorption of amidoxime grafted porous carbon framework.[33] After amidoximation, the adsorption CO_2/N_2 selectivity showed 10%-100% increase. Other AO work reported also provides solid support that the incorporation of CO_2-philic groups could help enhanced CO_2 sorption into the materials.[30, 31, 114]

Table 1.2 Binding Energy of CO_2 with different functionalities.

Functionality	Structure	Binding energy (kJ/mol)
Water[110]	H_2O	11.5
Methylamine	H_3C-NH_2	15
Tetrazole[109]	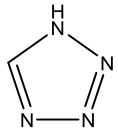	18
Imidazole[109]	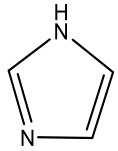	19
Tetrahydrofuran[110]	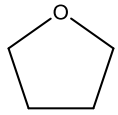	19
Triazole[110]	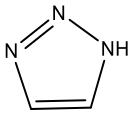	20
Amidoxime[34]	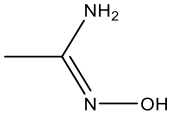	20
Me-PEO_4[110]	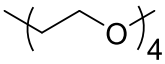	36
N,N,N'TMEDA-EO[111]	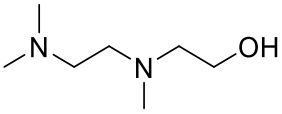	50
Piperazine[112]	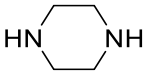	64
Monoethanolamine[112]	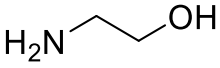	70

In Guiver et al's recent review paper,[104] many other basic functional groups, e.g. -NH_2, F^-, PO_4^{3-}, CO_3^{2-}, COO^-, etc., were highlighted to show enhanced CO_2/N_2 selectivity. Another extensively studied functionality is PEO. Due to the polar ether linkages, it has strong interaction with CO_2 molecules thus is an ideal candidate for CO_2 separation. As reported by Lin and Freeman, the amorphous PEO possess CO_2 permeability about 140 Barrer and CO_2/N_2 selectivity about 50. A great amount of research was followed to explore the PEO-based materials. Some of the Pebax membranes showed great CO_2/N_2 selectivity up to ~70 and demonstrated great potential for practical flue gas separation.[21-25, 115-121]

Overall, with the careful selection of CO_2-philic functionality and polymer matrix, it is possible to significantly enhance CO_2/N_2 separation performance.

1.6.Dual-mode model

To investigate the solubility selectivity, gas sorption measurements could help to determine the gas solubility of different membranes. A schematic representation of gas sorption in polymer membranes is illustrated in Figure 1.6.[122]

The sorption of polymer is typically explained by a dual-mode model,[123, 124] which deconvolute gas sorption into equilibrium and non-equilibrium regions in a polymer matrix.

$$C = k_D p + \frac{C'_H bp}{1 + bp} \tag{1.7}$$

where C is the equilibrium penetrant concentration in the polymer at pressure p, k_D is the Henry's law solubility parameter, which demonstrates penetrant dissolution into the

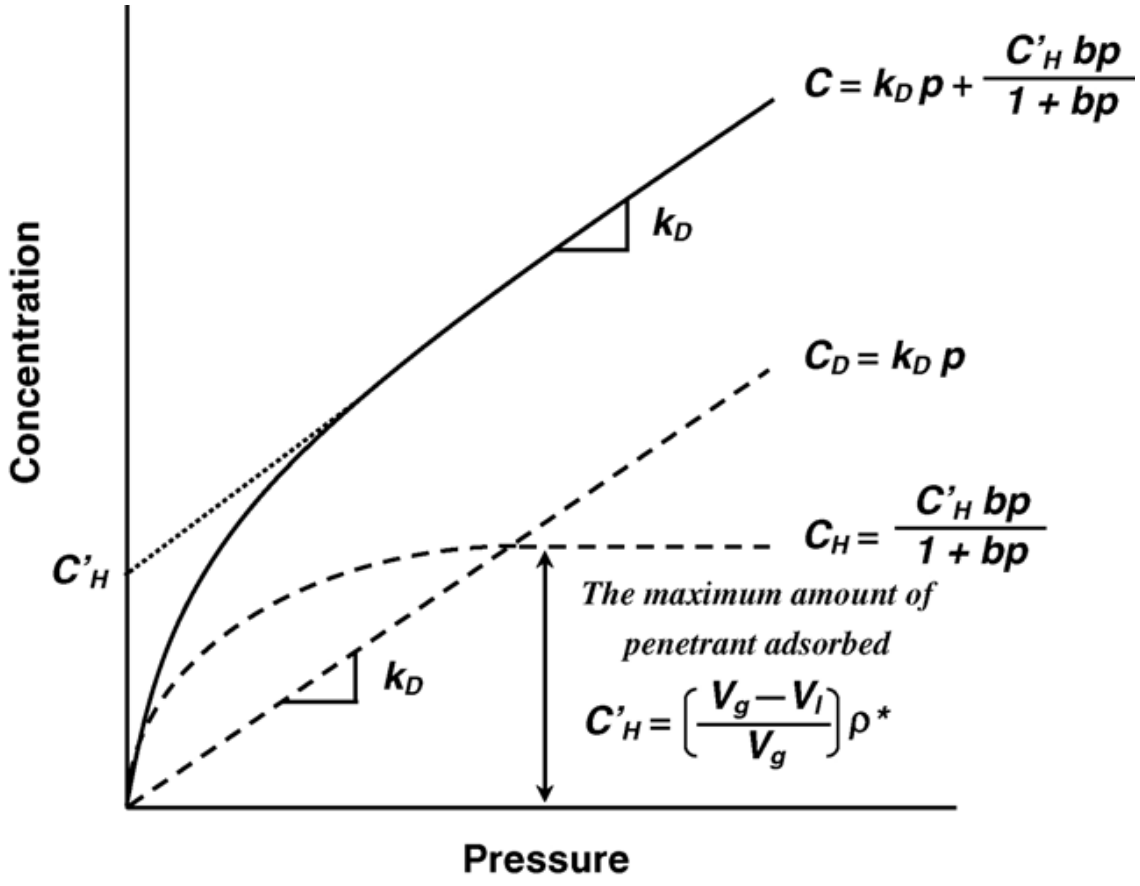

Figure 1.6 Schematic representation of a dual-mode sorption analysis using Eq.1.7.

equilibrium densified polymer matrix; C'_H is called Langmuir capacity parameter, which demonstrates the sorption capacity of the non-equilibrium excess FV characteristic of the glassy state; *b* is the Langmuir affinity parameter, an equilibrium constant describing the affinity of a penetrating gas for a Langmuir site. According to the dual mode model, the solubility coefficient *S*, is writen as:

$$S = \frac{C}{p} = k_D + \frac{C'_H b}{1 + bp} \tag{1.8}$$

The solubility selectivity is determined by the ratio of solubility coefficients of two gases.

1.7. Time lag and diffusion coefficient

The gas permeability, *P*, is typically calculated using the slope of pressure rise in the permeating side. However, before the steady state permeation is approached, there is typically an interval. This is due to the finite diffusion velocity of permeants/gas molecules within the membranes. In the Pressure-Time curve, the intercept *L* between *t*= 0 and the intersection for large *t* extrapolated back to the *t*-axis, provides an easy way of estimating diffusion coefficient (*D*). *L* is called the " time lag." A representative plot shown in Figure 1.7.

The origins of the “time lag ” method were explained early by Daynes[125] and Barrer.[126]

The basic law of the diffusion through a membrane is the Fick’s law:

$$J = -D\frac{\partial c}{\partial x} \tag{1.9}$$

where *J* is the diffusion flux, and *c* is the concentration of the permeants at position *x*, *D* is diffusion coefficient.

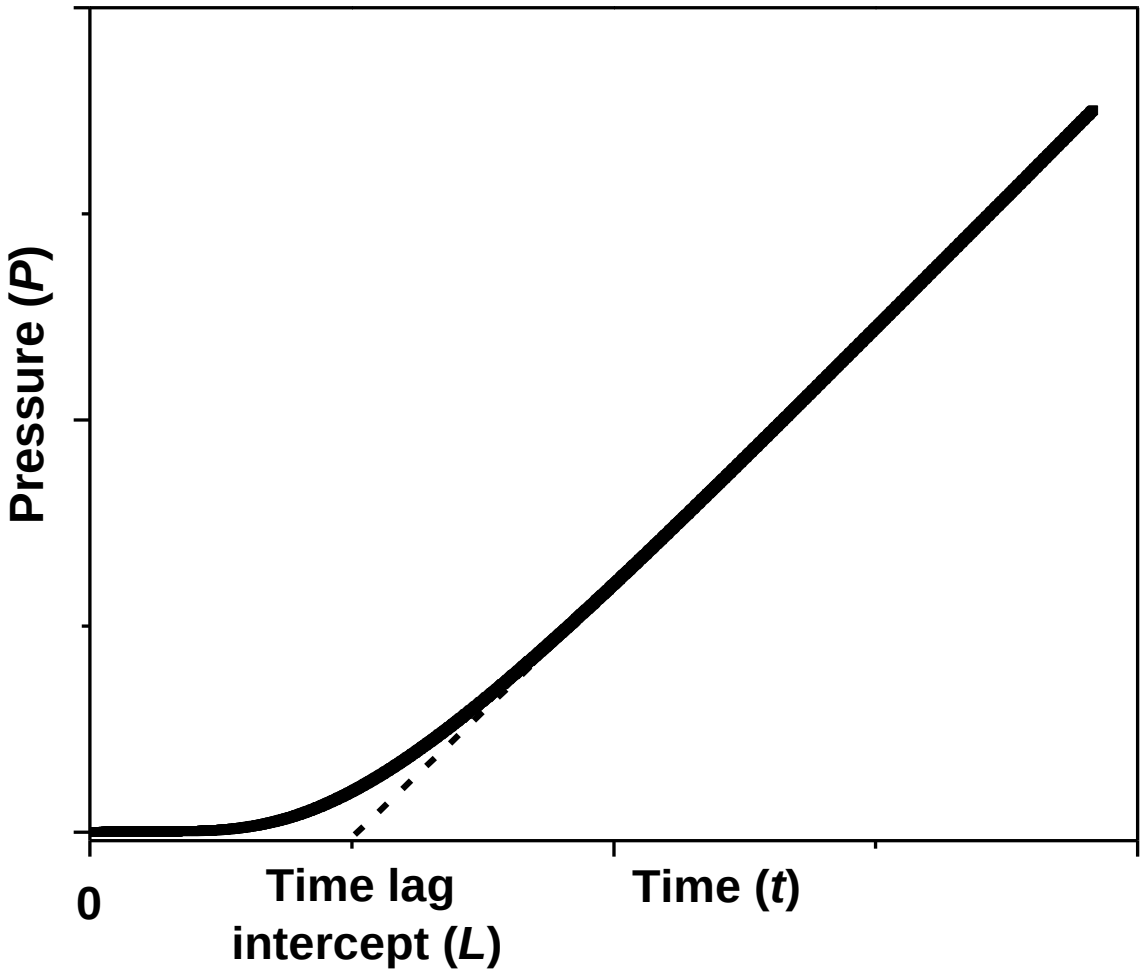

Figure 1.7 Pressure rise of a polycarbonate membrane indicating the "time lag" before the establishment of steady state of flow into the permeating side.

One model to analyze Eq. 1.9 is the Frisch method. This method is based on integrating the transport equation once in time and twice in space, and therefore, obtaining the integrated flux. The method was originally derived for systems with concentration-dependent diffusion coefficients *D(c)* without explicitly solving the diffusion equation. This method is elaborated by Rutherford[127] and reviewed by Strzelewicz[128] for quasi-linear, diffusion equation:

$$\frac{\partial c}{\partial t} = \frac{\partial}{\partial x}\left[D(c)\frac{\partial c}{\partial x}\right] \tag{1.10}$$

Time lag *L* is given then by the formula:

$$L = \frac{\int_0^l \int_x^l c_s(z)\, dz\, dx}{\int_0^{c_0} D(u)\, du} \tag{1.11}$$

where $c_s(z)$ is the steady-state concentration distribution, *l* is membrane thickness. When diffusion coefficient is constant, reduces Eq.1.11 to the form:

$$L = \frac{l^2}{6D} \tag{1.12}$$

Thus, by knowing the time lag *L* and membrane thickness *l*, the diffusion coefficient *D* of the membrane could be estimated.

1.8.Research objectives

In order to treat the large volumes of industrial flue gas efficiently and cost-effectively, high-performing polymeric membranes with excellent CO_2 permeability and decent CO_2/N_2 selectivity are in a desperate need. However, no current commercially available membranes could meet the practical target. Conventional glassy membranes based on size-sieving mechanism are inherently limited due to the similar kinetic size of CO_2 and

N_2 gas. A completely novel method based on non-size-sieving mechanism should be developed to break through and current limit.

Bear that goal in mind, this work targets on the development of high-performing, solubility selective membranes with excellent gas permeability and good selectivity. The carefully tailoring of polymer matrix, the controlled incorporation of CO_2-philic functionality and the deeper fundamental understanding will be illustrated in the following work.

CHAPTER II

EXPERIMENTAL TECHNIQUES

2.1 Gas permeation measurement

Gas permeation measurements are performed at room temperature (25 ± 1 °C) with single gas tests using a custom test chamber following the constant-volume variable-pressure method.[129, 130] A schematic drawing is present in Scheme 2.1 and a photo of instrument is shown in Figure 2.1. In this work, all the upstream and downstream parts were purchased from Swagelok. The upstream pressure was measured with a Honeywell STJE 1500 psig pressure transducer and the downstream pressure was measured by a MKS Baratron 626B capacitance manometer with a range of 0 to 10 torr (1.33 kPa).

In a typical gas permeation test, the fabricated membrane is cut and mounted on a 47-mm brass disc with a 10-mm hole in the center. The membrane edges were sealed using epoxy and the permeation area was determined using the ImageJ software. The thickness of a membrane is measured using a digital micrometer. The membrane sample is then carefully placed on a piece of filter paper that provided mechanical stability and negligible resistance to gases. Then the entire assembly is placed in a Millipore 47-mm diameter filter holder for testing. A photo of membrane sample in shown in Figure 2.2. After loading the membrane sample into the cell, all the valves (valve 0,1,2,3) are switched on and the whole system is vacuumed overnight to completely degas the membrane sample. When the permeability of the tested sample is very high, valve 5 is also switched on to provide extra permeation volume on the downstream side. After

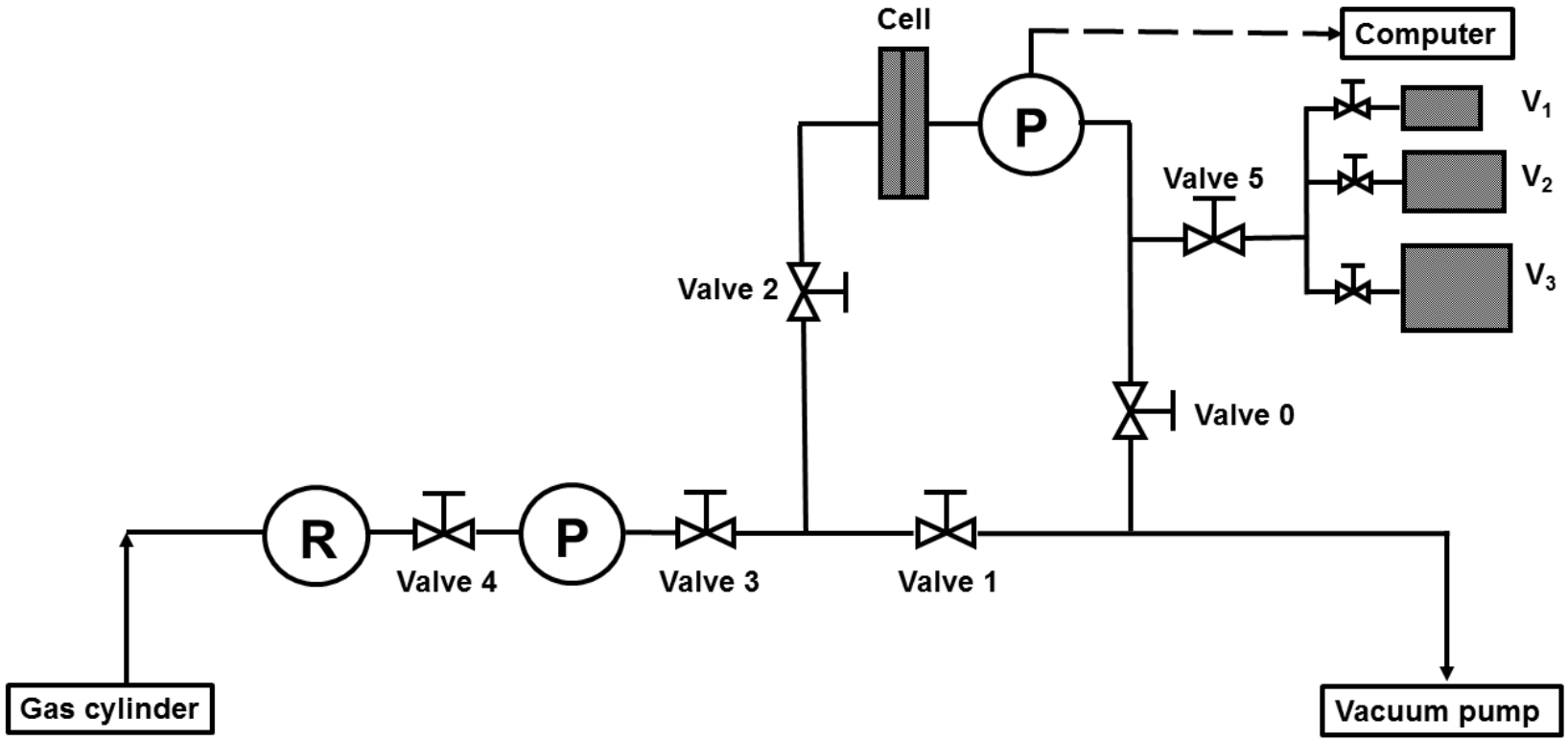

Scheme 2.1 Schematic drawing of a constant-volume variable-pressure apparatus for single gas permeability measurements (R is the regulator; P is pressure transducer; V_1, V_2 and V_3 are extra permeation volumes).

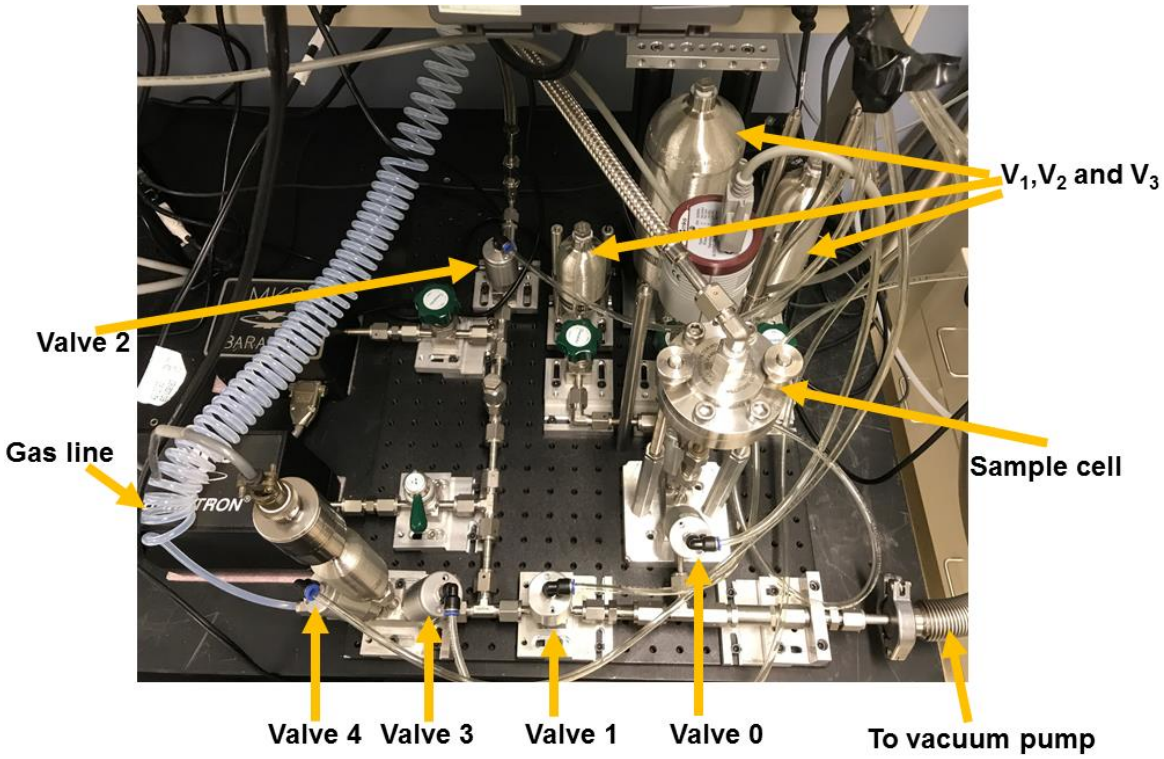

Figure 2.1 A photo of the gas permeation instrument.

Figure 2.2 A photo of a testing membrane sample. The membrane is typically mounted on a brass disc and the edge is sealed using epoxy.

degassing the sample, the valves connecting the permeation chamber to the vacuum pump (valve 0 and 1) are closed. A slow pressure increase in the downstream volume (i. e., system leak rate) is observed and recorded. After the leak test, valves 0,1,2,3 are closed and the valve 4 is switched on to introduce feed gas (from 0.1-2 atm) to the upstream side of the membrane. Then valve 2 and 3 are opened and the gas starts to permeate through the membrane sample. The pressure rise in the downstream volume is recorded by the program. Figure 2.3 demonstrates a typical pressure rise when gas permeates through a polymer membrane.

According to the following equation, single gas permeabilities are calculated using the pressure rise data collected from the linear regime.

$$P_A = \frac{V_c l}{RTA_m \Delta P}\left[\left(\frac{dP}{dt}\right)_{ss} - \left(\frac{dP}{dt}\right)_{leak}\right] \quad (2.1)$$

where P_A is the gas permeability, V_c is the permeate volume of the instrument, l is the thickness of the membrane, R is the ideal gas constant, A_m is the permeation area, ΔP is the pressure difference between the upstream and downstream, $\left(\frac{dP}{dt}\right)_{ss}$ is the rate of gas pressure increase on the permeate side at steady state, $\left(\frac{dP}{dt}\right)_{ss}$ is the system leak rate.

In order to obtain data with higher accuracy, it is important to insure the low pressure rise on the downstream side. Thus, when testing the sample with high P_A, V_1 and V_2 will be used to increase the total V_c to reduce the downstream pressure increase.

In the mixed gas permeation measurement, feed and permeate compositions were determined using a Buck Scientific gas chromatograph (GC) equipped with silica gel packed and molecular sieve 13x columns and TCD detector. The gas mixture was

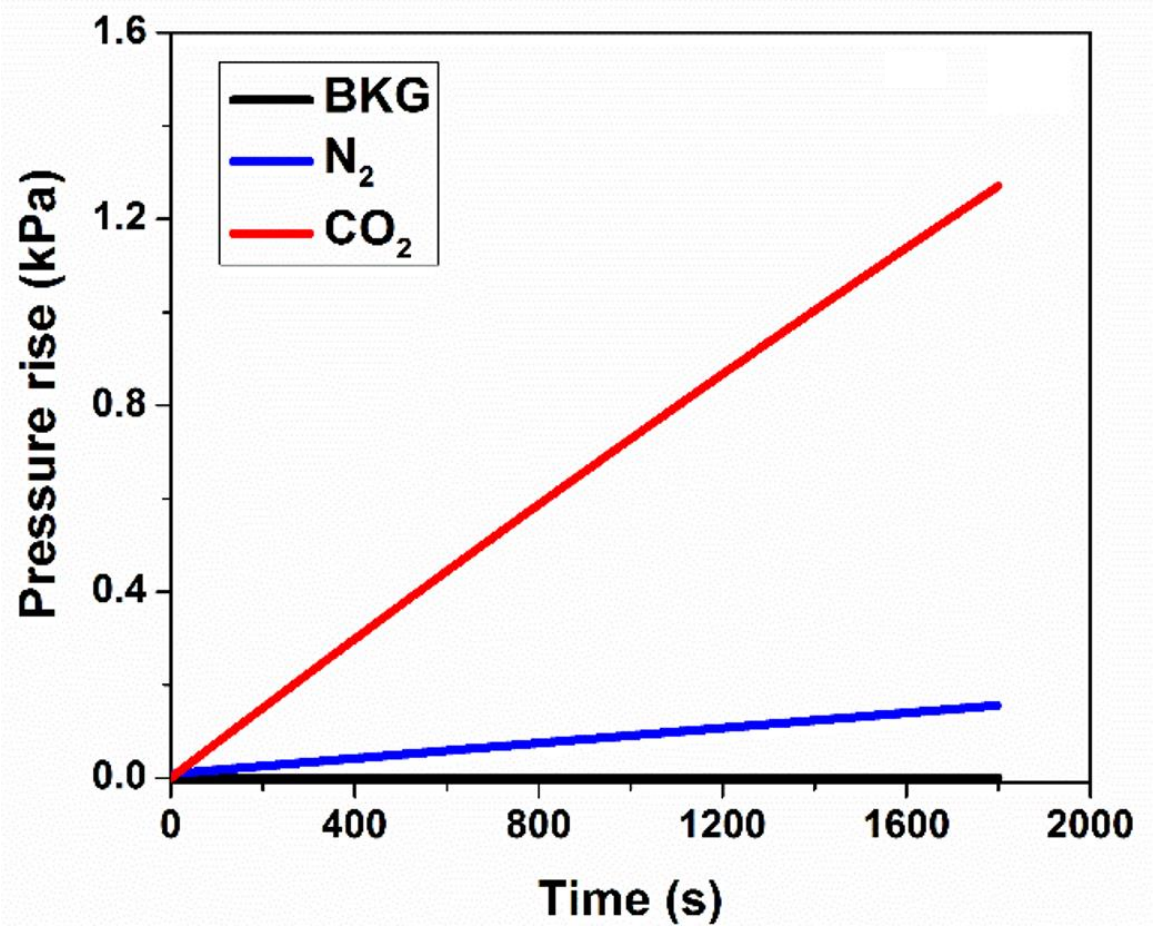

Figure 2.3 Pressure rise in the permeation chamber when gas permeates through a polymer membrane.

controlled using mass flow controllers (MKS Instruments). The CO_2/N_2 molar ratio in the feed gas is 1:1.

The permeability of different gases in the mixture was calculated using the following equation:

$$P_A = \frac{V_c l}{RTA_m \Delta P} \frac{dP_l}{dt} \frac{y_A}{x_A} \tag{2.2}$$

where y_A is the mol fraction of component A in the permeate side, x_A is the mol fraction of component A in the feed side.

2.2 Isothermal gravimetric gas adsorption

Gas sorption measurements of CO_2 and N_2 are performed using an Intelligent Gravimetric Analyzer (Hiden Analytical Limited, UK).[131] The machine generally measures the mass uptake in membrane samples. In a typical experiment, approximately 50 mg membrane sample is loaded into a quartz container and vacuumed to 0.003 bar at 150 ˚C for 6 h to degas and dry the sample. All measurements are performed at ambient temperature. The mass uptake (%) is measured as a function of feed pressure up to 10 atm to obtain the absorption isotherm.

The raw data is reported in mass uptake [(g/g) *100%]. To convert the data to sorption concentration [cm^3 (STP)/cm^3 polymer], following calculation is applied:

$$\frac{cm^3(STP)}{cm^3\ polymer} = \frac{m_{absorb}/\rho_{gas}}{m_{polymer}/\rho_{gas}} \tag{2.3}$$

Desorption isotherms are obtained subsequently by measuring the mass versus the decreasing pressure to ensure that the sorption behavior is reversible and to test the hysteresis effects.

Typically, the mass uptake data is converted to volume uptake and the sorption isotherms are fit using Eq. 1.7. The gas solubility is calculated by Eq. 1.8.

2.3 Differential Scanning Calorimetry (DSC)

Differential Scanning Calorimetry (DSC) is used to study the thermal transitions, e.g. melting, crystallization, and glass transition of a material. In a typical DSC measurement, one pan has sample in it and the other pan is always empty as the reference. During the measurement, both pans are heated at the same specific rate which is determined by the operator. Since one pan has sample the other pan doesn't, in order to keep the same heating rate, the sample pan needs more heat than the reference pan. The instrument measures how much more heat it has to supply for the sample pan than the reference pan. The quantity that describes how much heat Q a sample has to take for it to increase temperature by one degree is called heat capacity $Cp = Q/\Delta T$, in which ΔT is the change of temperature.

In this work, Temperature Modulated-DSC (TMDSC) is used to study the thermal transitions of membranes. The TMDSC can divide the total heat flow into two individual components, the reversing heat flow which contains information about processes such as glass transition and the non-reversing heat flow which includes those kinetic processes such as crystallization. Although a TMDSC experiment takes longer time than a

traditional DSC measurement, TMDSC can distinguish processes which might overlap in a standard DSC measurement.

TA Instruments Q1000 with standard aluminum pans is used. Temperature-modulated DSC (TMDSC) measurements were performed using the following procedure: sample was equilibrated at 100 °C, isothermal for 5 min to erase the thermal history, and then cooled to −160 °C at 3 °C/min with a modulation of ±1 °C/min, and then heated to 100 °C. The glass transition temperature (T_g) value was taken as the midpoint of the transition step in the heating process of the reversible heat flow signals. The glass transition temperature (T_g) can be estimated from both the transition process in reversible heat flow curves and the peak position in the derivative curves.

2.4 Broadband Dielectric Spectroscopy

Broadband dielectric spectroscopy is a useful tool to probe molecular dynamics on a wide range of time scales. Generally, in a dielectric measurement, a very small perturbation created by a sinusoidal external electric field is applied to the sample. The dipoles within the sample will try to align with the external field and then relax to a new equilibrium state. During this process, the neighboring dipoles, bonds or groups have to rearrange, in this way the dielectric spectroscopy probes different polarization processes, reflecting important properties of the materials. Properties like molecular relaxation can be determined in a broad temperature and frequency range by using dielectric spectroscopy. In this work, Broadband dielectric spectroscopy measurements are performed by using a Novocontrol Concept 80 system in the frequency range of 10^{-2} – 10^{7} Hz. The system has a ZGS active sample cell interface, an Alpha-A impedance analyzer, and a Quatro

Cryosystem unit for temperature control. Before measurement, the membrane samples are made as a circle with 8 mm diameter and placed between gold-plated electrodes. The system is quenched to -140 °C before the samples are placed into the cryostat to avoid the crystallization issues during the measurements. The experiments are performed from low temperature to high temperatures. Before the measurements, the sample is equilibrated at each temperature for 10–20 min. Detailed dielectric measurements analysis will be discussed in the next chapter.

2.5 Rheology

In order to determine cross-link density of membrane samples, small-amplitude oscillatory shear (SAOS) measurements of membrane samples are carried out on an AR2000ex rheometer (TA Instruments) with 4 mm plates parallel plate geometry. An environmental chamber with nitrogen as purge gas is used to control the test temperature. Prior to the measurement, the sample is purged for 3 h under a nitrogen atmosphere to achieve the equilibrium state. All the tests are performed at ambient temperature 298K with the frequency sweep from 0.01 to 100 Hz, where only the cross-link structure contribute to the obtained storage modulus. The cross-link densities of the membranes were calculated using the measured shear modulus,[132-134]

$$c_x = \frac{\rho}{2M_x} = \frac{G'}{2RT} \tag{2.4}$$

where c_x is the moles of cross-links per unit volume, ρ is the density of cross-linked polymer, M_x is the number-average molecular weight of the polymer segments between

cross-links, *G'* is the plateau value of real part of shear modulus, *R* is the gas constant, *T* is the temperature in Kelvin.

2.6 Density measurement

Density of the membrane samples could be determined by two methods: density-gradient column and by Archimedes Principle.

When using density-gradient column, the standard floats with density ranging from 0.95 g/cm^3 and 1.03 g/cm^3, and the accuracy to ± 0.0002 g/cm^3 are first added, and stay suspended in the column at the level where the density of reference floats is the same as that of the liquid. After the density floats reach stabilization status, the test membrane is added and allowed to descend to the different levels of the columns. A calibration chart is drawn to determine the densities of the membranes.

When using Archimedes Principle,[135] the density is calculated as follows:

$$\rho = \frac{M_A}{M_A - M_L}\rho_0 \tag{2.5}$$

where M_A is the film weight in air, and M_L is the film weight in the auxiliary liquid (methanol), and ρ_0 is the density of methanol at the temperature where the measurement was performed.

2.7 Fourier transform infrared spectroscopy (FTIR)

Fourier transform infrared spectroscopy (FTIR) of the polymer membranes was conducted in transmission mode using a Perkin-Elmer Frontier mid-infrared FT-IR instrument. A

minimum of 16 scans were signal-averaged with a resolution of 4 cm^{-1} to obtain the final spectrum. The background test is performed in air.

2.8 Thermogravimetric Analysis (TGA)

The thermal stability of the PEO-PDMSPNB membranes was examined using a TA Instruments Q-50 TGA. About 10 mg sample was placed in the platinum pan and equilibrated at room temperature. TGA measurements were conducted from room temperature to 800 °C under a nitrogen atmosphere at a rate of 20 K/min.

CHAPTER III

EFFECT OF CROSS-LINK DENSITY ON CARBON DIOXIDE SEPARATION IN POLYDIMETHYLSILOXANE-NORBORNENE MEMBRANES

Reproduced in part from "Effect of Cross-Link Density on Carbon Dioxide Separation in Polydimethylsiloxane-Norbornene Membranes" *ChemSusChem* 2015, 8, 3595 – 3604.

3.1 Introduction

The development of a new method based on a non-size sieving mechanism for gas separation could potentially offer a solution to the improvement of CO_2/N_2 separation efficiency. As a typical rubbery polymer at room temperature, polydimethylsiloxane (PDMS) is known to possess some of the highest permeabilities to various gases, e.g. the reported permeability is 3800 barrer for CO_2, 890 barrer for H_2, 400 barrer for N_2, *etc*.[86] It has drawn much attention also due to its good physical and mechanical properties (ductile), no aging issues, low cost, thermal stability and ease of processing.[76-85] For CO_2/N_2 separation, the reported selectivity of typical PDMS membranes is around 9.5.[86] If the CO_2/N_2 selectivity of those PDMS membranes can be improved while maintaining high permeability, the designed membrane would meet the practical target in efficiency and cost.[89] In PDMS-like rubbery polymer membranes, the liquid-like polymer matrix has poor size-sieving ability,[88] thus the overall selectivity is often determined by different gas solubilities in the membranes.[19, 86] If one compares various membranes made of PDMS polymer matrix, the gas solubilities should not be altered significantly, while diffusivity

can be tuned by controlling PDMS molecular architecture. One way to tune the gas diffusivity property of PDMS membranes is by introducing cross-linked networks. Many studies have been performed on cross-linked PDMS materials, due to their various applications in many fields.[136-143] The performance of cross-linked PDMS materials largely depends on the structure of the cross-linked networks and the residual end groups in the bulk material and interfaces. A previous study showed that increased cross-links in the PDMS network results in stronger elastic resistance and the diffusivity of a penetrant through the membrane decreases.[138] There has also been a previous study on cross-linked Matrimid membranes reporting the monotonous decrease of the permeability of different gas with the increase of cross-linking degree.[144] In some other cases, Lin *et al.* reported in their study of cross-linked poly (ethylene glycol diacrylate) (XLPEGDA) that gas permeability and solubility were independent of cross-link density.[145] Some papers even claimed an increase in gas permeability with the increase of cross-link density.[146] However, more comprehensive studies on the effect of the cross-link density for gas separation in rubbery polymers such as PDMS-based membranes are limited, and a better level of understanding is necessary for further development of gas separation membranes.

In this work, a facile membrane fabrication approach was applied for the preparation of PDMS-based membranes for CO_2 separation with a controlled degree of cross-linking. The room temperature chemical cross-linking reaction of (bicycloheptenyl) ethyl terminated polydimethylsiloxane (PDMSPNB) via ring-opening metathesis polymerization (ROMP) was developed by reacting PDMSPNB with Grubbs-II catalyst in a dichloromethane solution and drying under argon. The cross-link density was mainly controlled by the ratio

of PDMSPNB to Grubbs-II catalyst and was determined by rheological measurements. The use of difunctional PDMS macromonomers allowed for the preparation of free-standing films with much lower cross-link density than conventionally reported cross-linked PDMS membranes. Owing to the low cross-link density, the synthesized membranes provide very high permeability of CO_2 up to ~6800 Barrer with a good selectivity of CO_2/N_2~14 in single gas permeation measurements and show similar performance for mixed gas separation. The gas sorption, positron annihilation lifetime spectroscopy (PALS), and broadband dielectric spectroscopy (BDS) studies were carried out to provide a better understanding of the parameters controlling solubility and diffusivity.

3.2 Materials and methods

3.2.1 Materials

(Bicycloheptenyl) ethyl terminated polydimethylsiloxane (PDMSPNB) with an average molecular weight range from 12,000-16,000 g/mol was purchased from Gelest Inc. Sylgard® 184 silicone elastomer kit was obtained from Dow Corning. The Grubbs Catalyst, 2nd Generation (Grubbs-II) and anhydrous dichloromethane were purchased from Sigma-Aldrich. Nitrogen and carbon dioxide gas cylinders (99.99% purity) were obtained from Air Liquide. All materials were used as received.

3.2.2 Membrane synthesis

The scheme of the cross-linking reaction is shown in Scheme 3.1. The reaction was performed via ROMP of the norbornene groups on the telechelic position on PDMS.

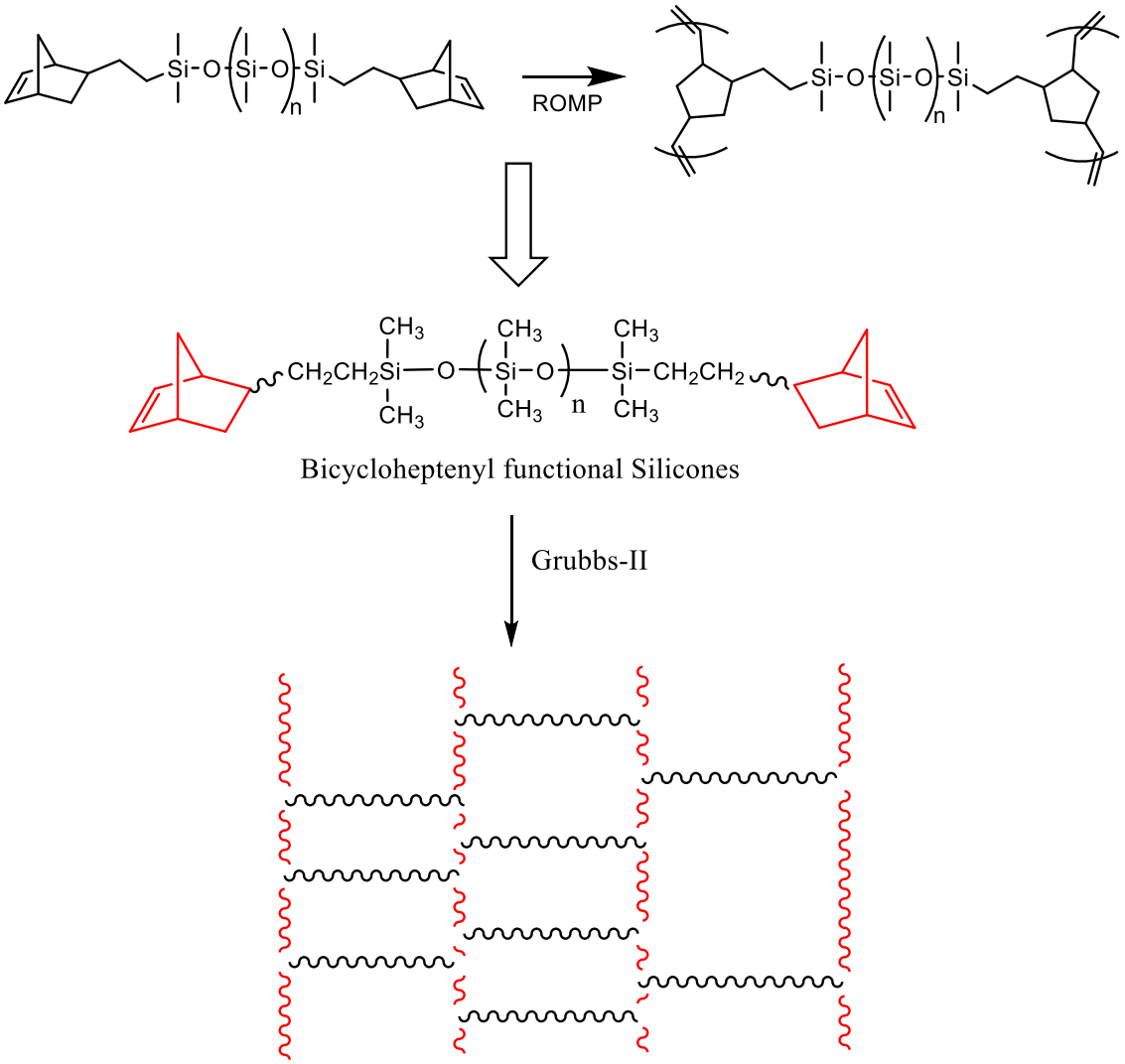

Scheme 3.1. Cross-linking reaction of PDMSPNB with different catalyst ratio.

In a typical experiment, PDMSPNB (0.515 g, 3.68×10^{-5} mol) was dissolved in DCM (6 mL) solution, while Grubbs-II catalyst (1.92 mg, 2.26×10^{-6} mol) was dissolved in DCM (2 mL) separately. Then 0.5 mL of 2 mL Grubbs-II stock solution was added to the PDMSPNB solution and the mixture was shaken for 60 seconds before poured into a 100 mL PTFE dish (with a diameter of 10 cm). The PTFE dish was then covered for 1 h and the *in-situ* cross-linked membrane was formed. A mixture of ethyl vinyl ether (2 mL) in DCM (6 mL) was added to the film to terminate the cross-linking reaction. The membrane was dried under argon atmosphere overnight and moved into a vacuum oven for three days to remove residual solvent completely. Finally, the cross-linked, free-standing polymer membrane was detached from the PTFE dish and cut into approximately 2 cm × 2 cm square membranes. The thickness of each membrane was determined using a micrometer. PDMSPNB/Grubbs-II molar ratios varied from 130/0.5 to 130/10 were used during the membrane casting process to control the cross-link density. All permeation measurements were performed within a similar time frame after curing.

A conventional cross-linked PDMS membrane was synthesized and characterized as a control experiment.[147] The membrane was fabricated by mixing the Sylgard® 184 silicone elastomer kit with the curing agent in a weight ratio of 10:1 using toluene as a solvent to dilute the mixture. The mixture was stirred for 15 min before casting onto a 10 cm × 10 cm glass plate. After 1 h curing at room temperature, the mixture was placed in an oven and heated for 3 h at 100 ˚C. It was then moved into the vacuum oven for three days at room temperature to remove residual solvent. Finally, the free-standing PDMS membrane was peeled off the glass substrate and cut for all the measurements carried out in this study.

3.2.3 Positron Annihilation Lifetime Spectroscopy (PALS)

Positron Annihilation Lifetime Spectroscopy (PALS) is widely used to analyze the free volume in the membrane structure.[148-150] Membranes with different cross-link densities were measured at room temperature, using a conventional sample-source-sample sandwich geometry.[151] The positron source was made from a ^{22}NaCl solution evaporated onto the surface of the samples. The stacked two identical membranes were wrapped by thin aluminum foil to generate a sample assembly. The 1.274 MeV gamma ray, indicating a positron emission event, and the 0.511 MeV annihilation gamma rays were detected using a fast scintillator (BaF_2), coupled with photomultiplier tubes (PMT). Different from the traditional experimental setup, a double-stop setup was employed in this work.[152, 153] Data were obtained using a digital oscilloscope with a system timing resolution of 158 ps.

3.3 Results

3.3.1 Cross-linked PDMSPNB with varied catalyst ratio

All membranes were formed *in-situ* via the cross-linking reaction of PDMSPNB with Grubbs-II catalyst in a PTFE dish. The as-prepared free-standing membranes showed a transparent, homogeneous and elastic nature with thickness ranging from 200-250 μm (Figure 3.1). With the change of PDMSPNB to Grubbs-II catalyst ratios, the membranes showed different ductility due to the difference in cross-link density. To elucidate the effect of the PDMSPNB to Grubbs-II catalyst molar ratio, the cross-link density was quantified by rheology using Eq. 2.3. The *G'* values as a function of polymer/catalyst ratio are shown in Figure 3.2 and summarized in Table 3.1.

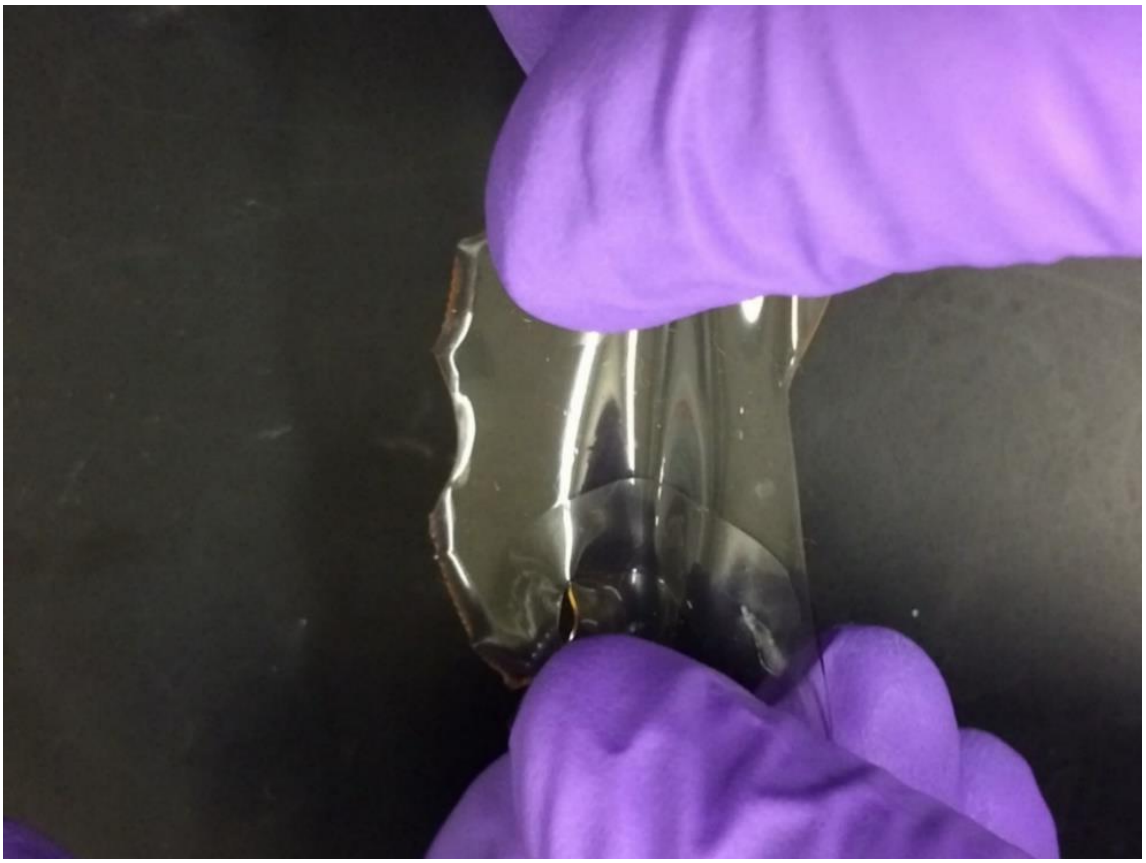

Figure 3.1 Picture of a cross-linked PDMSPNB membrane showing free-standing, transparent and mechanically strong properties.

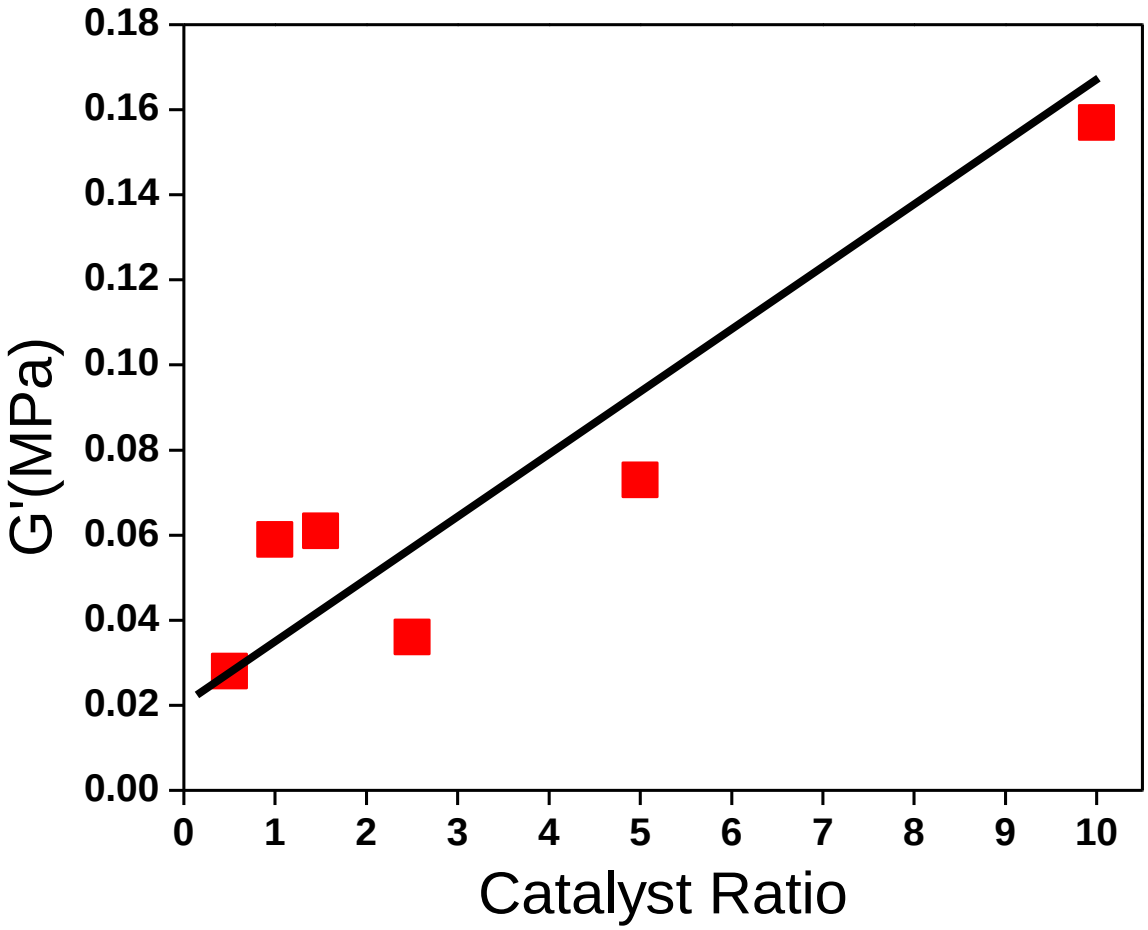

Figure 3.2 G' as a function of catalyst ratio for cross-linked PDMSPNB membranes. The line is present to guide the eye.

Table 3.1 Plateau value of *G'*, molecular weight between cross-links, cross-link density and glass transition temperature (T_g) as a function of different PDMSPNB/Grubbs-II ratios.

Sample code	PDMSPNB/Grubbs-II ratio	*G'* (MPa)	M_x (10^3 g/mol)	c_x (mol/cm^3) ×10^5	T_g (K)
A	130:0.5	0.028	86.0	0.57	148
B	130:2.5	0.036	67.1	0.73	148
C	130:1	0.059	41.2	1.19	148
D	130:1.5	0.061	39.0	1.23	148
E	130:5	0.073	33.3	1.47	148
F	130:10	0.157	15.5	3.17	148
-	PDMS	0.387	6.3	7.81	150

Density values for all the membranes including the conventional PDMS were obtained from density-gradient column measurements (0.9730 – 0.9881 g/cm^3) with an average value of 0.9800 g/cm^3 was applied for all the calculations of M_x (eq 2.3) and the cross-link density. The cross-link density of the conventional cross-linked PDMS membrane was also determined by rheology measurements and was calculated to be 7.81×10^{-5} mol/cm^3, which is consistent with previously reported values.[86]

3.3.2 Gas transport properties of cross-linked PDMSPNB membranes

Figure 3.3 shows a representative plot of the CO_2 and N_2 pressure rise, which are measured on the permeate side of the separation chamber in a single gas permeation test.

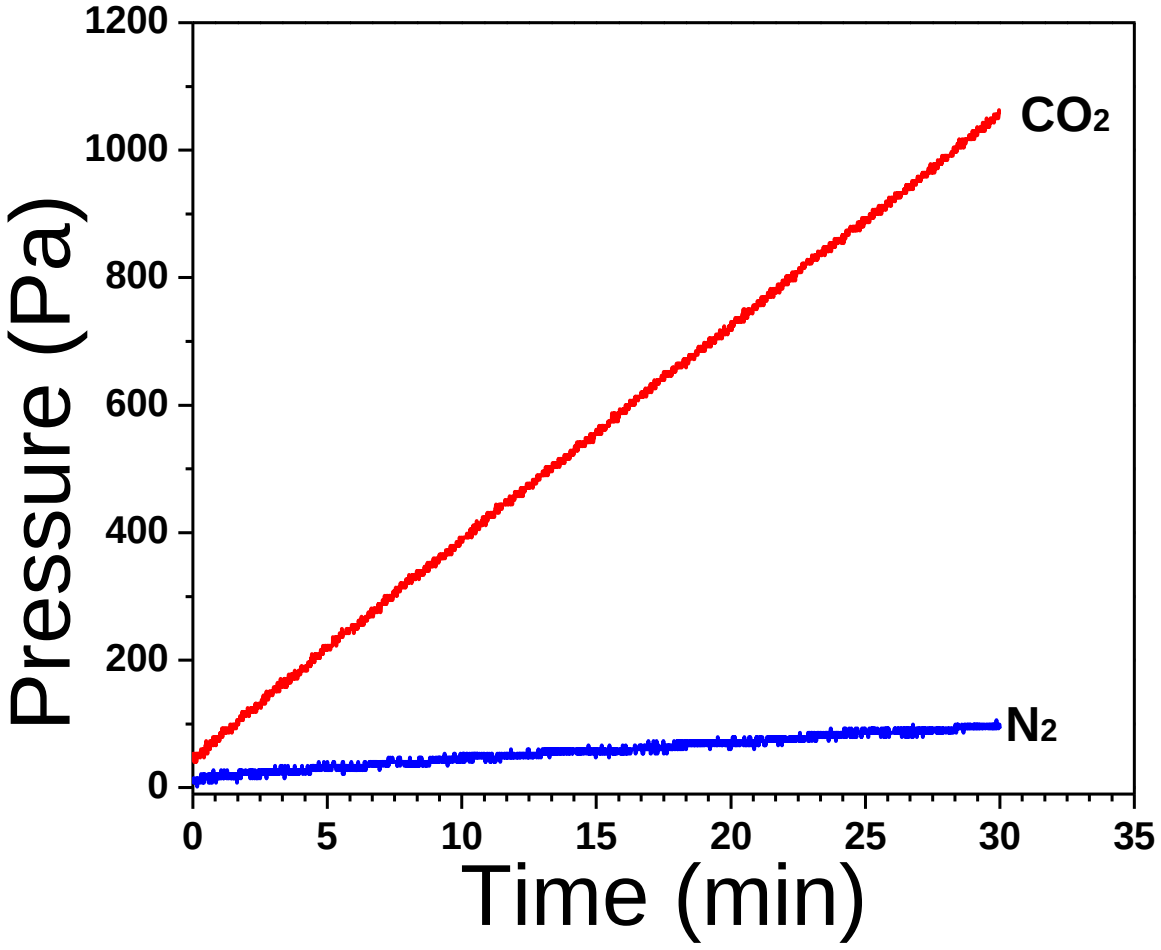

Figure 3.3 Pressure rise in the permeate chamber as CO_2 and N_2 diffuse through the PDMSPNB membrane with $c_x = 1.19\times10^{-5}$ mol/cm^3.

Single gas permeability values were calculated using the data collected in the linear regime according to equation 2.1. The selectivity was obtained by calculating the ratio of CO_2 permeability to N_2 permeability.

The permeability of each component in the gas mixture was calculated using equation 2.2. All single gas permeability and CO_2/N_2 selectivity data for PDMSPNB membranes with varied cross-link density as well as the conventional PDMS membrane are summarized in Figure 3.4 and Table 3.2. The mixed gas permeation data of sample C is included in Figure 3.5 and Table 3.2. The updated Robeson's upper bound for CO_2/N_2 with the cross-linked PDMSPNB in this study is shown in Figure 3.6. For comparison, the permeability and selectivity values of conventional cross-linked PDMS membrane is also included.

3.3.3 Gas sorption measurements

CO_2 mass uptakes for cross-linked PDMSPNB membranes with different cross-link densities and conventional cross-linked PDMS were measured (Figure 3.7). Due to the low absorption value, the change of mass was in the 0.15% to 0.20% (0.075 to 0.1 mg) range. The sorption isotherms were calculated from the mass uptake. From the sorption isotherms, the solubility of each membrane was obtained:

$$S \equiv C/p \tag{3.1}$$

where S is gas solubility, C is the sorption isotherm, p is the pressure.

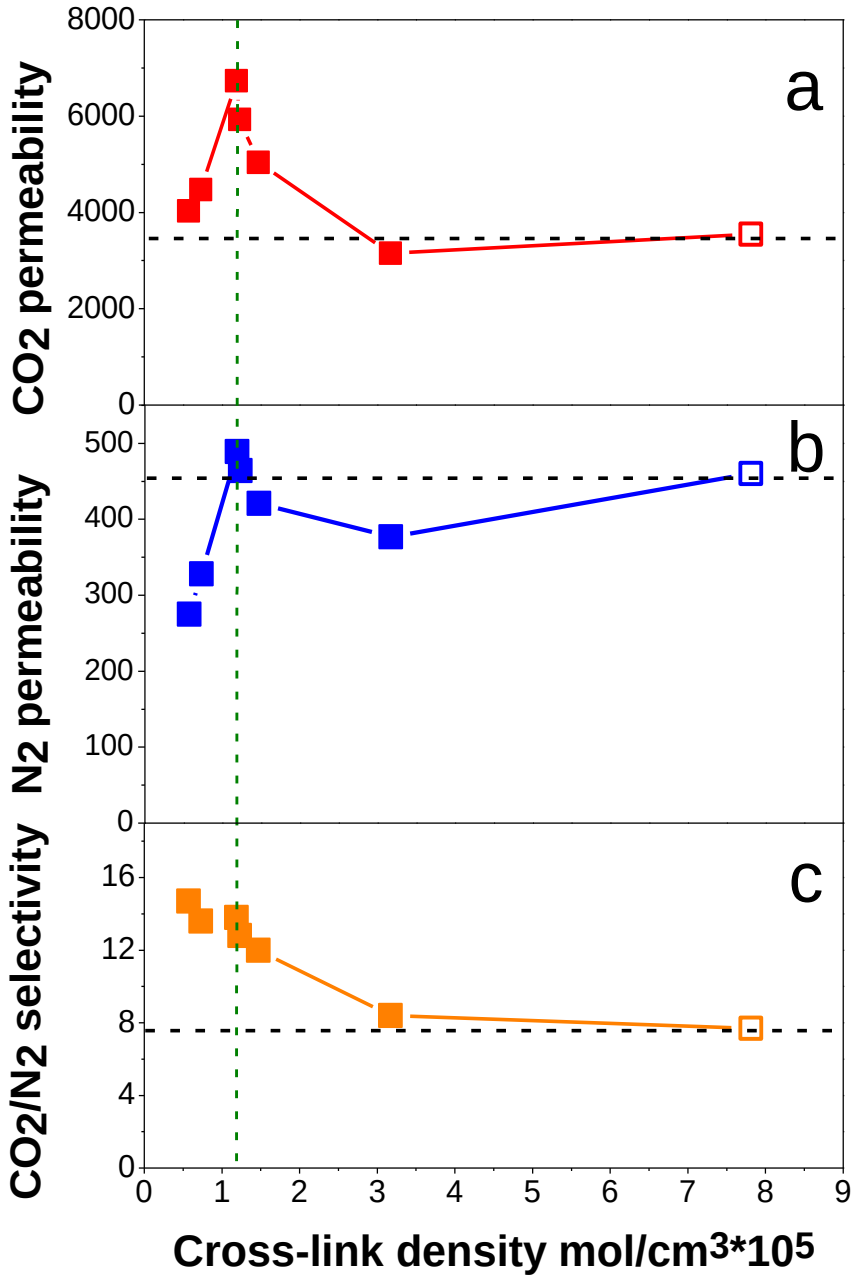

Figure 3.4 (a) CO_2 permeability (b) N_2 permeability and (c) CO_2/N_2 selectivity as a function of cross-link density for the cross-linked PDMSPNB membranes. Open squares represent the results of a conventional cross-linked PDMS membrane. Horizontal dashed lines represent the gas permeability and selectivity value for conventional cross-linked PDMS, vertical dashed lines mark the sample with highest CO_2 permeability.

Table 3.2 Summary of gas transport propoerties as a function of cross-link density.

Sample code	c_x(mol/cm^3) ×10^5	CO_2 Permeability (Barrer)	N_2 Permeability (Barrer)	CO_2/N_2 Selectivity
A	0.57	4030	275	14.7
B	0.73	4474	329	13.6
C	1.19	6734	489	13.8
D	1.23	5929	464	12.8
E	1.47	5040	422	12.0
F	3.17	3154	377	8.4
-	7.81 (PDMS)	3545	460	7.7
C-mixed gas	1.19	6343	434	14.6

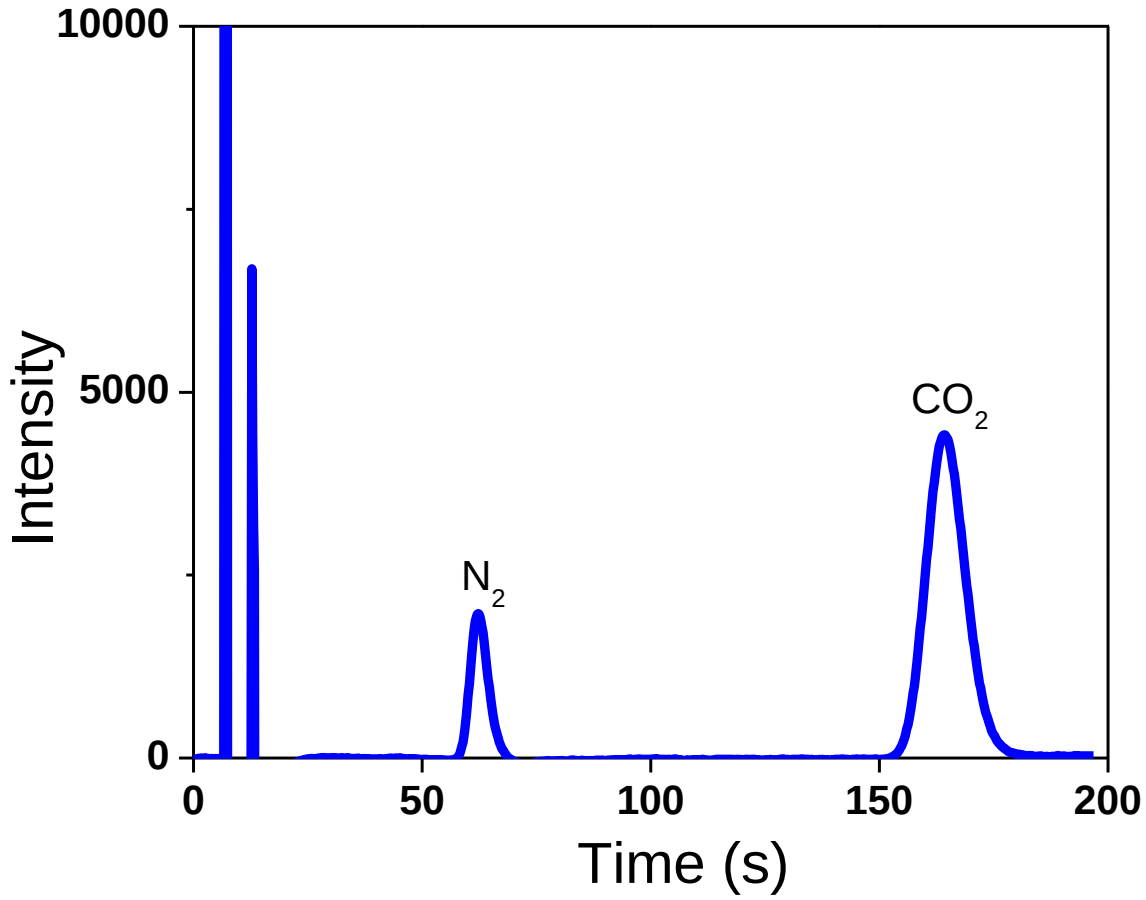

Figure 3.5 Mixed gas permeability data measured by gas chromatography (GC) in the permeate chamber as CO_2 and N_2 diffuse through the PDMSPNB membrane with $c_x = 1.19\times10^{-5}$ mol/cm^3. The sharp peaks before t=25s relate to the injection of the gas into the GC and can be ignored. The N_2 and CO_2 peaks are noted in the figure.

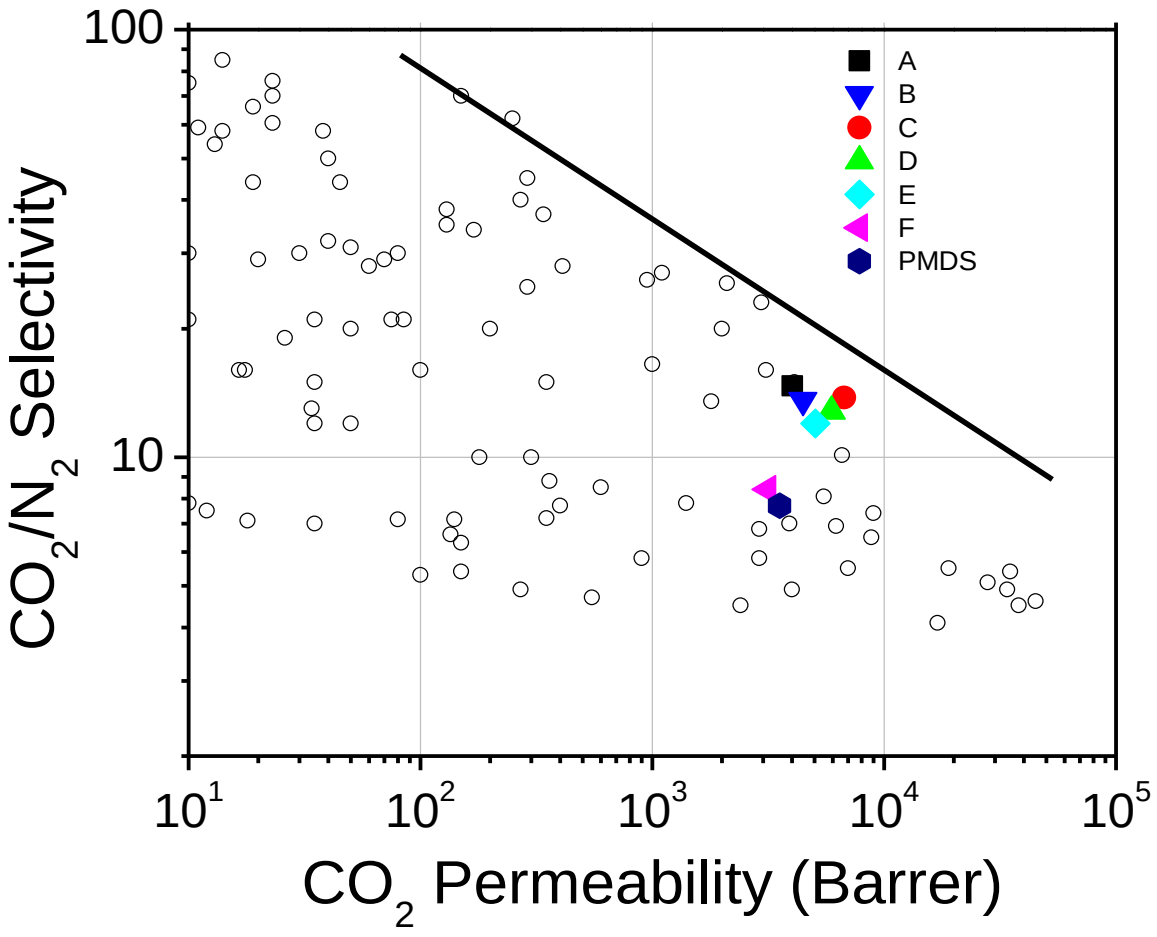

Figure 3.6 Summary of the cross-linked PDMSPNB and conventional PDMS membranes in Robeson plot.

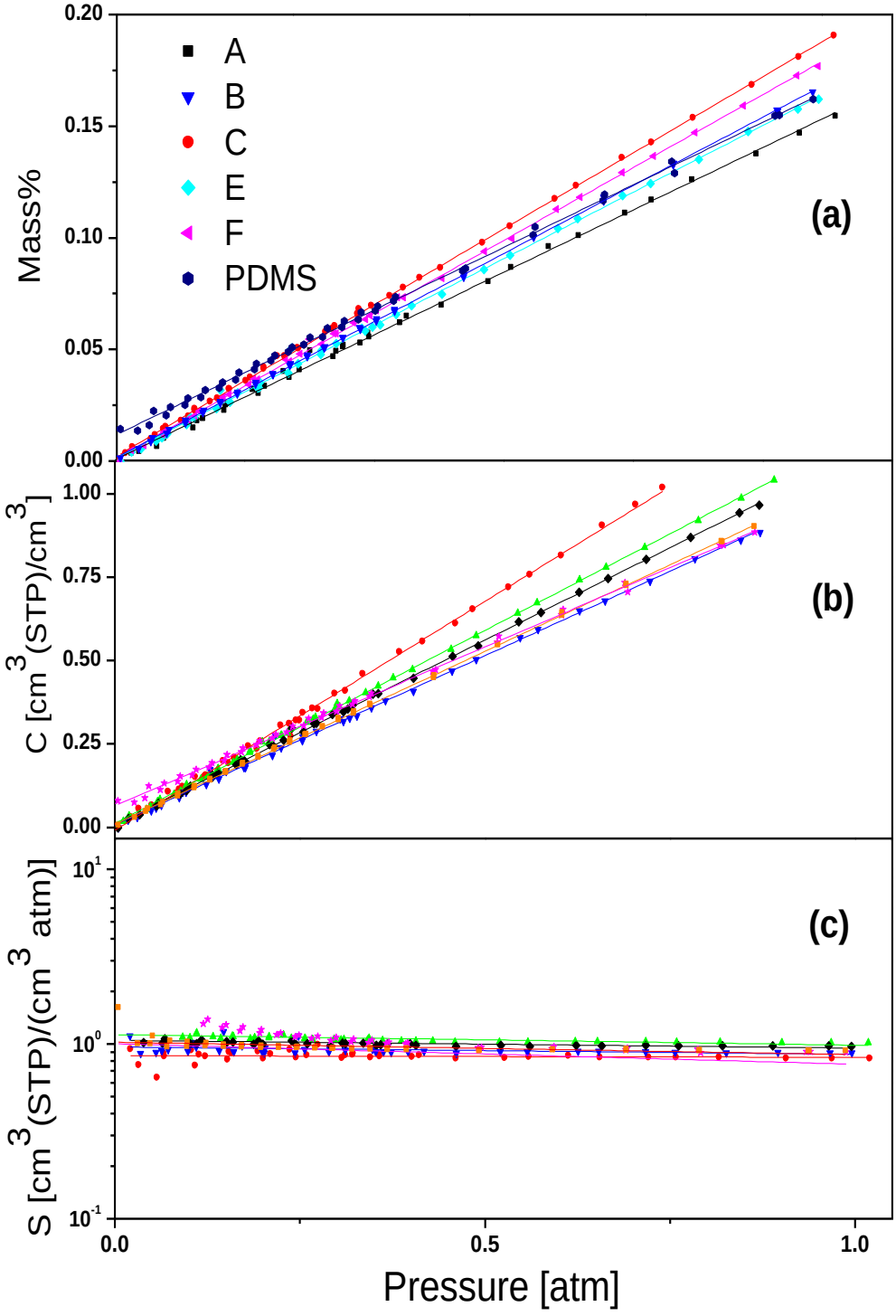

Figure 3.7(a) Mass uptake of CO_2 (b) Sorption isotherms and (c) CO_2 solubility in cross-linked PDMSPNB membranes.

It can be noted in Table 3.3 that the calculated CO_2 solubility showed very small differences as a function of cross-link density. When compared to the conventional cross-linked PDMS membrane, the solubility of the cross-linked PDMSPNB membranes showed a slight decrease.

3.3.4 PALS measurements

For rubbery polymeric membranes, we expect the diffusivity to be influenced by both the free volume and segmental dynamics. In order to study free volume effect, PALS measurements were carried out. Three separate positron lifetimes are commonly observed in polymers. The first lifetime (τ_1) indicates the positrons being annihilated in the bulk of the materials (< 200 ps). The second lifetime, τ_2, is attributed to the positrons being

Table 3.3 Summary of gas solubility and PALS results *versus* cross-link density.

c_x(mol/cm^3)× 10^5	S [cm^3(STP)/ cm^3.atm]	Average Positron lifetime (ns)	Pore diameter (nm)	Average trapping rate (ns^{-1})	Relative pore concentration
0.57	0.86 ± 0.030	2.647	0.676	1.9664	1.00
0.73	1.04 ± 0.053	2.751	0.691	2.6633	1.35
1.19	1.10 ± 0.012	2.537	0.659	2.3937	1.21
1.47	0.97 ± 0.035	2.511	0.655	3.0143	1.53
3.17	1.03 ± 0.011	2.431	0.643	2.6459	1.34
7.81 (PDMS)	1.25 ± 0.044	2.615	0.671	2.6794	1.36

annihilated in defects (300-500 ps). The third lifetime, τ_3, refers to ortho-positronium (o-Ps), a parallel spin complex of a positron and electron, which forms in low electron density regions of the polymer, such as free volumes, holes, interfaces, and pores. The o-Ps lifetime and intensity are often associated with the size and concentration of the open volume in a polymer, respectively. Therefore, the experimentally obtained positron lifetime was fitted by three exponential components. From the fitting procedure, one obtains positron lifetimes and intensities. The o-Ps lifetime, τ_3, is typically related to the average radius of a free volume element, r, which is assumed to be spherical, by Tao-Eldrup model.[154, 155]

$$\tau_3 = \frac{1}{2}\left(1 - \frac{r}{r+\Delta r} + \frac{1}{2\pi} sin\left[2\pi \frac{r}{r+\Delta r}\right]\right)^{-1} \tag{3.2}$$

Trapping model[156] is applied here to extract the average concentration of the free volume.

$$\begin{aligned} \kappa_2 &= \frac{I_2}{I_1}[I_3(\lambda_2 - \lambda_3) + (\lambda_1 - \lambda_2)] \\ \kappa_3 &= \frac{I_3}{I_1}[I_2(\lambda_3 - \lambda_2) + (\lambda_1 - \lambda_3)] \end{aligned} \tag{3.3}$$

where κ_2 and κ_3 are positron trapping rates in the defects and free volume, annihilation rate λ_i is equal to the reciprocal lifetime τ_i, λ_1 is the bulk annihilation rate, I_i are corresponding intensities and hence through the relation

$$\kappa_i = \mu_i C_i \tag{3.4}$$

where μ_i is the specific trapping coefficient for one trapping site, the trapping site density could be obtained. Assuming μ_3 is the same for all of the membranes considered in this

study, the concentration of free volume is proportional to the trapping rate calculated by Eq. 3.4.

Figure 3.8 represents the PALS data for six different membranes. It can be noticed that the positron lifetime did not show any significant changes with different cross-link density, which revealed a similar pore size inside the dense membranes to be around an average of 0.67 nm (Table 3.3). The trapping parameters did show some fluctuations within the range of study, which indicated some minor changes in the pore concentration.

3.3.5 Dynamics study by Broadband Dielectric Spectroscopy

Dynamics of the synthesized membranes were measured using broadband dielectric spectroscopy. Figure 3.9 shows the representative dielectric loss spectra and their fits at -114 °C.

Two Havriliak-Negami (HN) functions are used to describe the main relaxation process in the dielectric spectrum:

$$\varepsilon^*(\omega) = \varepsilon_\infty + \frac{\Delta\varepsilon_1}{[1 + (i\omega\tau_{HN1})^{\alpha_1}]^{\beta_1}} + \frac{\Delta\varepsilon_2}{[1 + (i\omega\tau_{HN2})^{\alpha_2}]^{\beta_2}} \quad (3.5)$$

where $\varepsilon^*(\omega)$ is the complex dielectric permittivity, $\varepsilon_\infty = \lim_{\omega\to\infty} \varepsilon'(\omega)$ is the value of $\varepsilon'(\omega)$ at infinite frequency, $\Delta\varepsilon$ is the dielectric relaxation strength, $\omega = 2\pi f$ is the angular frequency, τ_{HN} is the Havriliak-Negami relaxation time, α, β are the shape parameters.

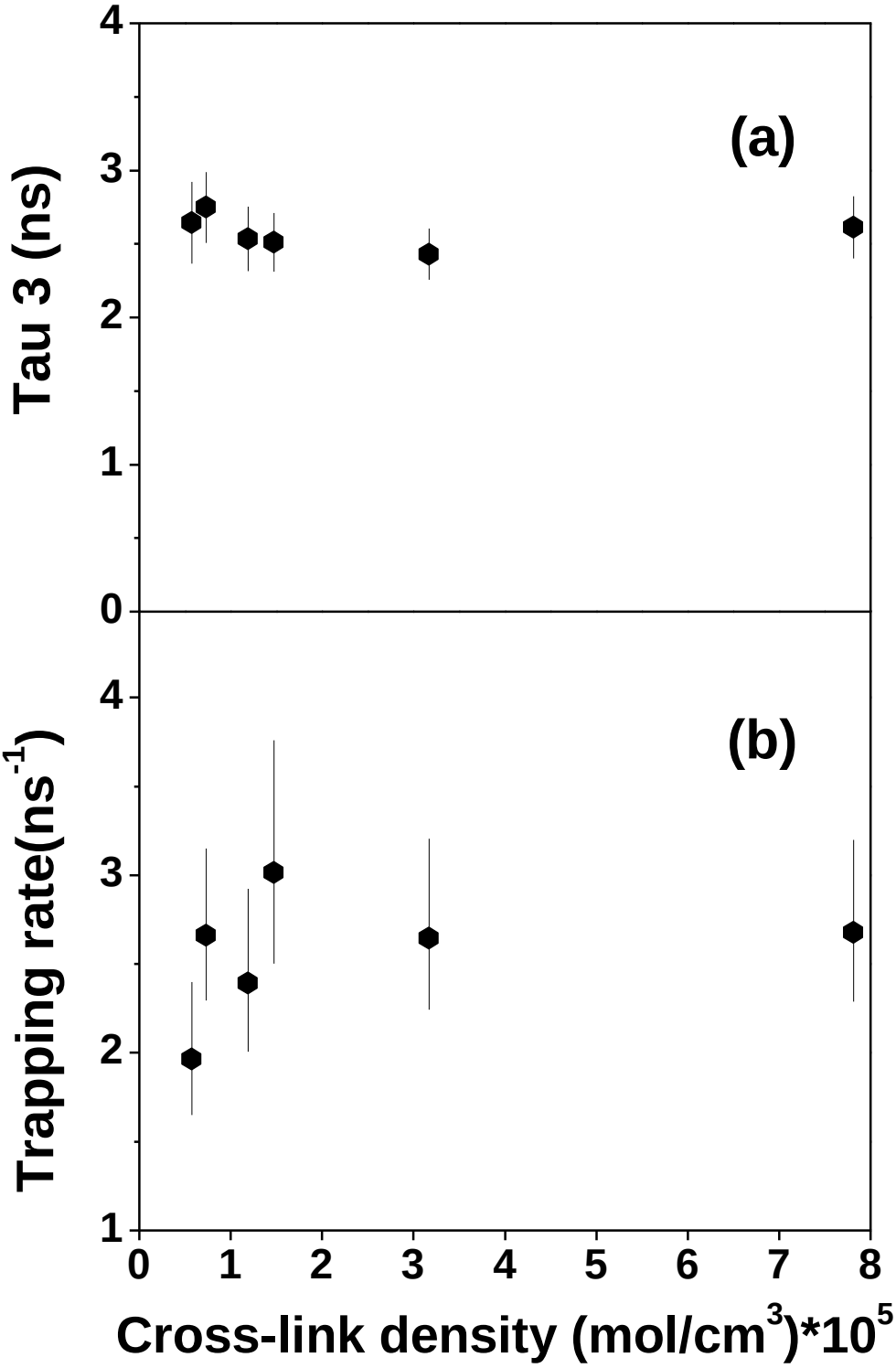

Figure 3.8 Influence of cross-link density on (a) τ_3 **and** (b) **trapping rate.**

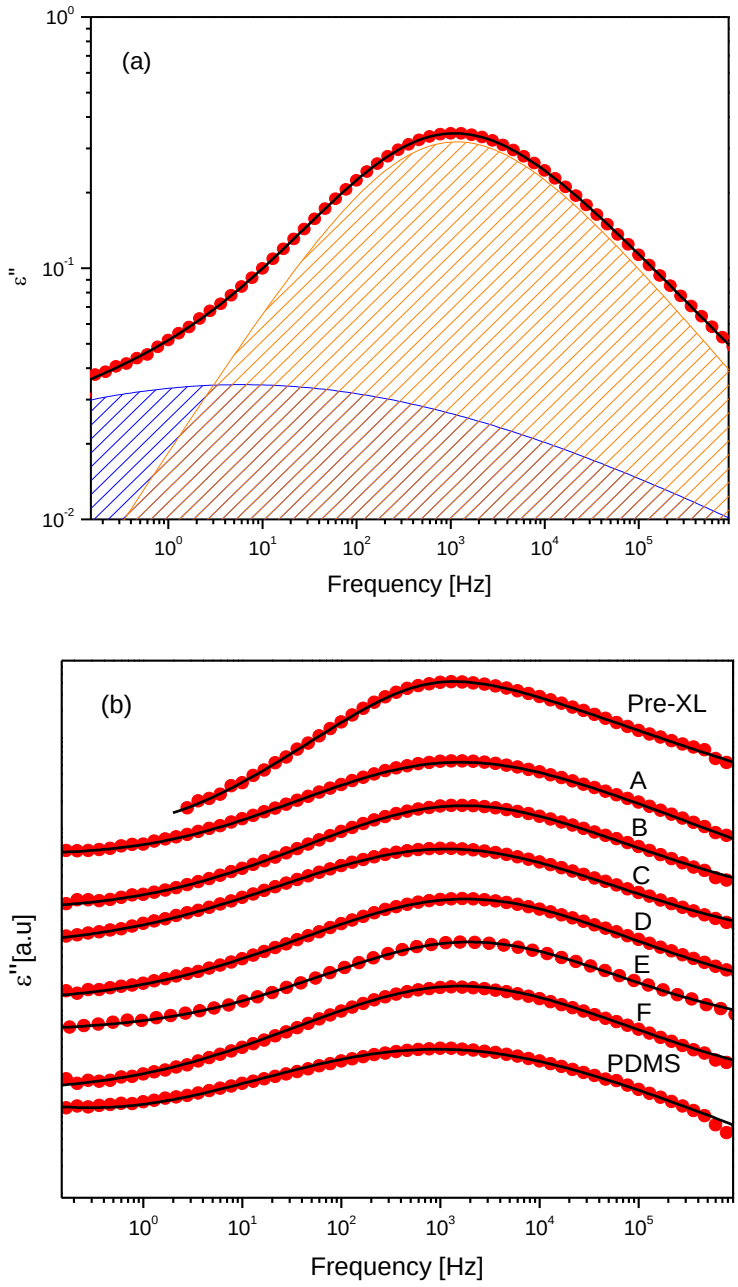

Figure 3.9(a) Dielectric loss spectra of sample C (c_x =1.19×10^{-5} mol/cm^3) at -114 °C (red solid symbols). Lines show the fit of the dielectric spectrum, and two relaxation processes are used (b) Dielectric loss peaks for the pre cross-linked PDMSPNB, PDMSPNB and conventional PDMS membranes at -114 °C. The peaks have been shifted vertically to illustrate the systematic change of the peak shape and position. The black curves show the fits to Havriliak-Negami function.

The frequency of the ε'' maximum is used to calculate the relaxation time (τ_{max}). The τ_{max} is related to the Havriliak-Negami relaxation time τ_{HN}, the shape parameters α and β by the following equation:

$$\tau_{max} = \tau_{HN}\left(sin\frac{\alpha\beta\pi}{2+2\beta}\right)^{1/\alpha}\left(sin\frac{\alpha\pi}{2+2\beta}\right)^{-1/\alpha} \quad (3.6)$$

The temperature dependence of the segmental relaxation time (higher frequency peak) of different samples determined from the Havriliak-Negami fitting function (Eq.3.5) is presented in Figure 3.10. The behavior is described by the well-known Vogel-Fulcher-Tammann (VFT) equation in the studied temperature range:

$$\tau = \tau_0 exp\left(\frac{B}{T-T_0}\right) \quad (3.7)$$

where τ_0 is the infinite temperature relaxation time, T_0 is the so-called VFT temperature, and B is a material specific parameter.

The dynamic glass transition temperature (T_g) is usually defined at the temperature where the segmental relaxation time τ = 100 s. By extrapolating the VFT curves to τ = 100 s, a glass transition temperature can be estimated. The calculated T_g of all samples are shown in Table 3.1.

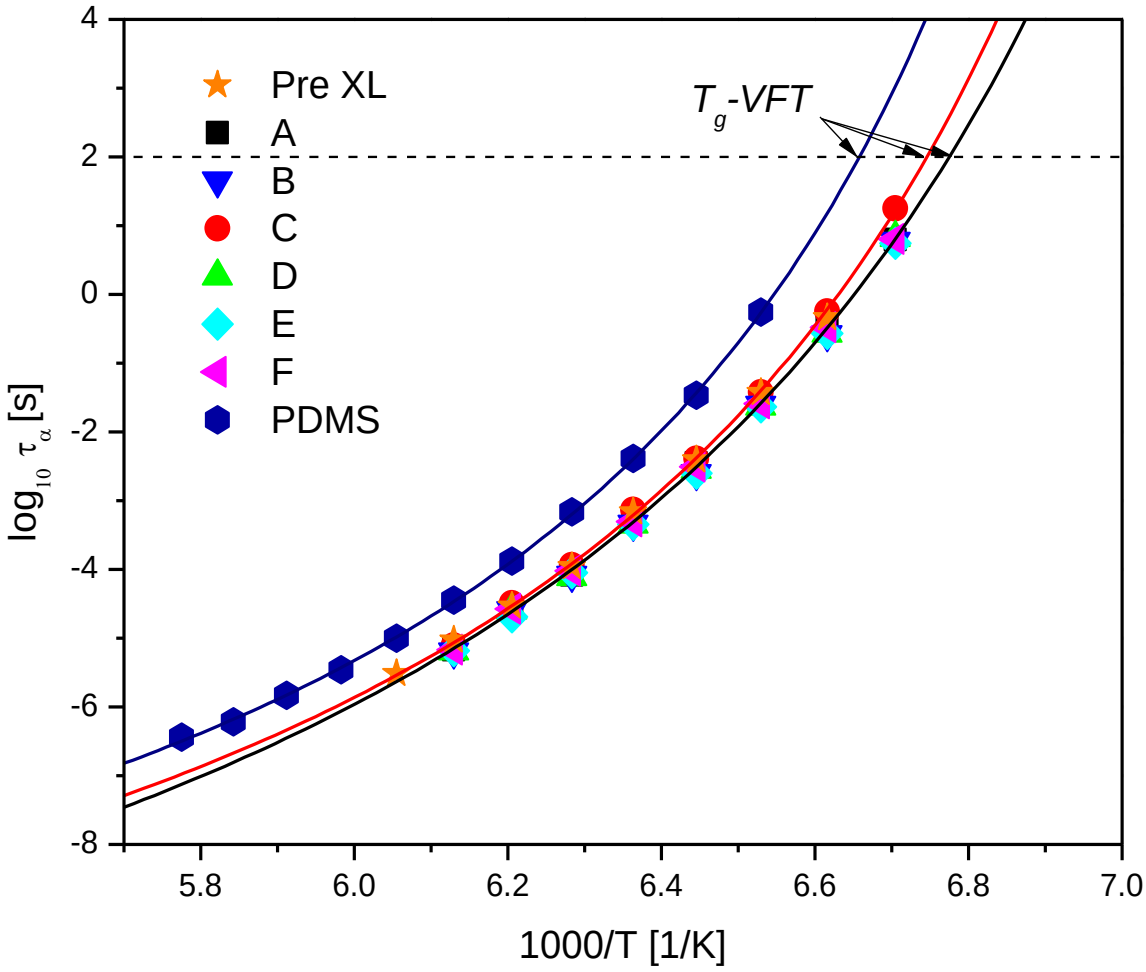

Figure 3.10 Temperature dependence of segmental relaxation time measured by broadband dielectric spectroscopy for different samples. Solid lines were fit to the VFT equation. The glass transition temperature (T_g) was determined by VFT extrapolation of the segmental relaxation time to $\tau_\alpha = 100s$ ($log_{10}\ \tau_\alpha = 2$).

3.4 Discussion

3.4.1 Effect of catalyst ratio on cross-link density

As shown in Figure 3.2 and Table 3.1, the *G'* values generally increase with the higher catalyst ratio, while the calculated M_x values show a decreasing trend. In case of a linear polymer with monofunctionality, the amount of catalyst controls the resulting molecular weight; however, for the difunctional PDMSPNB, the catalyst ratio should control the cross-link density as well as the reaction kinetics. From the rheology data, a higher catalyst ratio resulted in a stronger shear response, because the higher catalyst ratio increased the numbers of cross-link junctions in the membrane, thereby generating shorter average chain lengths between cross-links. It is also worth mentioning that the cross-link density in the PDMSPNB membranes is controlled by multiple factors. The catalyst ratio is a dominant factor but the reaction kinetics during *in-situ* membrane formation could also influence the cross-link density. However, due to the fast reaction rate, it is difficult to kinetically control the formation of cross-link networks within the time range demonstrated in this study. The deviation of the trend for G' vs. catalyst ratio in Figure 3.2 is likely due to a combination of variation of reaction kinetics and other possible factors.

3.4.2 Gas transport properties of cross-linked PDMSPNB membranes

The slopes of the CO_2 and N_2 permeabilities in Figure 3.3 clearly show much higher CO_2 permeability than that of N_2. As seen in Figure 3.4(a) and 3.3(b), for cross-linked PDMSPNB membranes, the permeability of both the CO_2 and N_2 showed an increasing trend with the initial increase of cross-link density, and then permeability reaches a

maximum (c_x =1.19×10^{-5} mol/cm^3) and decreases with farther increase in cross-link density. The permeation of CO_2 and N_2 of the cross-link density 1.19×10^{-5} (mol/cm^3) showed the highest flux than any other membranes in this study. From the Robeson plot (Figure 3.6), the cross-linked PDMSPNB membrane achieved much better CO_2/N_2 separation property than the majority of polymers.[4, 157] The mixed gas permeation measurements of sample C showed very comparable results to that of single gas measurements (Table 3.2), which suggests that the PDMSPNB membranes perform similarly well in a mixed gas permeation, which is more relevant to real industrial circumstances.

Compared to conventional cross-linked PDMS, the cross-linked PDMSPNB membrane show higher permeability and higher selectivity, and the performance is very close to the Robeson upper bound. The conventional cross-linked PDMS utilizes short chains of PDMS as precursor and requires high cross-link density to make it a free-standing film. The use of difunctional macromonomer PDMSPNB in this work allowed us to prepare free-standing films with much lower cross-link density. This membrane fabrication approach to prepare cross-linked membranes has revealed that tuning cross-link densities of PDMSPNB using these macromonomers can improve the performance of CO_2/N_2 separation significantly. Our best performance membrane with cross-link density 1.19×10^{-5} (mol/cm^3) is approximately a factor of two improvement in CO_2 permeability and CO_2/N_2 selectivity over the well-studied conventional cross-linked PDMS. The excellent permeability and good selectivity of the cross-linked PDMSPNB membranes provides a promising perspective (Figure 3.4 and 3.6) for future development of membranes for CO_2

separation. However, a deeper understanding of the physical and chemical mechanism behind the outstanding gas separation property is also crucial. To elucidate how cross-links affect the solubility and diffusivity, the study of CO_2 solubility and free volume were carried out.

3.4.3 Influence of gas solubility and free volume

As described in the Introduction, researchers reported different trends of gas permeability change with the change of cross-link density. However, for our rubbery cross-linked membranes, the permeability does not follow a monotonous trend. We expected the change in gas permeability to be a combined effect of many factors. From the CO_2 solubility measurements, all the tested cross-linked PDMS membranes are similar within the range of uncertainty (Table 3.3), which indicates that the solubility did not play a key role in the enhancement of permeability and selectivity for the PDMSPNB membranes. The N_2 solubility of the PDMSPNB membranes was lower than the measurable limit of the device and could not be measured.

The PALS measurements show that the pore size of the PDMS was similar to that of PDMSPNB membranes (Table 3.3), indicating that the difference of the cross-link density did not influence much the pore size, which is within our expectation due to the use of the same polymer matrix. With the increase of cross-link density, the concentration of pores shows fluctuations, which could be interpreted as the small changes in the total free volume. However, due to the relatively large error bar, the fluctuations still lie well within the range of uncertainty for these measurements.

3.4.4 Effect of dynamics on gas permeability

Dielectric loss peaks in Figure 3.9 shows that the α-relaxation of all the cross-linked samples broadened at the low frequency side compared to that of the pre cross-link sample. Similar results were reported for cross-linked PDMS networks [158] and other polymers.[159] The authors ascribed the broadening of the peaks to the slowing down of segments in the proximity to the cross-link junction. For our end cross-linked PDMSPNB membranes, the mobility of the segments near the end junctions are expected to be restricted, which could explain the broadening of the peak at lower frequencies. It can also be noticed that the peak position of the conventional cross-linked PDMS membrane, which has much higher cross-link density than those of the PDMSPNB membranes, was shifted around one order in frequency. This indicates approximately ten times faster segmental motion in our membranes relative to conventional cross-linked PDMS at the studied (by dielectric spectroscopy) temperatures. However, our PDMSPNB membranes were only slightly cross-linked, i.e. the concentration of junctions was very small. Thus, compared to pre-XL sample, no apparent shift of the peak position to lower frequencies was observed. The pre-XL and cross-linked PDMSPNB samples did not show any changes in T_g (Table 3.1), indicating that although some segmental motions in cross-linked PDMSPNB samples were restricted, the influence on average segmental relaxation time was not significant. However, the cross-linked PDMSPNB did show faster dynamics than the conventional cross-linked PDMS membranes, which in part, might explain the significant increase in gas permeability between these two types of membranes. To relate quantitatively the observed increase in gas diffusivity to change in segmental dynamics,

measuring the dynamics at the same ambient temperature would be ideal, while unfortunately PDMS segmental dynamics at T=298 K is too fast for our spectrometer. Despite the difference of the measured temperature range, this dynamic study indicates that the most significant enhancement of CO_2 separation of PDMSPNB over conventional cross-linked PDMS should be ascribed to the much faster segmental dynamics despite their similar free volume.

3.5 Conclusion

A facile room temperature cross-linking reaction of PDMSPNB membranes was developed via *in-situ* ROMP. The resulting free-standing films were ductile and flexible, and could be readily fabricated to different shapes and coatings. Our membrane fabrication approach to preparing cross-linked PDMS has revealed that tuning cross-link densities of PDMS membranes using these macromonomers can improve CO_2/N_2 separation significantly. The novel cross-linked PDMSPNB membranes achieved excellent CO_2 permeability with good selectivity (a factor of two improvement in CO_2 permeability and CO_2/N_2 selectivity over the well-studied conventional cross-linked PDMS), and their performance is very close to the Robeson upper bound line. The unprecedented performance by a careful design of the macromolecular architecture and cross-link mechanism has revealed the strong potential of the rubbery polymer, PDMS, for gas separation. This finding can open up a new approach to enhance performance for gas separation and could elucidate additional factors for the gas separation mechanisms in rubbery polymers. To the best of our knowledge, this study is the first report to identify that lightly cross-linked PDMS membranes synthesized by difunctional PDMS

macromonomers enhance both CO_2 permeability and CO_2/N_2 selectivity. Moreover, from an industrial viewpoint, according to Merkel *et al.*'s study,[89] the cross-linked PDMSPNB membrane could offer the permeance of ~ 6,300 gpu if 1 μm membranes could be cast and coated on the gas separation media. This should allow reduction of CO_2 capture cost to less than $20 per ton. Although the complete quantitative level of understanding of the obtained results has not yet been achieved, we could ascribe the key factor to the faster segmental dynamics in our membranes and probably improved solubility selectivity. Our next goal is to incorporate CO_2-philic groups into the PDMSPNB matrix, to achieve a better selectivity without significant loss in permeability. These findings will contribute to the fundamental understanding of gas transport through polymer membranes, with potentially broad applications.

CHAPTER IV

IMPACT OF AMIDOXIME FUNCTIONALITY IN RUBBERY AND GLASSY POLYMERIC MEMBRANES FOR CARBON DIOXIDE SEPARATION

Reproduced in part from "Impact of tuning CO_2-philicity in polydimethylsiloxane-based membranes for carbon dioxide separation" *Journal of Membrane Science* 2017, 530, 213 – 219.

Reproduced in part from "Gas separation mechanism of CO_2 selective Amidoxime-poly(1-trimethylsilyl-1-propyne) membranes" *Polymer Chem*istry 2017,8, 3341-3350.

4.1 Introduction

In Chapter 3, we demonstrated the cross-linked PDMSPNB matrix with excellent CO_2 permeability and decent CO_2/N_2 selectivity. However, the gas separation performance has still not achieved Robeson upper bound. The major drawback of PDMS-based membranes is their relatively low CO_2/N_2 selectivity.[64, 160] In order to obtain high-performing materials to meet the required performance for practical deployment, the selectivity of PDMSPNB membranes needs to be further improved.

A common approach to improve gas selectivity is to enhance diffusivity selectivity by tuning the pore size, thereby increasing the membrane's size-sieving capability.[11-14] However, this method is not sufficient for CO_2/N_2 separations due to the similar kinetic diameters of CO_2 and N_2 (CO_2~3.30 Å, N_2~ 3.64 Å). Another approach, to which less attention has been paid, is to enhance solubility selectivity.[19, 20] For instance, a number of

studies on Pebax membranes, which exhibits high CO_2 solubility due to the strong affinity of the polar ether linkages in the structure, have demonstrated the potential of enhancing CO_2 solubility in order to improve the CO_2 separation performance.[21-25] Thus, our strategy focuses on the incorporation of CO_2-philic groups into the polymer matrix, thereby tuning the CO_2/N_2 solubility selectivity. Among the various CO_2-philic groups that have been reported,[28-33, 114, 161-163] we choose to evaluate the incorporation of amidoximes (AO) within PDMS matrix for CO_2 separation.[30]

Moreover, in this chapter, another polymer matrix is also discussed. Most study in this dissertation focuses on the development of rubbery, high permeable PDMS-based membranes. However, in the membrane gas separation field, glassy membranes also play an important role. For instance, poly(1-trimethylsilyl-1-propyne) (PTMSP),[157] polymers of intrinsic microporosity (PIMs), [15-17] thermally rearranged (TR) polymers, [12, 13, 18] etc., are well-known high-performing glassy materials. Among them, PTMSP is known to be one of the most permeable polymer (CO_2 permeability~ 29,000 Barrer) which owns orders of magnitude higher permeability than other polymers. The high permeability is attributed to the exceptionally large free volume and large intersegmental gaps in the polymer matrix.[164] However, the rather low gas selectivity is one of the major drawbacks that limits its deployment in various applications.

Researchers have reported the enhancement of CO_2 selectivity by introducing CO_2-philic groups in glassy systems. Du *et al.* reported the successful incorporation of tetrazole(TZ) groups into the highly-permeable PIM-1 polymer,[28] and the CO_2/N_2 selectivity showed a factor of 2 improvement and reached ~30, Later, thioamide-PIM-1[113], AO-PIM-1[165],

PIMCO1-CO15-50[166], Carboxylated[167, 168], *etc*. were also reported to significantly enhance CO_2/N_2 permeability.

Moreover, much research has been reported to modify PTMSP to obtain enhanced gas separation performance. Freeman *et al.* reported highly-loaded titanium oxide (TiO_2) nanoparticle-filled PTMSP that showed higher light gas permeability than neat PTMSP.[169] Hill *et al.* studied that addition of fumed silica nanoparticle (FS) to PTMSP matrix facilitates the diffusion of CH_4 significantly (~180% higher than that of untreated polymer).[170] However, the gas solubility in these composite membrane was unaffected by the addition of nanoparticles. Moreover, Buhr *et al.* investigated the gas transport properties of poly(1-trimethylsilyl-1-propyne)-*block*-poly(4-methyl-2-pentyne) (PTMSP-*b*-PMP) block copolymers. They showed rather high permeability (1100 Barrer for CH_4, 20000 Barrer for C_4H_{10}).[171] PTMSP grafted PDMS also showed enhanced permselectivity of ethanol.[172] However, few research groups have conducted studies on tuning the CO_2-philicity of PTMSP matrix.

Herein, we introduce an efficient method to prepare novel AO-PDMSPNB and AO-PTMSP membranes for CO_2/N_2 separation. The synthesized membranes exhibit a systematic increase in CO_2/N_2 selectivity and improved overall performance in CO_2/N_2 separation comparing with that of neat PDMSPNB and PTMSP membranes. The separation performance of the best membranes has achieved above/on the Robeson upper bound. Key parameters for tuning the gas transport properties are discussed based on calculated CO_2-AO complex binding energies, CO_2 sorption measurements and fractional free volume (FFV) estimations.

4.2 Materials and methods

4.2.1 Materials

(Bicycloheptenyl)ethyl terminated polydimethylsiloxanes (PDMSNB) with weight-average molecular weights ranging from 12,000-16,000 g/mol were purchased from Gelest Inc. Grubbs catalyst, 2nd generation (Grubbs-II), dicyclopentadiene, fumaronitrile, hydroxylamine solution (50 wt. % aqueous solution) and anhydrous dichloromethane (DCM) were purchased from Sigma-Aldrich. Nitrogen and carbon dioxide gases (99.99% purity) were obtained from Air Liquide. All chemicals were used as received. All ^{1}H and ^{13}C NMR spectra were collected using a Bruker ADVANCE III spectrometer operating at 400 MHz for ^{1}H and 100 MHz for ^{13}C. Chemical shifts are reported in ppm downfield from tetramethylsilane. $CDCl_3$ was used as the solvent for all NMR samples. Elemental analyses were performed by Galbraith Laboratories, Inc.

4.2.2 Synthesis of bicyclo[2.2.1]hept-5-ene-2,3 dicarbonitrile (dicyanonorbornene, diCyNb)

Dicyclopentadiene (7.2 g, 54.4 mmol) and fumaronitrile (9.3 g, 108.8 mmol, 2.2 equiv.) were added to a 300 mL round bottom flask with stir bar. The mixture was heated at 190 °C under an inert atmosphere. After 48 h, the product-diCyNb (5.30 g, 72% approx. yield) was isolated from the product mixture by distillation. ^{1} H NMR (400 MH_Z, $CDCl_3$): δ= 6.18 (m, 2H, -C<u>H</u>=C<u>H</u>-); 3.23-3.20 (m, 2H, -C<u>H</u>-CN); 3.07(t, 1H, $^{3}J_{23}$ = 7.9, =CH-C<u>H</u><); 2.38 (m, 1H, =CH-C<u>H</u><); 1.44-1.54 (m, 2H, >C<u>H_2</u>). ^{13}C NMR (100 MH_Z, $CDCl_3$): δ=136.55 (-

CH=CH-); 134.70 (-CH=CH-); 119.45 (-CH-CN); 119.07 (-CH-CN); 47.44 (=CH-CH<); 46.30(=CH-CH<); 45.46(>CH_2); 33.64 (-CH-CN); 33.41 (-CH-CN).

4.2.3 PDMSPNB-co-PdiCyNb precursor synthesis and post-modification

The precursor membranes were synthesized *via* the *in-situ* ring-opening metathesis polymerization (ROMP) of PDMSNB and dicyanonorbornene (diCyNb) (Scheme 4.1). In a typical process, PDMSNB (375 mg, 2.68×10^{-5} mol) and diCyNb (125 mg, 8.68×10^{-4} mol) were dissolved in DCM (6 mL). In a separate vial, Grubbs-II catalyst (10 mg, 1.18×10^{-5} mol) was dissolved in DCM (2 mL). Then 1 mL of the Grubbs-II catalyst stock solution was added to the monomer solution and shaken for 60 s before being poured into a 100 mL PTFE dish (with a diameter of 10 cm). The PTFE dish was covered with aluminum foil for 72 h in which the *in-situ* cross-linked membrane was formed. A mixture of ethyl vinyl ether (2 mL) in DCM (6 mL) was added to the film to terminate the metathesis reaction. The membrane was dried under argon atmosphere overnight and moved to a vacuum oven for 3 days to remove residual solvent. Finally, the cross-linked free-standing polymer membrane was detached from the PTFE dish and cut into pieces for further functionalization or testing.

The PDMSPNB-*co*-PdiCyNb membranes were synthesized with varying feed compositions of diCyNb ranging from 10 to 30 wt%. No uniform membranes with diCyNb feed contents higher than 30 wt% were successfully made due to the heterogeneity between two components in PDMSPNB-*co*-PdiCyNb. From elemental analysis results, the ratio of diCyNb:PDMSNB incorporated in the copolymer membrane was lower than the feed ratio. For example, at 25 wt% feed contents only produced about 17 wt% composition.

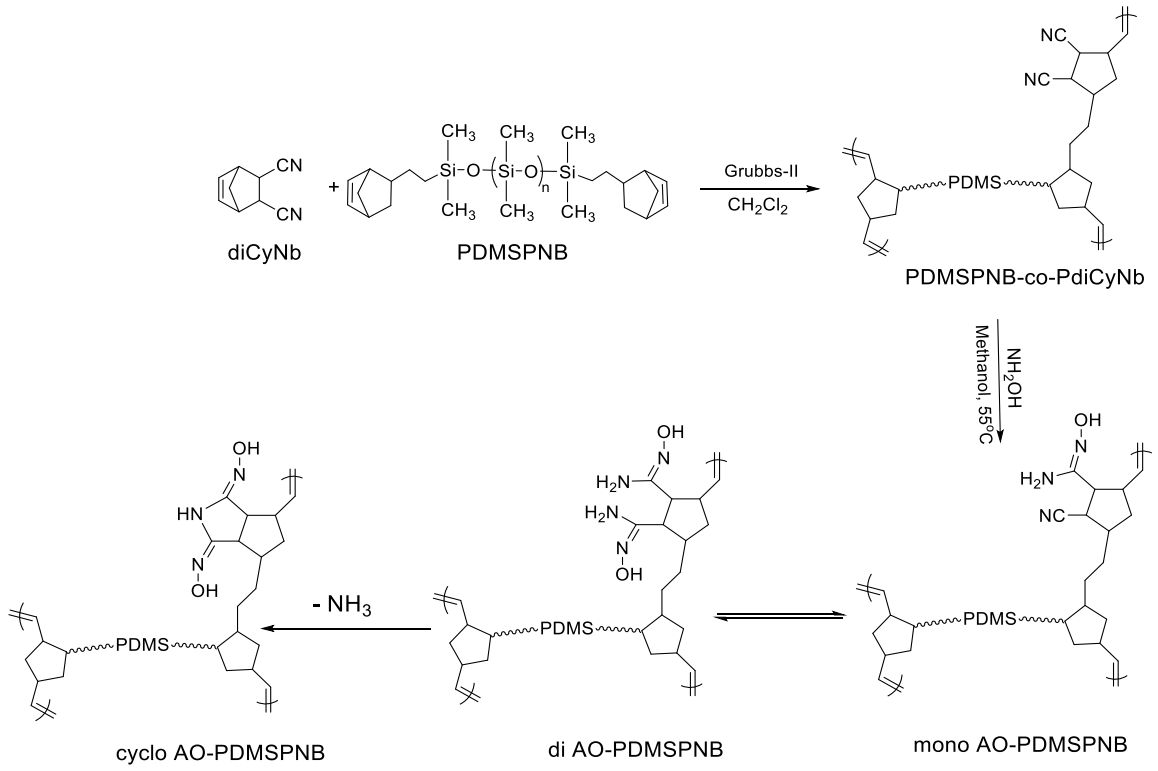

Scheme 4.1. ROMP reaction of the diCyNb-PDMSPNB membrane and post-modification.

The gas permeability of PDMSPNB-*co*-PdiCyNb membranes were tested and the CO_2/N_2 selectivity was calculated. Due to the optimum balance of CO_2 permeability and CO_2/N_2 selectivity obtained in the permeation data of PDMSPNB-*co*-PdiCyNb membranes, the precursor with 25 wt% feed of diCyNb was selected for use in further experiments.

Each batch of amidoxime-PDMSPNB membranes were functionalized from one specific PDMSPNB-*co*-PdiCyNb membrane, which was cut into small pieces and treated for amidoximation. In a typical amidoximation experiment, 0.1g of cross-linked PDMSPNB-*co*-PdiCyNb membrane was added to methanol (10 mL), followed by the addition of hydroxylamine solution (0.12g, 1.82 mmol, 3 equiv). The mixture was placed in a 56 °C oil bath. A control experiment using only methanol but without hydroxylamine was also performed and the results showed no CN group conversion and extended cross-link density (Figure 4.1). By varying the amidoximation time from 6 h to 48 h, membranes with varied amidoximation extent were obtained. The membranes were then washed with methanol and DI water several times and dried in a vacuum oven for another 3 days at room temperature. The thickness of the membranes ranged from 100-130 μm. The density of all the membranes were obtained from density-gradient column measurements (0.9780-0.9840 g/cm^3) and the estimated fractional free volume using Bondi's method[173] ranged from 0.190-0.195, which is comparable with previously reported data.[174] The resulting membranes were cut into approximately 2 cm × 2 cm squares for permeation measurement. The as-prepared membranes were labeled as "AO-amidoxime time (h)." For example, AO-12-PDMSPNB is the membrane with 12 h amidoximation. The compositions of the membranes were determined by elemental analysis.

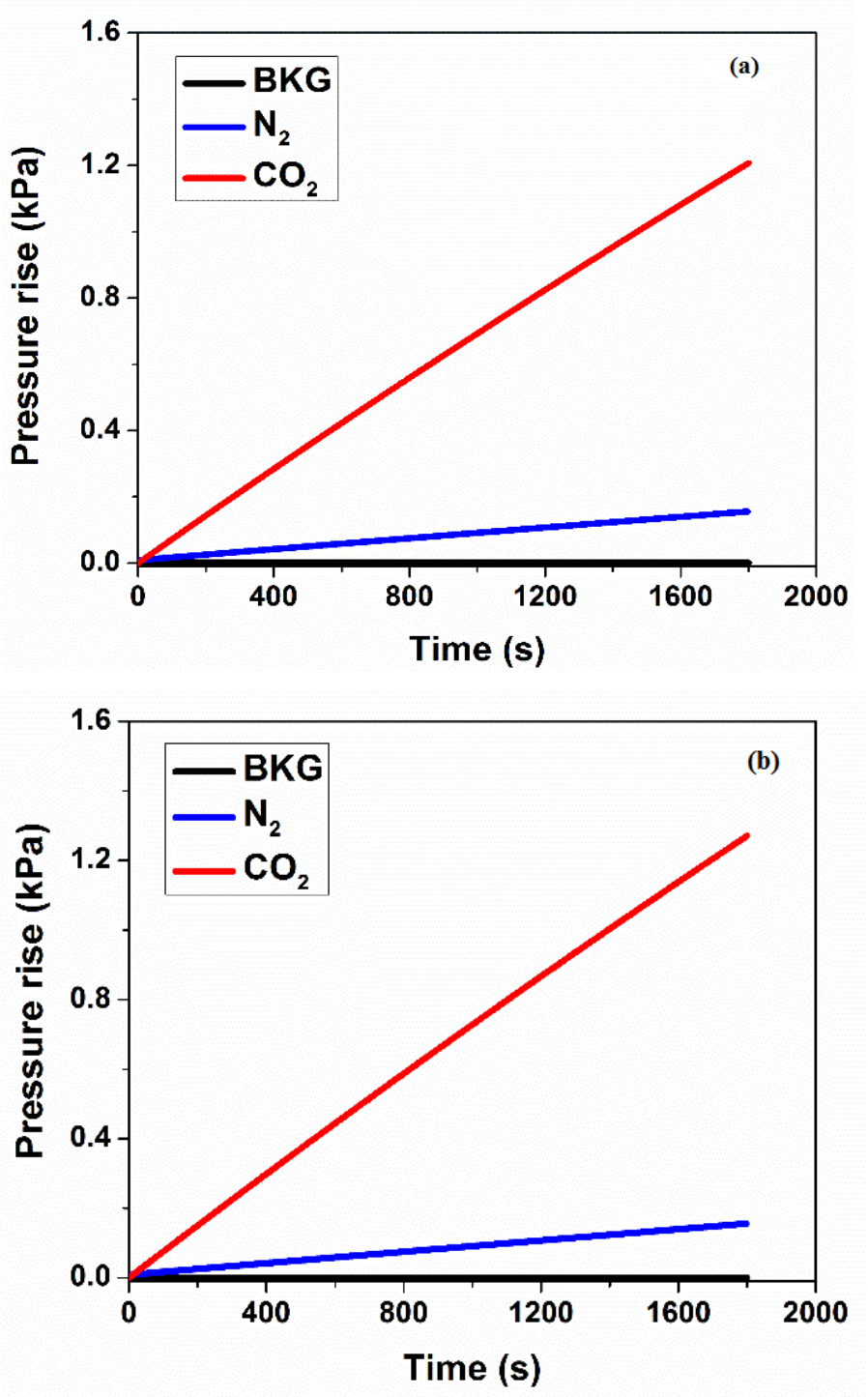

Figure 4.1. Pressure rise of cross-linked PDMSPNB-co-PdiCyNb membrane (a) before and (b) after methanol treatment.

4.2.4 AO-PTMSP membrane fabrication

The synthetic route of AO-PTMSP is demonstrated in Scheme 4.2. For detailed synthesis procedures, please see *Polymer Chemistry* 2017,8, 3341-3350. Membranes were prepared using solution casting method. In a typical example, a solution of AO-PTMSP (0.2 g) was prepared in toluene (15 mL) at a concentration of 1.5 wt% and was dispersed onto a PTFE dish (with a diameter of 6 cm) after filtration using a 0.45 μm PTFE filter. The homogeneous and clear membrane was then formed by slow evaporation of the solvent in an isolating container at ambient temperature after two days. All the resulting membranes had thicknesses of 70-90 μm and were soaked in methanol to remove residual solvent and prevent the aging effect. Each membrane was removed from the methanol solvent and dried in air for 24 h prior to any measurements.

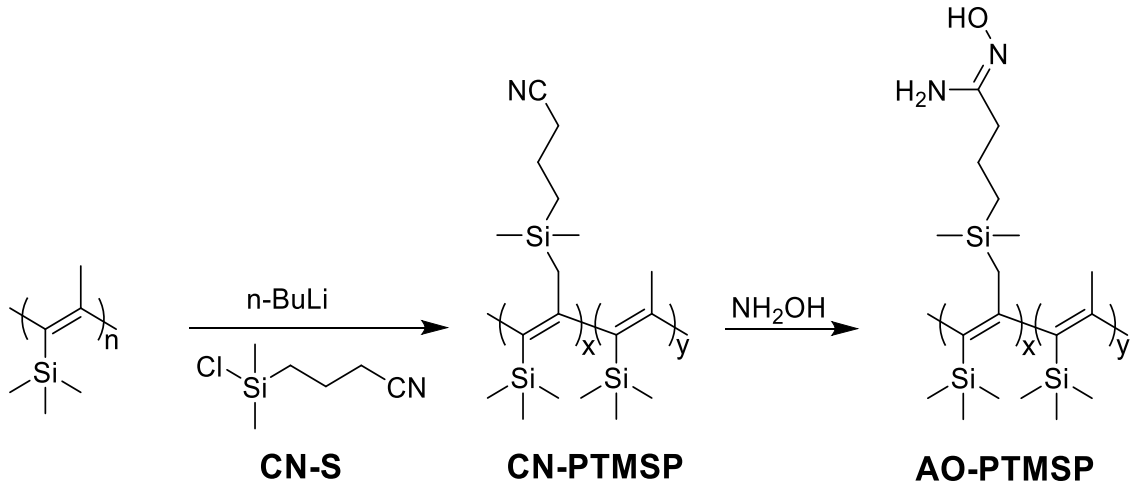

Scheme 4.2. The synthetic scheme of AO-PTMSP.

4.2.5 AO-PDMSPNB Membrane Characterizations

Temperature-modulated DSC (TMDSC) measurements were performed using the following procedure: sample was equilibrated at 100 °C, isothermal for 5 min to erase the thermal history, and then cooled to −160 °C at 3 °C/min with a modulation of ±1 °C/min, and then heated to 100 °C. The glass transition temperature (T_g) value was taken as the midpoint of the transition step in the heating process of the reversible heat flow signals. Representative curves of AO-PDMSPNB membranes are presented in Figure 4.2, in which the inset shows the derivative curves of the heat flow change. The glass transition temperature (T_g) can be estimated from both the transition process in reversible heat flow curves and the peak position in the derivative curves. In all AO-PDMSPNB membranes, only one T_g for PDMS and crystallization at higher temperature (not shown) are observed. The data reveal no changes in T_g (T_g of all samples are -125°C) for AO-PDMSPNB membranes with different amounts of AO groups.

4.2.6 Calculation of binding energies

CO_2 affinities were estimated by calculated binding energies (BE) between CO_2 and polymer units. Structures of complexes and monomers were optimized at the RI-MP2/def2-TZVPP level with the Turbomole 6.5 software package.[175] We have shown that weak interactions between CO_2 and dipolar molecules can be reproduced accurately at this level.[110] Basis set superposition error (BSSE) was further corrected for reported BEs with counterpoise correction.

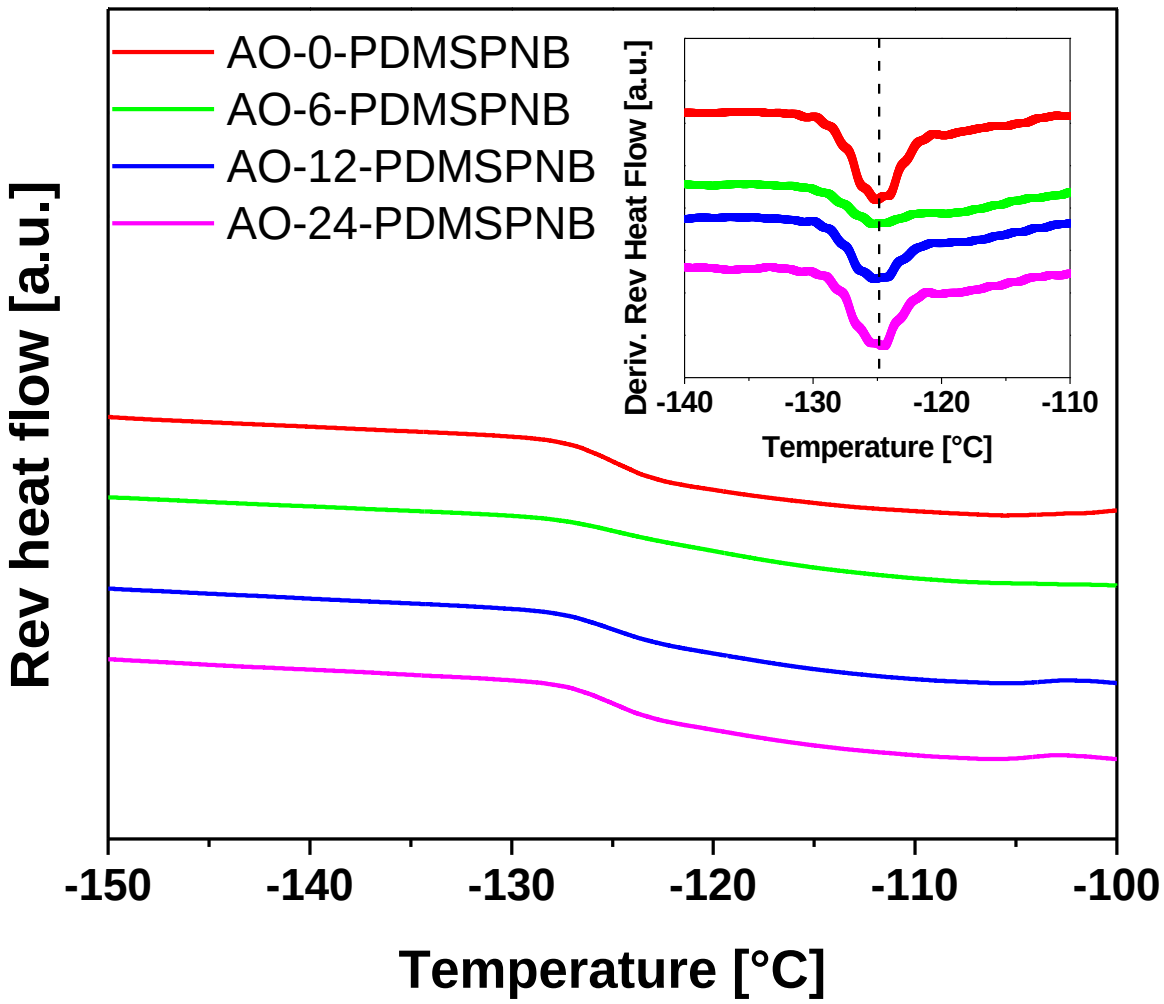

Figure 4.2 DSC curves for AO-PDMSPNB membranes illustrating the glass transition step. Inset is the derivative of reversible heat flow change. All curves have been shifted vertically to illustrate the systematic change of the peak shape and position.

4.2.7 Fractional free volume (FFV) estimation

The FFV of the membranes was estimated using the following group contribution method,

$$FFV = \frac{V - V_0}{V} \tag{4.1}$$

where V is the specific volume of the AO-PTMSP polymer obtained from density measurements at the temperature of interest; V_0 is the specific occupied volume at 0 K, which was estimated as 1.3 times the van der Waals volume calculated using Bondi's group contribution method.[176, 177]

4.3 Results

4.3.1 Determination of AO-PDMSPNB membrane compositions

The compositions of the PDMSPNB-*co*-PdiCyNb and AO-PDMSPNB membranes were determined using a combination of FTIR spectroscopy and elemental analysis. The IR spectra of AO-PDMSPNB series membranes are shown in Figure 4.3. It can be noticed that the band associated with the C≡N group at 2250 cm^{-1} disappears with the conversion to AO groups. The broad bands in the region of 3000–3500 cm^{-1} represent the N-H and O-H stretching vibration while the band at 1660 cm^{-1} represents the C=N stretch vibration.[178, 179] These peaks confirm the conversion from CN groups to AO groups. The band at 1260 cm^{-1} is related to the Si-CH_3 symmetric deformation[180, 181] in the PDMS matrix, which remains constant during the amidoximation.

The conversion percentage of the CN group is calculated from the change of the integrated area of the CN peak (2250 cm^{-1}) relative to the Si-CH_3 symmetric deformation peak (1260 cm^{-1}).

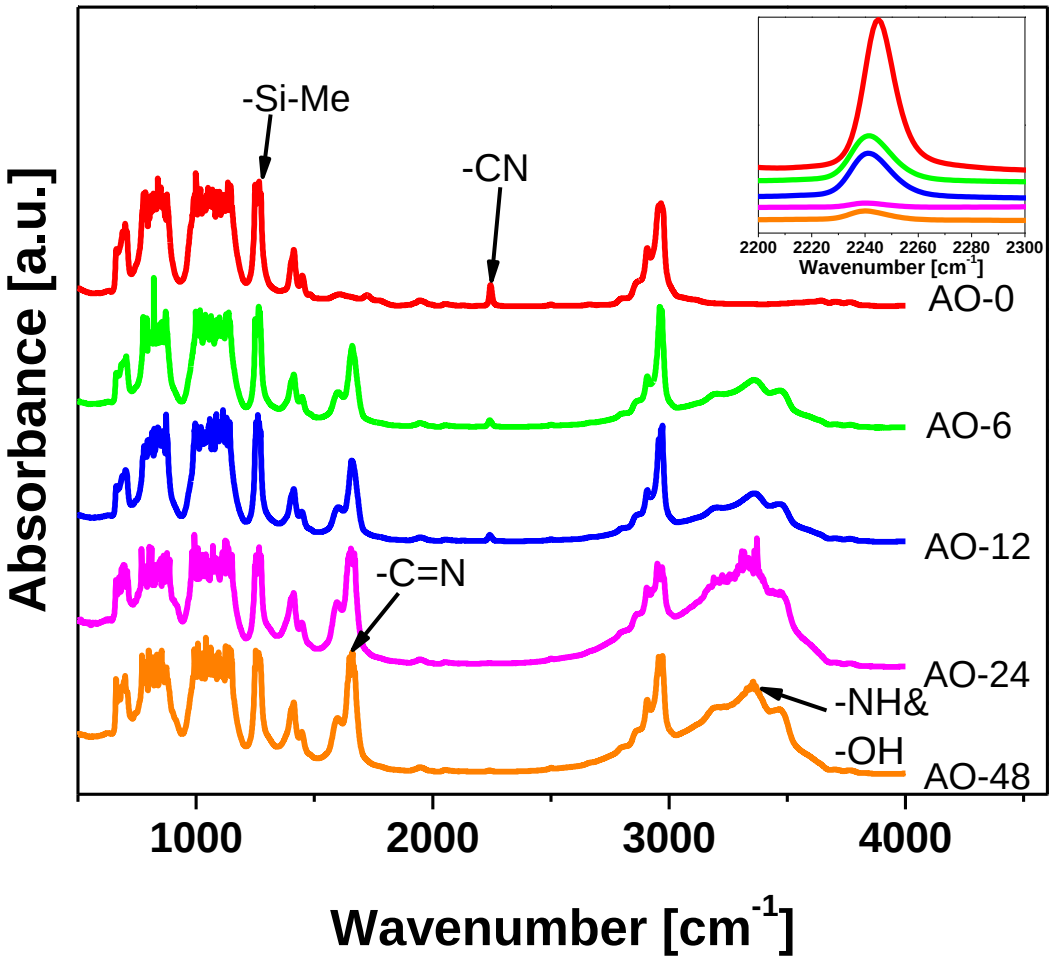

Figure 4.3 FTIR spectra of AO-PDMSPNB series membranes. Inset: change of CN peaks at 2250 cm^{-1}. All spectra have been shifted vertically to illustrate the systematic changes of the peak.

The calculation results are shown in Figure 4.4 and Table 4.1. Moreover, Table 4.2 shows the amount of linear and cyclo-AO composition in the polymer membranes. The conversion of the CN groups increases with increasing amidoximation time and reached a plateau after 24 h. Previous studies reported an amidoximation time around 20 h to reach the plateau[32, 114, 182], which is consistent with our results. The post-modification of the hydrophobic cross-linked membranes may limit diffusion and penetration of the hydroxylamine through the membrane matrix,[183] thus resulting in slightly less than 100% conversion. No further measurements of the 48 h sample were taken due to its similarity to the 24 h sample.

4.3.2 Gas transport properties of AO-PDMSPNB membranes

To study the effects of amidoximation on gas separation performance, each membrane was tested using the constant-volume variable-pressure gas flux method. All the membranes show much higher CO_2 permeability than that of N_2. The results of the single-gas permeability and CO_2/N_2 selectivity values are summarized in Table 4.3 and Figure 4.5. As seen in Figure 4.5a and 4.5b, for AO-PDMSPNB membranes, the CO_2 and N_2 permeabilities show a monotonic decrease with increasing AO conversion. The CO_2/N_2 selectivity increases as a function of AO content, but reaches a maximum at ~39% conversion, and further increase in AO conversion results in decreased selectivity (Figure 4.5c). When these values are plotted on a 2008 Robeson plot (Figure 4.6), the highest performing membrane, AO-12-PDMSPNB has exceeded the Robeson upper bound, showing great enhancement as compared with the majority of the membranes.

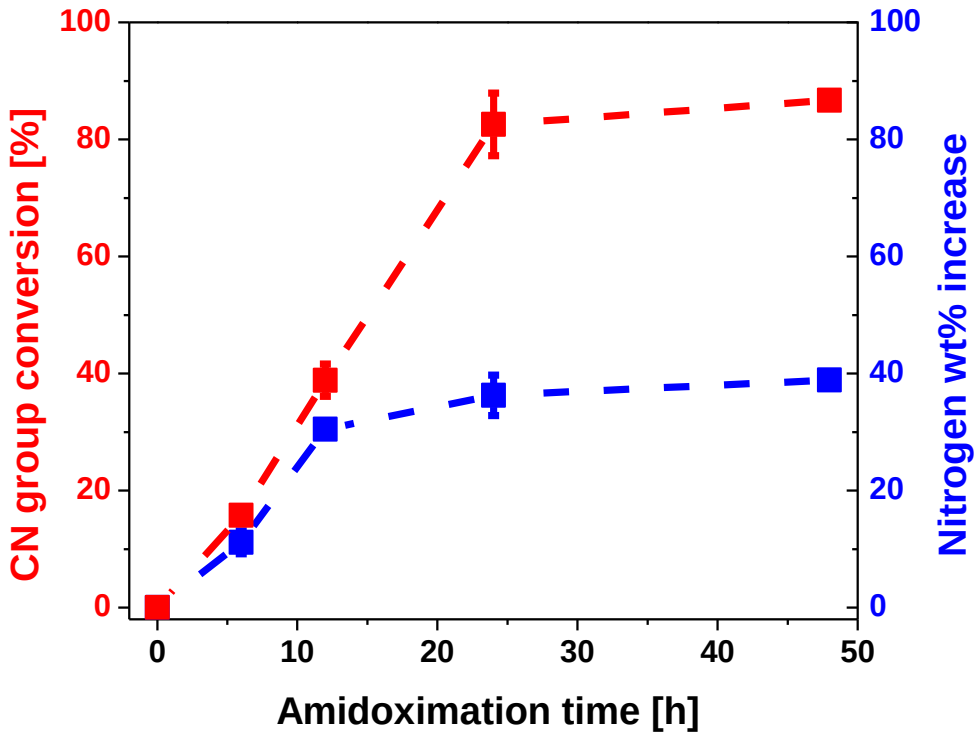

Figure 4.4 Red circles represent the conversion of CN groups in AO-PDMSPNB series calculated from FTIR mode at 2250 cm^{-1}. Blue squares represent the increase of Nitrogen wt% calculated from elemental analysis.

Table 4.1 Summary of elemental analysis and FTIR calculation results.

AO time(h)	Carbon wt%	Nitrogen wt%	Nitrogen/Carbon ratio %	Nitrogen% increase	CN % conversion
0	42.01 ±0.07	3.27 ±0.10	7.79 ±0.23	0	0
6	39.49 ±0.65	3.42 ±0.10	8.65 ±0.10	11.2 ±2.0	15.8 ±1.0
12	39.48 ±0.61	3.96 ±0.13	10.16 ±0.31	30.5 ±0.2	38.9 ±2.8
24	38.67 ±0.04	4.10 ±0.02	10.60 ±0.04	36.3 ±3.5	82.6 ±5.4
48	38.40	4.03	10.50	38.9	86.7

Table 4.2 Summary of AO vs cyclo-AO amount in two series AO-PDMS membranes.

Sample code	CN conversion (%)	AO amount (%)	Cyclo-AO amount (%)
AO-0-PDMSPNB	0	0	0
AO-6-PDMSPNB	15.8 ±1.0	6.6 ±3.0	9.2 ±2.0
AO-12-PDMSPNB	38.9 ±2.8	22.0 ±2.4	16.9 ±5.2
AO-24-PDMSPNB	82.6 ±5.4	0	82.6 ±5.4

Table 4.3 Summary of gas permeability and CO_2/N_2 selectivity for prepared samples.

Sample code	CN conversion (%)	P_{CO_2} (Barrer)	P_{N_2} (Barrer)	CO_2/N_2 Selectivity
AO-0-PDMSPNB	0	10500 ±2400	1540 ±110	6.8 ±1.2
AO-6-PDMSPNB	15.8 ±1.0	7600 ±1200	670 ±210	11.3 ±2.1
AO-12-PDMSPNB	38.9 ±2.8	6800 ±1200	360 ±90	18.8 ±2.2
AO-24-PDMSPNB	82.6 ±5.4	4800 ±1300	320 ±80	15.0 ±0.2
PDMSPNB[160]	-	6734	489	13.8

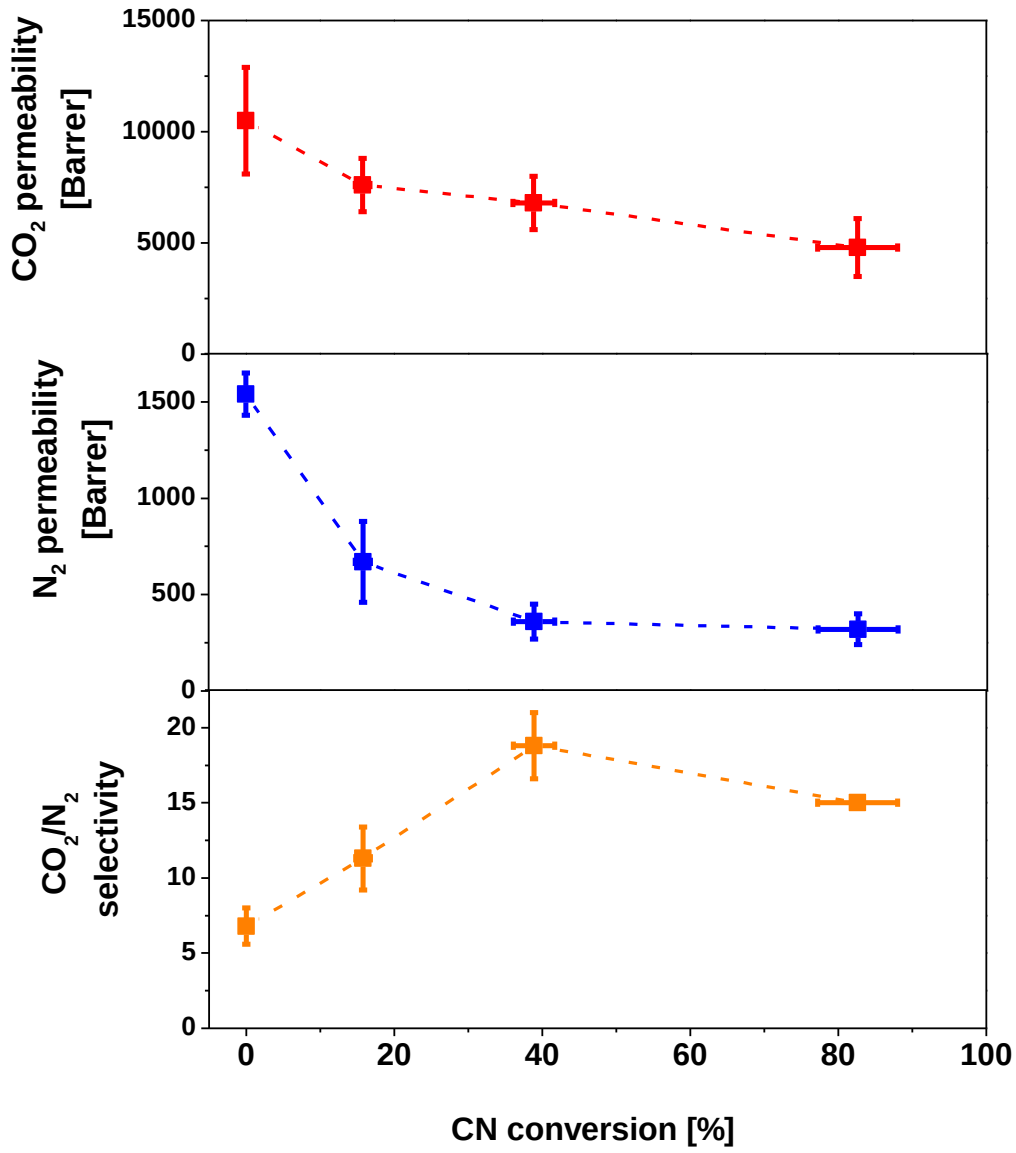

Figure 4.5 (a) CO_2 permeability, (b) N_2 permeability, and (c) CO_2/N_2 selectivity versus degree of CN group conversion (%) for the AO-PDMSPNB membranes.

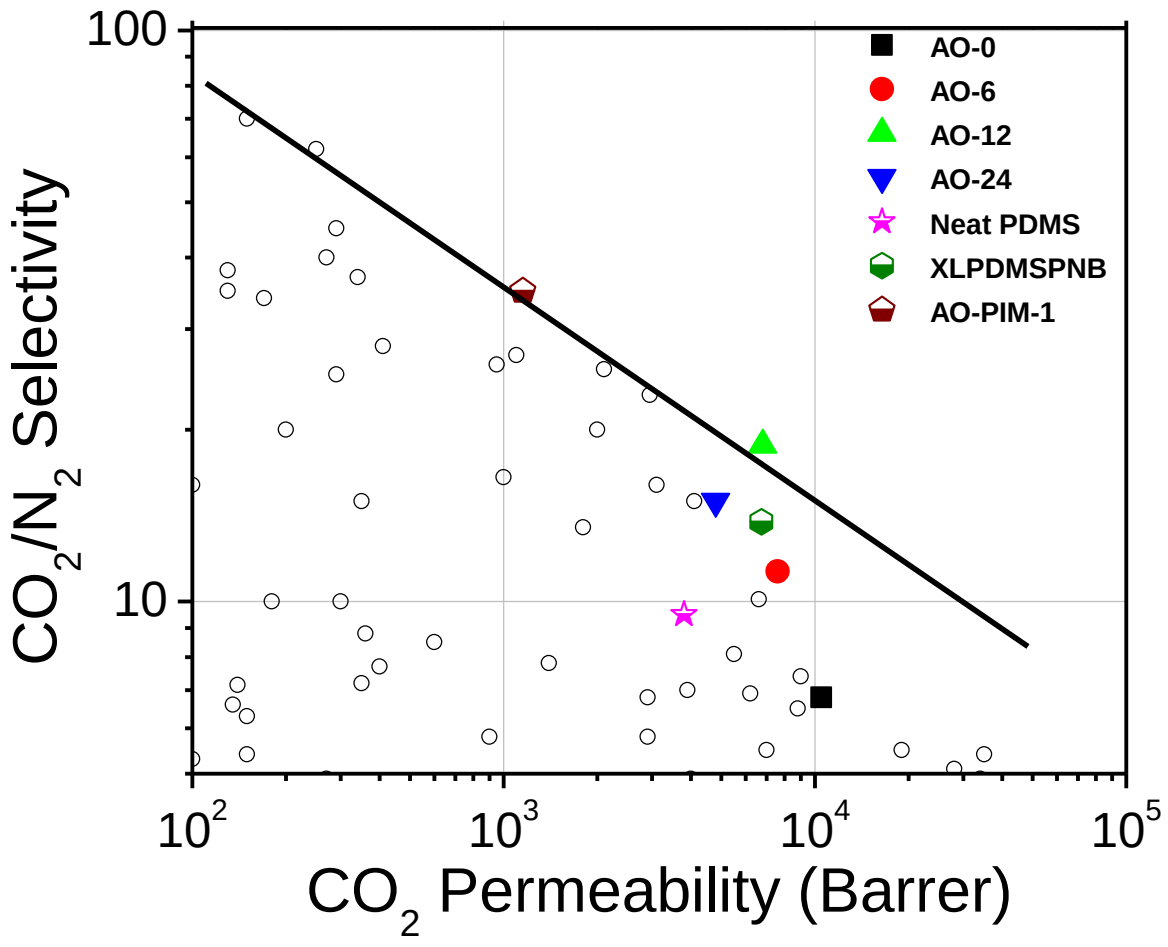

Figure 4.6 Summary of the AO series membranes (measured at 25 °C) as a function of amidoximation time in 2008 Robeson plot. The conventional PDMS[64], PDMSPNB[160] and AO-PIM-1[32] data are from references. The averaged permeability values are used and the error bar is not included.

BE calculations (Figure 4.7) show that the conversion of CN groups to AO groups (Figure 4.7a to Figure 4.7b, 4.7c) leads to an approximately 45% increase in the BE, which should lead to an increase in CO_2 solubility. Interestingly, the cyclo-AO structure (Figure 4.7d), which typically forms during the amidoximation reaction[184-186], shows weaker BE than AO groups (Figure 4.7b, 4.7c). Thus, the conversion from the AO structure to the cyclo-AO structure is expected to result in a slight decrease in CO_2 solubility due to the decrease of the BE from about -20 kJ/mol to -17 kJ/mol.

4.3.3 Gas transport properties of AO-PTMSP membranes

The composition of AO-PTMSP membranes are determined by a combination of NMR and TGA measurements. The data is present in Table 4.4. The grafting yield of AO functionality is ranged from 8% to 31%.

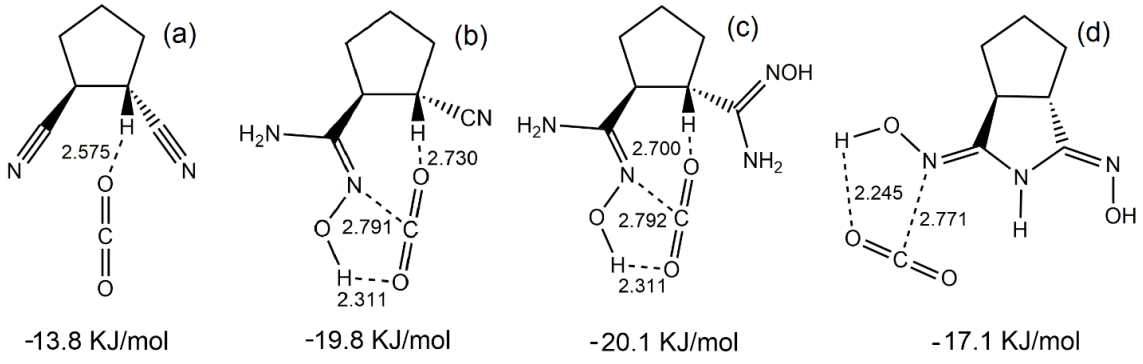

Figure 4.7 Summary of the calculated structure and binding energy (BE) for CO_2-CN and CO_2-AO complexes.

Table 4.4 General characterization of AO-PTMSP.

Sample	Grafting yield (%)		AO functionality (mmol/g)	T_d (°C)*
	NMR	TGA		
PTMSP	-	-	-	341
AO-8-PTMSP	7.9	11.3	0.71	218
AO-20-PTMSP	20.0	20.5	1.43	206
AO-31-PTMSP	31.5	30.9	2.67	200

* Reported as the temperature at ~5% weight loss.

The effect of AO grafting on gas permeation properties was investigated by evaluating the membrane permeability using the constant-volume variable-pressure gas flux method. The results for gas permeability and CO_2/N_2 selectivity values are summarized in Table 4.5 and Figure 4.8. Generally, the reported CO_2/N_2 separation performance of PTMSP membranes ranges from a CO_2 permeability from 20000 - 35000 Barrer and CO_2/N_2 selectivity from 3.5 - 11, due to different testing conditions and the aging effect of samples.[157, 169, 187-189] Our measured gas permeability of neat PTMSP (CO_2 permeability 30000 Barrer and CO_2/N_2 selectivity 3.5) is comparable to those previously reported data. With the higher incorporation of AO moiety, the permeability of both CO_2 and N_2 show a monotonic decrease, while the CO_2/N_2 selectivity increases as a function of AO grafting content. When these values are plotted on a 2008 Robeson plot (Figure 4.9), the highest performing AO-31-PTMSP, has achieved very close to the Robeson upper bound.

Table 4.5 Summary of density, FFV and gas transport properties for AO-PTMSP.

Sample code	Density (g/cm^3)	FFV	Permeability (Barrer)		α (PCO_2/PN_2)
			CO_2	N_2	
PTMSP	0.79	0.25	30000	8600	3.5
AO-8-PTMSP	0.84	0.21	20000	3300	6.1
AO-20-PTMSP	0.90	0.16	6500	480	13.5
AO-31-PTMSP	0.96	0.11	6000	350	17.2

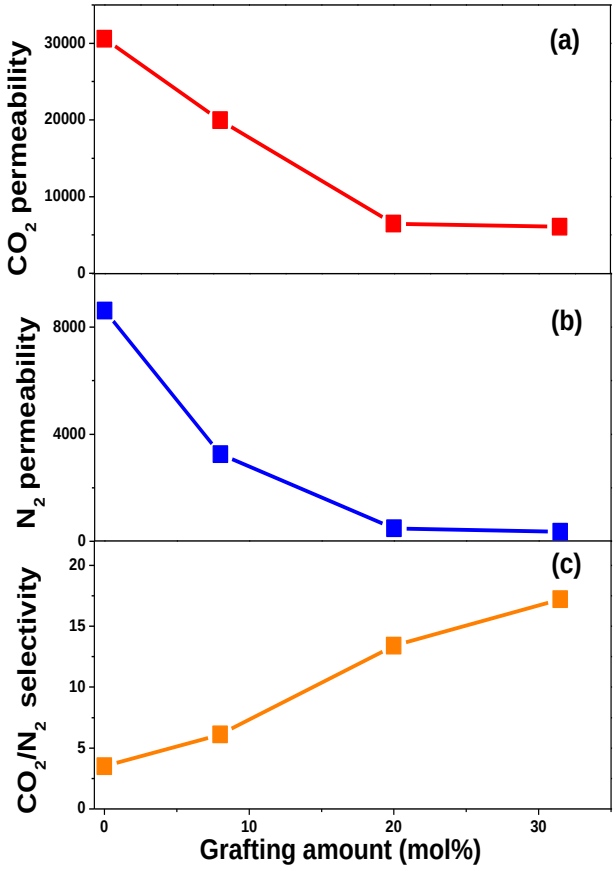

Figure 4.8 (a) CO_2 permeability, (b) N_2 permeability and (c) CO_2/N_2 selectivity versus grafting ratio (mol%) for the AO-PTMSP membranes.

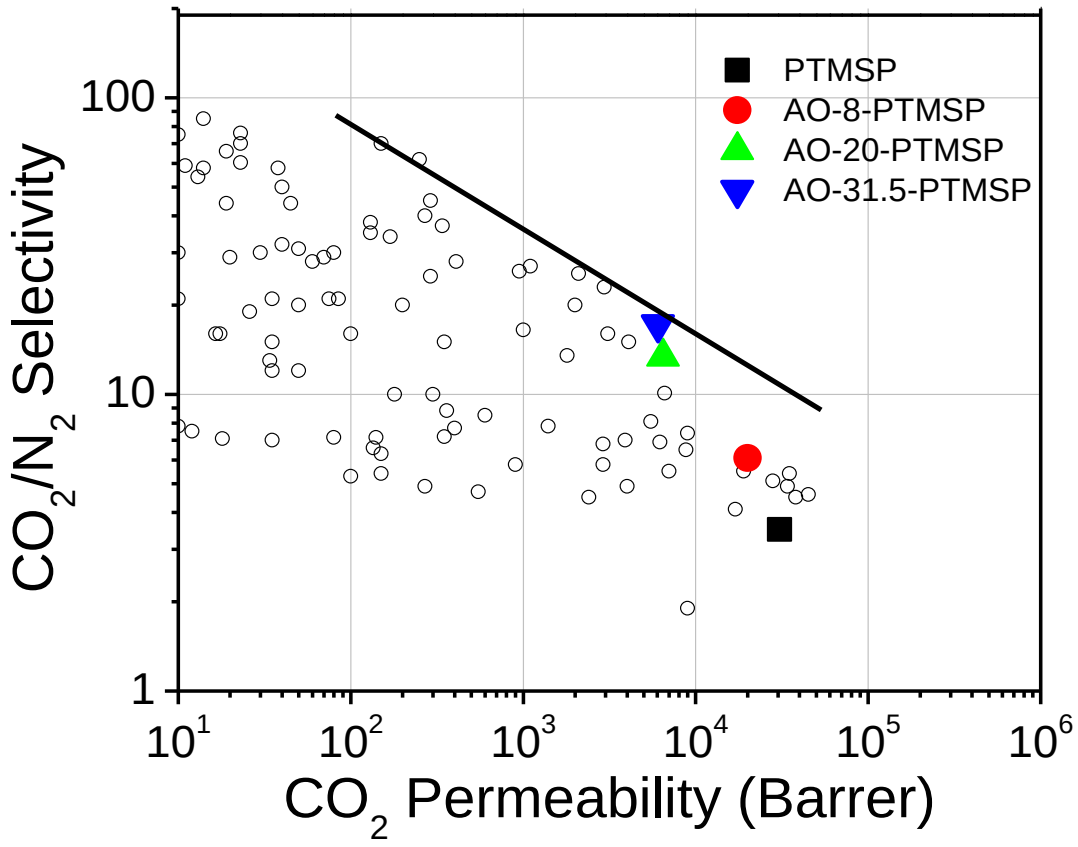

Figure 4.9 Summary of the AO-PTMSP membranes in a 2008 Robeson plot.

4.3.4 Impact of amidoximation on gas diffusivity in AO-PTMSP membranes

The effect of AO group incorporation into PTMSP membranes on gas diffusivity was investigated by evaluating density, FFV, and gas permeability, and the results are summarized in Table 4.5. The measured density and FFV of neat PTMSP are 0.79 g/cm^3 and 0.25, respectively, which are consistent with previously reported values.[187] With higher AO incorporation, the density increased while FFV showed a monotonic decrease. For example, AO-31-PTMSP, the membrane with the highest incorporation of AO at 31%, showed an increase in density (~20%) and decrease of FFV (~50%). Meanwhile, both CO_2 and N_2 permeabilities showed a decreasing trend with higher AO content

4.3.5 Effect of amidoximation on gas solubility in AO-PTMSP membranes

The sorption isotherms for both CO_2 and N_2 in AO-PTMSP membranes are depicted in Figure 4.10. The sorption isotherms are described by the dual-mode model and the fitting parameters are summarized in Table 4.6. For each polymer, the fitting parameters k_D and b (Eq. 1.6) were constrained to a range which correlated to the critical temperature of permeating gas.[188] The neat PTMSP data is consistent with reported values.[164, 188-190] A slight variability of sorption data compared with previously reported values is likely from the film preparation process and processing history of the sample.[191, 192]

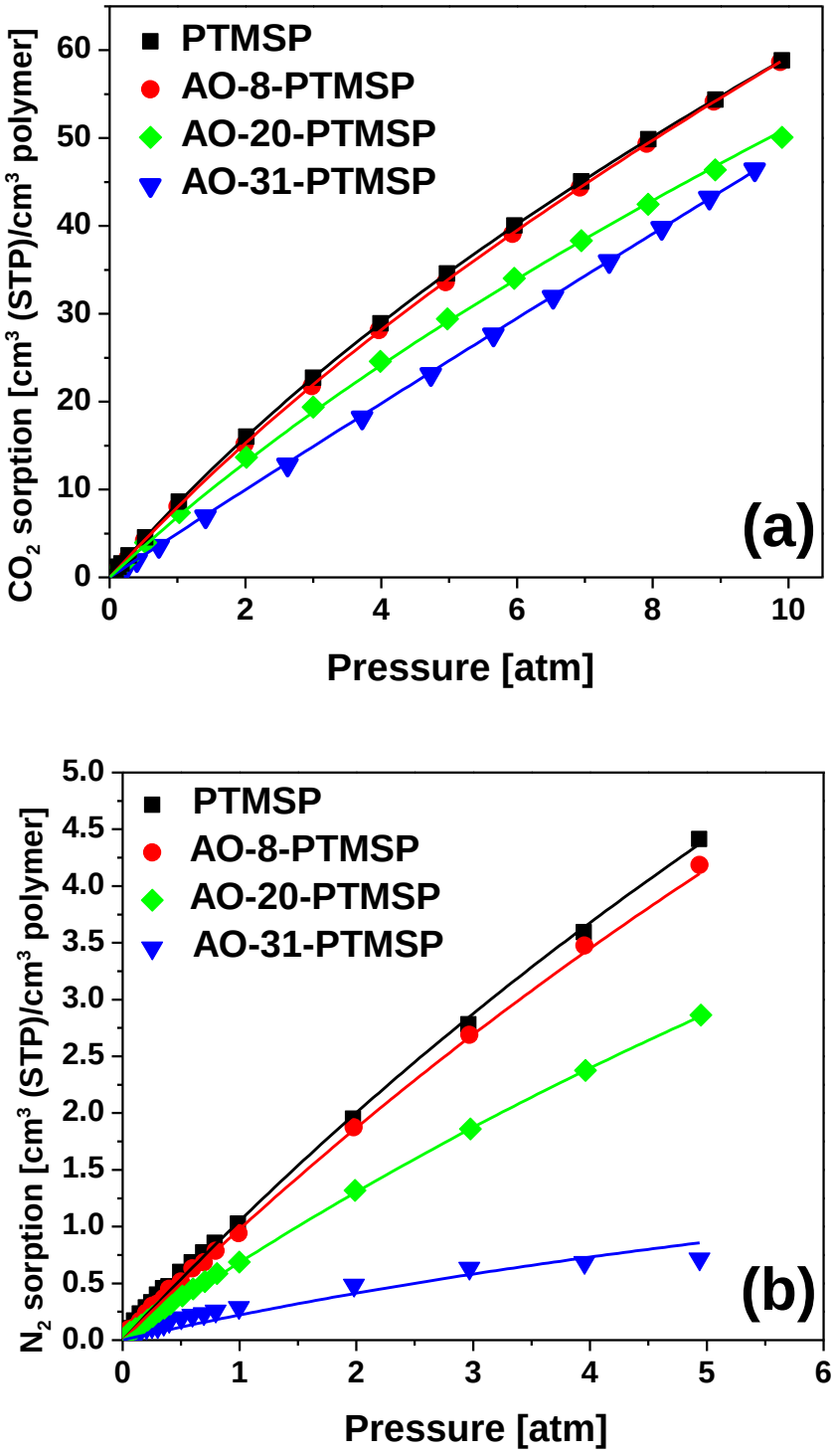

Figure 4.10 (a) CO_2 and (b) N_2 sorption isotherms for AO-PTMSP membranes. The solid curves show the fits to the dual-mode sorption model.

Table 4.6 Summary of dual-mode model parameters, gas solubility and solubility selectivity for AO-PTMSP membranes.

Sample code	k_D $\left[\frac{cm^3(STP)}{cm^3\ atm}\right]$		C'_H $\left[\frac{cm^3(STP)}{cm^3}\right]$		b $[atm^{-1}]$		S $\left[\frac{cm^3(STP)}{cm^3\ atm}\right]$		$\alpha[S_A/S_B]$
	CO_2	N_2	CO_2	N_2	CO_2	N_2	CO_2	N_2	
PTMSP	2.71	0.01	66	22	0.094	0.050	8.49	1.07	7.9
AO-8-PTMSP	3.06	0.02	61	20	0.088	0.050	8.09	0.98	8.3
AO-20-PTMSP	3.10	0.01	43	14	0.095	0.050	6.86	0.68	10.0
AO-31-PTMSP	4.64	0.01	5	3	0.080	0.050	5.02	0.15	32.4

4.4 Discussion

4.4.1 AO-PDMSPNB Membrane characterization

As illustrated in Scheme 4.1, the CN group can be converted into three different AO structures within the polymer matrix. Thus, it is of high importance to determine the actual compositions of each structure. When one CN group is converted to an AO group, one extra nitrogen atom is gained, which should result in a 100% increase in nitrogen wt% for the film. However, the elemental analysis results show a lower value than what was expected for 100% weight increase, which is attributed to the subsequent conversion of some di-AO groups to the cyclo-AO analogue.[179, 184, 185] The formation of a cyclo-AO group from two AO groups results in the loss of one equivalent nitrogen atom. In other words, if two CN groups are converted to one cyclo-AO group, only 50% extra nitrogen amount is gained. Therefore, by monitoring the nitrogen increase *via* elemental analysis

(Table 4.1), the amount of the cyclo-AO structure present in the matrix can be estimated (Table 4.2). The full conversion of CN groups to cyclo-AO groups in AO-24-PDMSPNB membranes should result in about 41% increase of nitrogen wt%, while the data showed a slightly lower value. Considering the experimental and fit errors, the value is within the range of uncertainty, and the majority of CN groups in AO-24-PDMSPNB membranes should be converted to cyclo-AO groups.

As shown in Figure 4.2, the T_g values obtained from DSC do not show any changes, and are consistent with our previously reported XLPDMSPNB membranes[160]. Although the conversion from CN groups to AO groups introduces sterically bulky functional groups as well as H-bonding, the overall influence on the averaged segmental dynamics in the PDMS matrix is negligible, which we attribute to PDMS being the major component within the polymer matrix. Thus, the observed changes in gas permeability are not related to changes in polymer segmental dynamics.

4.4.2 Impact of amidoximation on gas permeability of AO-PDMSPNB

Generally, with higher diCyNb content in the precursor, gas permeability increases, while the CO_2/N_2 selectivity showed a decreasing trend. The gas transport property data of membranes with 10, 25, and 30% diCyNb is summarized in Table 4.7. Due to the optimum balance of CO_2 permeability and CO_2/N_2 selectivity obtained in the permeation data of PDMSPNB-*co*-PdiCyNb membranes, AO-25 was selected for use in further experiments. It is reported that with the formation of AO groups, the intermolecular hydrogen bonding can be stacked up between the structures.[30, 193]

Table 4.7 Summary of gas permeability and CO_2/N_2 selectivity as a function of diCyNb Feed wt%.

diCyNb Feed wt%	CO_2 Permeability (Barrer)	N_2 Permeability (Barrer)	CO_2/N_2 Selectivity
10	5537	571	9.7
25	12563	1586	7.9
30	15084	2743	5.5

The H-bond rich structure can result in significant reduction of the gas diffusivity,[20, 194] which explains the monotonic decrease in gas permeability with the conversion from CN to AO groups (Figure 4.5a, 4.5b). Several reported studies on CO_2 separation and capture have achieved enhanced selectivity of CO_2over other gas pairs with the addition of AO groups.[30-33, 114] In this study, the increase of CO_2/N_2 selectivity from AO-0-PDMSPNB to AO-12-PDMSPNB (Figure 4.5c) agrees well with the enhanced performance by the addition of CO_2-philic AO groups. However, the observed maximum in CO_2/N_2 selectivity was not expected and requires a separate explanation.

The BE calculations of these complexes (Figure 4.7) can elucidate the different performance in gas transport properties of AO-PDMS membranes. The increase in BE upon the conversion of the CN groups to AO groups is likely the source of the observed increase in CO_2/N_2 selectivity (Figure 4.7 (a)-(c)). When CN conversion is less than 39% (AO-12-PDMSPNB), the enhanced CO_2 solubility partly compensates the loss of gas diffusivity caused by H-bonding. This is the major reason why the CO_2 permeability

decreases less than that of N_2, although they have a similar kinetic size. When the CN conversion is higher than 39%, the cyclo-AO structures become dominant in the polymer matrix (Figure 4.7c to Figure 4.7d), which results in decreasing BE to -17 KJ/mol (~15%) and corresponding decrease in CO_2/N_2 selectivity from AO-12-PDMSPNB to AO-24-PDMSPNB. Therefore, a decrease in CO_2-philicity with cyclization of AO groups is most likely a major reason for the decrease of selectivity at higher CN conversion. Thus, the CN conversion to various AOs structures should be carefully tuned in order to explore the optimum range.

4.4.3 Effect of AO functionality on diffusivity of AO-PTMSP

As shown in Table 4.5, the incorporation of AO groups resulted in a decrease of FFV and gas permeabilities. This is like due to the reason that the bulkier AO group contributes to occupying excess free volume. Moreover, the formation of intermolecular H-bonding between the AO structures could also hinder gas diffusion, leading to a decrease of gas permeability in AO-PTMSP membranes. Despite the decrease of gas permeability, the CO_2/N_2 selectivity demonstrates a five-fold increase. The enhancement of CO_2 selectivity by AO incorporation is attributed to the higher CO_2 affinity[30, 31, 33, 114, 165], and it is further examined by sorption measurements.

4.4.4 Effect of AO functionality on solubility of AO-PTMSP

The high sorption efficiency in PTMSP polymers is typically attributed to their high FFV and microporosity.[164] For AO functionalized membranes, the decrease of gas sorption capability is expected due to the reduction of FFV. In Table 4.6, when comparing the

Henry's law parameter, k_D, an increasing trend with higher AO content is observed. More than 70% increase is achieved from neat PTMSP to AO-31-PTMSP. Typically, k_D describes penetrant dissolution into the densified equilibrium regions of a polymer matrix. For membranes with no gas-polymer interaction, k_D is generally related to the critical temperature of permeating gas. In our study, the k_D values of CO_2 and N_2 in pure PTMSP are comparable with previously reported data. However, the AO-PTMSP membranes show much higher CO_2 k_D values than that of PTMSP. The high CO_2 k_D values clearly indicate that the dissolution of CO_2 into the polymer are significantly enhanced, which should originate from the strengthened CO_2-polymer interaction/philicity by the presence of the AO moiety. On the other hand, the Langmuir capacity parameter, C'_H, represents the maximum number of penetrant molecules that can be accommodated in the excess free volume of a glassy polymer. With functionalizing PTMSP to AO-PTMSP membranes in C'_H showed a decreasing trend, clearly reflecting the decreased amount of gas absorbed via Langmuir sorption. The amidoximation of the PTMSP matrix causes a great reduction of FFV, therefore it imparts a deleterious effect on Langmuir sorption.

The solubility selectivity could be calculated using the following equation[188]:

$$\alpha[S_A/S_B] = \frac{[(C_2 - C_1)/(P_2 - P_1)]_A}{[(C_2 - C_1)/(P_2 - P_1)]_B} \tag{4.2}$$

where $\alpha[S_A/S_B]$ are solubility selectivity, C the penetrant concentrations, p the pressure. When P_2-P_1=0, the solubility can be calculated as:

$$\lim_{\Delta p \to 0} \left(\frac{C_2 - C_1}{p_2 - p_1}\right) = k_D + \frac{C'_H b}{(1 + bp)^2} \tag{4.3}$$

The calculated solubility values for all AO-PTMSP membranes are summarized in Table 4.6. When considering the overall CO_2 sorption (Henry's law plus Langmuir), it is higher (~40%) in the pure PTMSP than in AO-31-PTMSP. However, the Langmuir sorption becomes the predominant factor for N_2 sorption due to the relative low k_D values for all PTMSP samples. The N_2 sorption of AO-31-PTMSP shows significant (~85%) decrease compared with pure PTMSP. Overall, when focusing on the sorption capability, although both CO_2 and N_2 sorption capacity show decreases to some extent, the decreasing percentage in N_2 is much higher than in CO_2. Thus, the overall solubility selectivity shows a four-fold enhancement after amidoximation.

4.4.5 Importance of tuning gas solubility

Our results clearly demonstrate that tuning the CO_2-philicity of PDMS-based and PTMSP-based membranes indeed improves CO_2/N_2 selectivity. It is of great fundamental interest to understand the optimum range of CO_2 BE, in which a balance of increased selectivity with the decrease in diffusivity should be met. More specifically, if the BE is too low, the membrane could not offer high enough gas solubility, while if the BE is too high, the strong CO_2 affinity may cause capture of the CO_2 molecule within the membranes and a strong reduction in its diffusivity and overall efficiency of the CO_2 separation. It is of great importance to study the correlation between BE and CO_2 separation performance, while simultaneously investigating other factors such as polymer dynamics and H-bonding, in order to develop a roadmap to design and synthesize high performance CO_2 separation membranes in the future.

4.5 Conclusion

In this chapter, we first showed the successful incorporation of CO_2-philic amidoxime groups into the PDMS matrix by using an *in-situ* ROMP technique, followed by a post-polymerization modification. Moreover, AO-PTMSP membranes were synthesized *via* hydrosilylation, followed by amidoximation reaction. The degree of amidoximation was found to significantly alter gas separation performance in both systems, which has been attributed to CO_2 binding affinity and H-bonding within the AO functionalities. Furthermore, these results demonstrate that by careful tuning of the CO_2-philicity of polymer membranes, it is possible to significantly increase CO_2/N_2 selectivity with a minimum loss in permeability. The highest performing membranes (AO-12-PDMSPNB and AO-31-PTMSP) shows significantly enhanced performance relative to previously reported pristine PDMSPNB and PTMSP membranes. These significant gains allowed AO-12-PDMSPNB and AO-31-PTMSP to exceed/achieve the Robeson upper bound at very high permeability (6800 Barrer and 6000 Barrer, respectively), which is critical for practical applications in treating the enormous amount of flue gases generated by power plants. This systematic report provides strong evidence detailing how AO content influences gas transport properties in polymer membranes. These findings provide a path to future CO_2 separation material development, as well as fostering fundamental understanding of the gas separation process using polymer membranes.

CHAPTER V

EFFECT OF POLY(ETHYLENE OXIDE) FUNCTIONALITY IN POLY(DIMETHYLSILOXANE) MEMBRANES FOR CARBON DIOXIDE SEPARATION

Reproduced in part from "Highly-permeable Poly(ethylene oxide)-co-Poly(dimethylsiloxane) Membranes for Carbon Dioxide Separation" *Advanced Sustainable Systems,* submitted.

Reproduced in part from "Robust and Elastic Polymer Membranes with Tunable Properties for Gas Separation" *ACS Applied Materials & Interfaces,* 2017, 9, 26483-26491.

5.1 Introduction

In Chapter 4, the amidoxime (AO) functionality was successfully incorporated into the PDMS and PTMSP membranes, and the synthesized materials showed significantly enhanced CO_2/N_2 solubility selectivity and improved gas separation performance. In this chapter, another CO_2-philic group, poly(ethylene oxide)(PEO), will be discussed.

Due to its polar nature, PEO shows high affinity for quadrupolar CO_2 molecules[23, 25, 195-199]. As estimated by Lin and Freeman, the CO_2/N_2 selectivity in amorphous PEO could reach 48, which far exceeds the practical CO_2/N_2 selectivity requirement for flue gas treatment.[200] However, as compared to some highly permeable polymers, e.g. poly (1-trimethylsilyl-1-propyne),[48, 57, 189] polymers of intrinsic microporosity,[15, 201-203] poly(dimethylsiloxane) (PDMS),[64, 160] PEO shows one or two orders of magnitude lower

gas permeability. For example, PDMS, a typical highly permeable rubbery polymer, exhibits about 25 times higher CO_2 permeability than that of amorphous PEO, which primarily originates from significantly different gas diffusivity between those two. [64, 200] Moreover, the undesirable semi-crystalline nature of PEO at room temperature additionally reduces gas diffusivity, leading to a further loss of gas permeability. Generally, high molecular weight PEO exhibits better mechanical properties, but higher crystallinity and lower gas permeability. Low molecular weight PEO shows a lower crystallinity and better gas transport properties, but exists in liquid form and cannot be directly used as a free-standing gas separation membranes. Due to inherently low permeability of PEO of either molecular weight, the design of free standing PEO-containing membranes owning high gas permeability is challenging. Researchers reported a variety of modifications of PEO-containing materials, hoping to achieve better gas transport properties as well as acceptable mechanical strength. Recently, various highly-permeable PEO-containing materials have been reported by different researchers.[104, 198, 199, 204, 205] Some combination of PDMS and PEO could potentially offer great advantages in high-performance gas separation membranes due to PDMS's high permeability and PEO's high selectivity for CO_2 separation. The majority of previous studies on PEO-PDMS systems focus on the polymer blend. The permeability of such membranes is usually under 700 Barrer. From practical aspect, the development of high permeable materials is required to further reduce the capture cost.

In Chapter 3, we reported lightly cross-linked polydimethylsiloxane-norbornene (XLPDMSPNB) membranes that exhibit excellent CO_2 permeability (~6800 Barrer). This

is due to the significantly lower cross-link density which offers much faster dynamics, and thus contributing to the increased gas diffusivity.[34, 160] Moreover, our previous simulation data reveal that the EO functionality could offer high binding energy with CO_2 molecules.[110] Herein, we report the successful copolymerization to produce PEO-PDMS materials with enhanced CO_2/N_2 separation performance, combining the advantage of fast PDMS dynamics and strong EO-CO_2 interactions. The utilization of short chain PEO in the copolymer matrix helps to overcome the crystallinity issue, while the cross-linking technique provides free-standing films. By the careful alternation of PEO versus PDMS composition, the membranes showed controlled CO_2 solubility. The combination of CO_2-philic PEO groups and highly permeable PDMSPNB matrix results in one of the highest CO_2 permeabilities in PEO-containing films (3400 Barrer) and achieves performance very close to the Robeson upper bound.

Moreover, in this chapter, another route to synthesize cross-linked PEO-PDMS membranes will also be discussed. In our previously chapters, the reported PDMS-based membranes were synthesized *via* the *in-situ* ROMP reaction. The versatility of the ROMP technique allowed us to incorporate various CO_2-philic groups into the PDMS matrix, providing tunable gas separation performance for membrane development.

Currently, chemical cross-linking *via* urea/urethane units is also widely used due to its facile mechanism.[206] In conventional poly-condensation technique, the reaction typically occurs between amine terminated pre-polymers and urea functionality.[207] However, the reaction kinetics is relatively slow. Herein, we report a series of urethane-rich PDMS-based polymer membranes (U-PDMS) formed by the reaction between the amine-terminated

PDMS and multifunctional isocyanate cross-linker. The novel membrane material exhibits the advantages of fast processing, *in-situ* film formation and absence of by-products. Modifying the molecular weights of the PDMS chain provides an efficient way to tune both cross-link density and physical interactions, which showed huge influence on gas diffusivity. Moreover, the successfuls incorporation of PEO moiety into the U-PDMS matrix offered a factor of 3 increase of CO_2/N_2 selectivity.

5.2 Materials and methods

5.2.1 Materials

(Bicycloheptenyl) ethyl terminated polydimethylsiloxane (PDMSNB) with a weight-average molecular weight ranged from 12,000-16,000 g/mol was purchased from Gelest Inc. trans-5-Norbornene-2,3-dicarbonyl chloride (NB-COCl), Poly(ethylene glycol) methyl ether (PEO), Pyridine, 4-(Dimethylamino)pyridine (DMAP), Grubbs catalyst, 2nd generation (Grubbs-II), Tetrahydrofuran (THF) and anhydrous dichloromethane (DCM) were purchased from Sigma-Aldrich. Nitrogen and carbon dioxide gas cylinders (99.99% purity) were obtained from Air Liquide. All used as received. All ^{1}H and ^{13}C NMR spectra were collected using a Bruker ADVANCE III spectrometer operating at 400 MHz for ^{1}H and 100 MHz for ^{13}C. Chemical shifts were reported in ppm downfield from tertamethylsilane. $CDCl_3$ (deuterated chloroform) was used as the solvent for all NMR samples.

Aminopropyl-terminated polydimethylsiloxane with labeled molecular weight (M_n) of 900g/mol, 1600g/mol, 3000g/mol, 5000g/mol and 30000g/mol were obtained from Gelest,

Inc and used directly. Poly(oxyethylene bis(amine)), Mw=1000 g/mol from Alfa Aesar was dried under vacuum prior to use. Poly(hexamethylene diisocyanate) was obtained from Sigma-Aldrich.

5.2.2 Synthesis of norbornene- poly (ethylene oxide) (NB-PEO)

The NB-PEO monomers were prepared by adding 2.5 equivalents of pyridine (45.65 mmol, 3.68 mL) *via* syringe into a flask equipped with 1 equivalent (18.26 mmol) NB-COCl, 0.05 equivalent (0.913 mmol) DMAP, 2 equivalents (36.52 mmol) PEO-OH, and 100 mL dry THF cooled in an ice bath. The reaction was stirred under argon for 72h at 40 °C. The pyridine salts were filtered out and remaining pyridine was removed by rotary evaporation as an azeotrope with n-heptane. The yield of the reaction was in 80%-90% range, all monomers are yellow to orange viscous liquids. ^{1}H NMR ($CDCl_3$, 400 MHz): 6.24 ppm (bs, 1H, CH=CH), 6.04 (bs, 1H, CH=CH), 4.30-4.10 (m, 4H, C=O(O)CH_2), 3.79-3.56 (m, 8H, CH_2OCH_2), 3.52 (m, 4H, CH_2OCH_3), 3.40 (t, 1H, nb), 3.35 (bs, 6H, OCH_3), 3.26 (bs, 1H, nb), 3.12 (bs, 1H, nb), 2.71 (d, 1H, nb), 1.59 (d, 1H, nb), 1.42 (d, 1H, nb).

5.2.3 PEO-PDMSPNB membrane fabrication

The PEO-PDMSPNB membranes were synthesized via the in-situ ring-opening metathesis polymerization (ROMP) of PDMSNB and NB-PEO (Scheme 5.1). In a typical process, PDMSNB (300 mg, 2.14×10^{-5} mol) and NB-PEO (200 mg, 3.07×10^{-4} mol) were dissolved in DCM (6 mL). In a separate vial, Grubbs-II catalyst (10 mg, 1.18×10^{-5} mol) was dissolved in DCM (2 mL). Then 1 mL of the Grubbs-II catalyst stock solution was added to the monomer solution and shaken for 60 s before being poured into a 100 mL PTFE dish (with

a diameter of 10 cm). The PTFE dish was covered with aluminum foil for 24 h in which the *in-situ* cross-linked membrane was formed. A mixture of ethyl vinyl ether (2 mL) in DCM (6 mL) was added to the film to terminate the metathesis reaction. The membrane was dried under argon atmosphere overnight and moved to a vacuum oven for 3 days to remove residual solvent. Finally, the cross-linked free-standing polymer membrane was detached from the PTFE dish and cut into pieces for further testing. The membrane thickness is ranged from 140-170 μm.

5.2.4 U-PDMS Membrane preparation

The cross-link network is formed *via* isocyanate-amine ([NCO]-[NH_2]) reaction. For detailed synthesis and characterization procedures, please see "A Robust and Elastic Polymer Membrane with Tunable Properties for Gas Separation" *ACS Applied Materials & Interfaces,* submitted.

The synthetic route of U-PDMS is demonstrated in Scheme 5.2. PDMS with 5 different molecular weight (MW), 900g/mol, 1600g/mol, 3000g/mol, 5000g/mol and 30000g/mol, were used for membrane fabrication. And the membrane sample was named as U-MW-PDMS. For example, a U-0.9K-PDMS membrane is synthesized using PDMS with 900 MW. The molecular weight between cross-links (M_x) and cross-link density is estimated from rheology data.

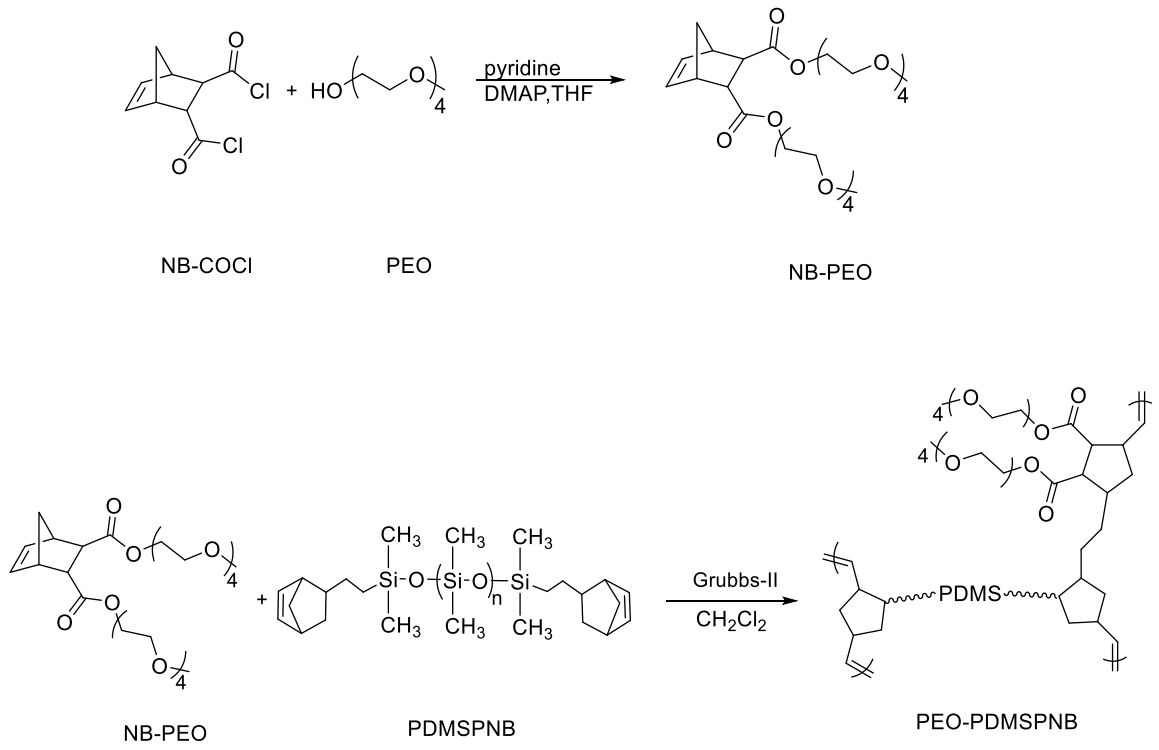

Scheme 5.1 Synthesis of NB-PEO and ROMP reaction of the PEO-PDMSPNB membranes.

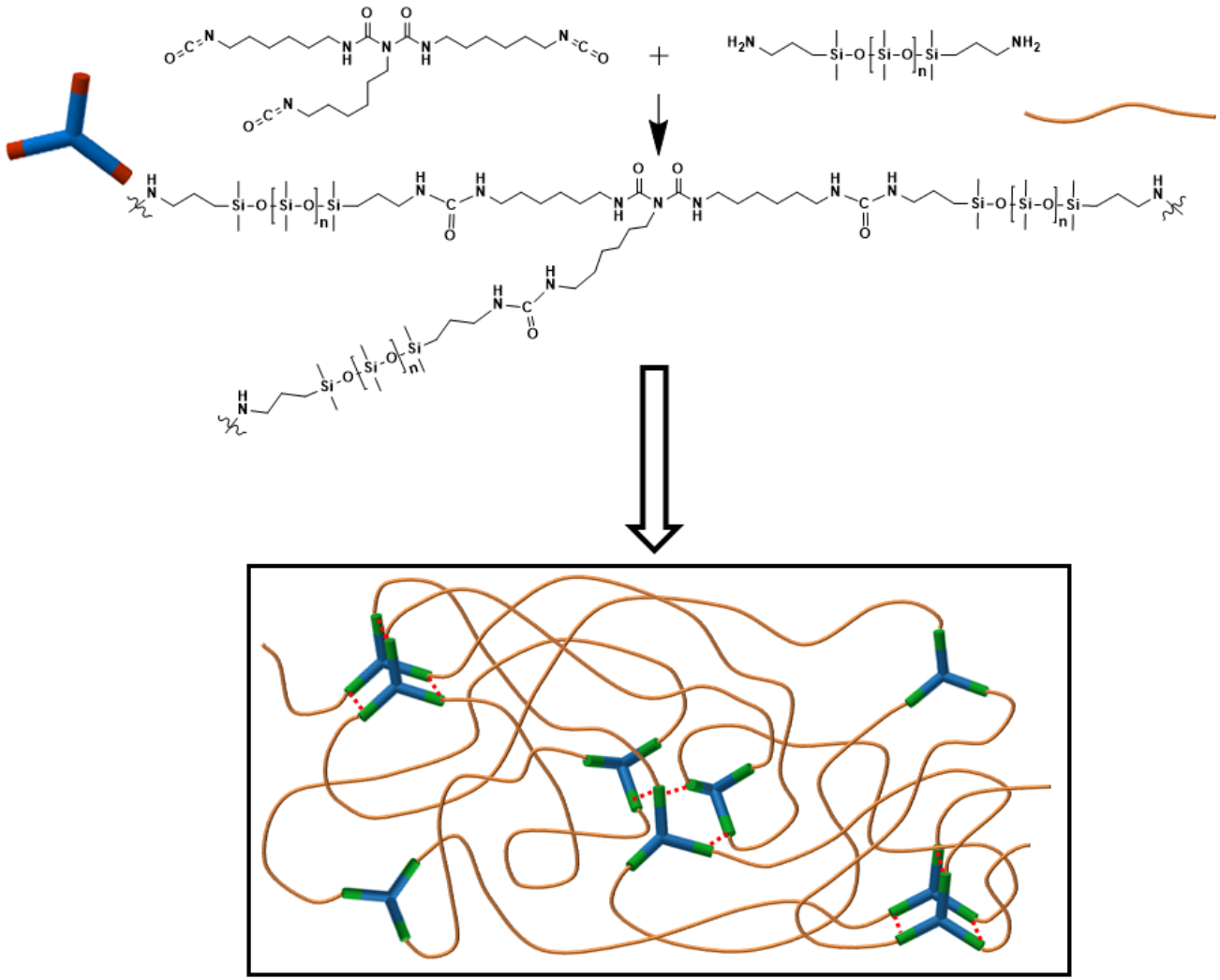

Scheme 5.2 Illustration of urethane-rich PDMS-based network (U-PDMS).

5.2.5 Dynamic Mechanical Analysis (DMA)

DMA tests were performed using a TA Q800 Instrument. Films were cut into approximately (6.0 × 5.0 × 0.1) mm specimens for tensile test. All samples were elongated until failure/break with a constant strain rate (10%/min) at 25 ^{o}C. The modulus was determined using the 1% secant method to the minimize error.

5.2.6 X-ray photoelectron spectroscopy

X-ray photoelectron spectroscopy (XPS) was performed using a Thermo Scientific Model K-Alpha XPS instrument. The instrument uses a monochromated, micro-focusing, Al Kα X-ray source (1486.6 eV) with a variable spot size (30-400 μm). Analyses of all samples were conducted with a 400 μm X-ray spot size for maximum signal and to obtain an average surface composition over the largest possible area. The instrument has a hemispherical electron energy analyzer equipped with a 128 multi-channel detector system. The base pressure in the analysis chamber is typically 2×10^{-9} mbar or lower. Samples were prepared for analysis by attaching them to the sample holder with metal clips. Wide energy range survey spectra (0-1350 eV) are acquired for qualitative and quantitative analysis using an analyzer pass energy of 200 eV. For assessing the chemical bonding of identified elements, narrow energy range core level spectra were acquired with an analyzer pass energy of 25 eV. Charging was reduced by using a charge neutralization system that uses a combination of low energy electrons and low energy argon ions for optimum charge compensation. The typical pressure in the analysis chamber with the flood gun operating was 2 x 10^{-7} mbar. The scanning condition for all measurements was as follows: 100

ms/step, 0.1 eV/step and 30 sweeps. Data were collected and partially processed using the Thermo Scientific Advantage XPS software package (v 4.61). Further detailed analysis was done using CasaXPS (v 2.3.16 PR 1.6).

5.3 Results and discussion

5.3.1 General characterization of PEO-PDMSPNB membranes

The compositions of PEO-PDMSPNB membranes were determined using FTIR (Figure 5.1). For the PEO moiety, the CH_2 scissoring and CH_2 asymmetric bending bands are observed at 1448 cm^{-1} and 1351 cm^{-1}, respectively.[208-210] The absorption band located at 1110 cm^{-1} for the C-O-C stretching mode is covered by Si-CH_3 symmetric deformation. For PDMS, the CH_3 asymmetric deformation is observed at 1408 cm^{-1}.[181] The systematic change of PEO and PDMS peaks can be observed in Figure 5.1(b). With increasing PEO feed ratio, the CH_2 scissoring and CH_2 asymmetric bending peaks show an increase relative to the CH_3 asymmetric deformation peaks of PDMS, indicating higher PEO content in the copolymer membranes.

The tensile properties, e.g. Young's modulus(Et), ultimate tensile strength (MPa) and elongation at break(ε), of PEO-PDMSPNB membranes were tested by Dynamic Mechanical Analysis (DMA). The data are shown in Figure 5.2 and Table 5.1. The obtained results agree well with the previously reported PDMS materials.[211, 212] Due to the rubbery nature of PEO-PDMSPNB membranes, Young's modulus values are ranged from 0.15 to 0.40 MPa, while the elongation is around 100-200%.

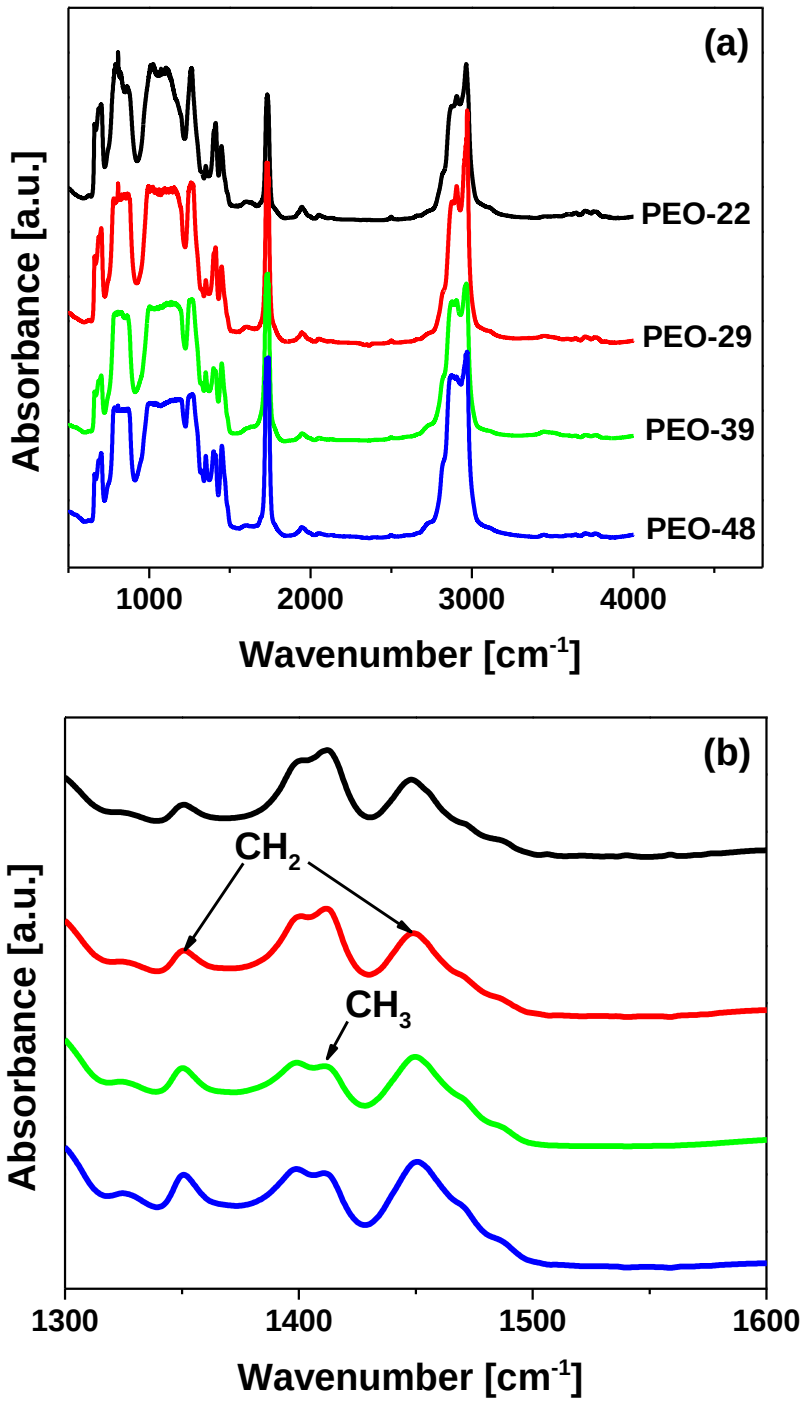

Figure 5.1 (a) FTIR spectra of PEO-PDMSPNB membranes and (b) zoomed in spectra (1300 cm^{-1} to 1600 cm^{-1}) demonstrating the systematical change of CH_2 scissoring and CH_2 asymmetric bending peaks of PEO and CH_3 asymmetric deformation peaks of PDMS.

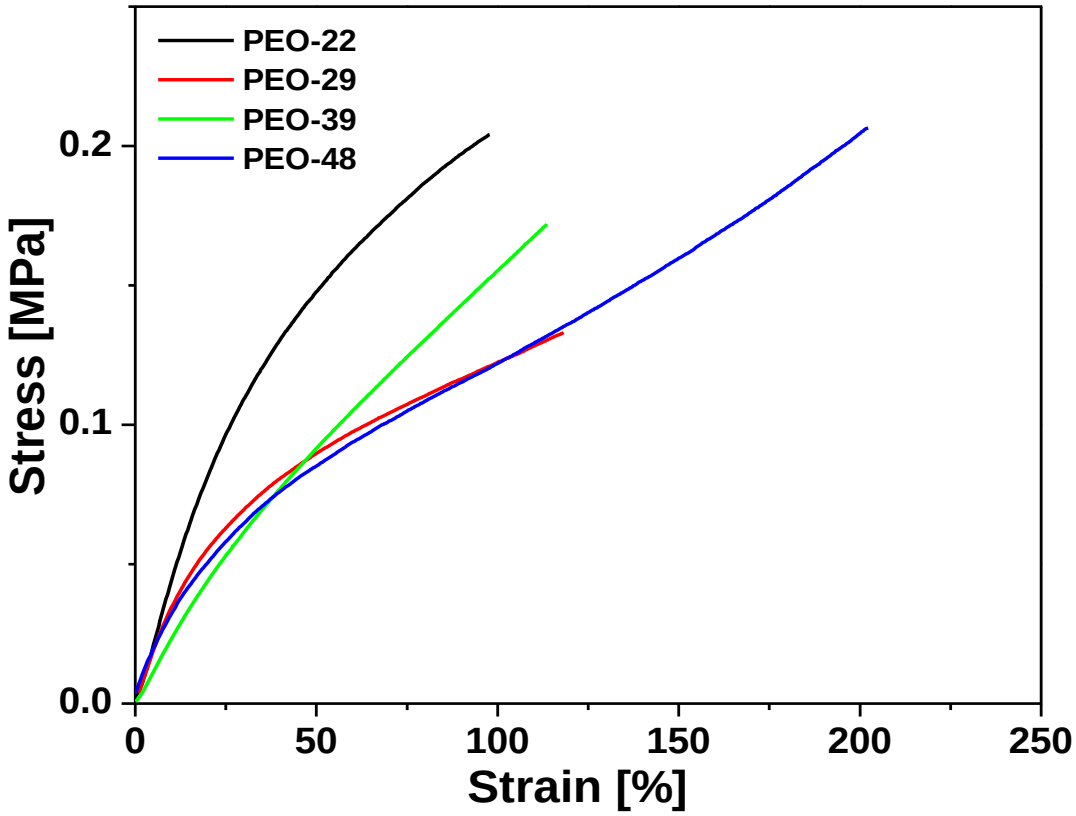

Figure 5.2 Tensile property of PEO-PDMSPNB membranes.

Table 5.1 Tensile test data of PEO-PDMSPNB membranes.

Sample	Et(MPa)	Ultimate tensile strength (MPa)	ε (%)
PEO-22	0.21	0.20	97.9
PEO-29	0.39	0.13	118.2
PEO-39	0.14	0.17	113.6
PEO-48	0.37	0.21	202.3

The differential scanning calorimetry (DSC) data for PEO-PDMSPNB membranes are present in Figure 5.3, and the glass transition temperatures (T_g) are summarized in Table 5.2. The glass transition process for PDMS can be estimated from both the transition process in reversible heat flow curves (Figure 5.3 (a)) and the peak position in the derivative curves (Figure 5.3 (b)). The glass transition process for PEO segment is masked by the PDMS melting process and can only be seen from the derivative curves. The T_g values for both PDMS ($T_{g,1}$,-124 °C) and PEO ($T_{g,2,}$ around -58°C) agree well with previously reported data.[213, 214]

The presence of two T_g values suggests the occurrence of phase separation between the two chemical compositions. The morphology of the PEO-PDMS membrane was further investigated by Small-Angle X-ray Scattering (SAXS) measurement (Figure 5.4). The appearance of a broad peak at 0.02 $Å^{-1}$ confirms the phase separation of the two polymer components. However, SAXS data also indicate the lack of long-range order in their morphology due to no presence of ordered multiple peaks and the formation of the very broad first diffraction peak.

For all measured samples, the crystallization and melting processes of PDMS are observed (Figure 5.3 (a)). However, the PEO melting temperature is usually around 70 °C,[200, 215] which was not observed in DSC thermograms, indicating no measurable crystallization of PEO segments. This is likely due to the use of short chain PEO (4 repeating units), as well as the introduction of cross-linking, which prevent the polymer chains from forming an ordered crystalline region. The suppression of crystallization could well contribute to the improvement of gas diffusivity.

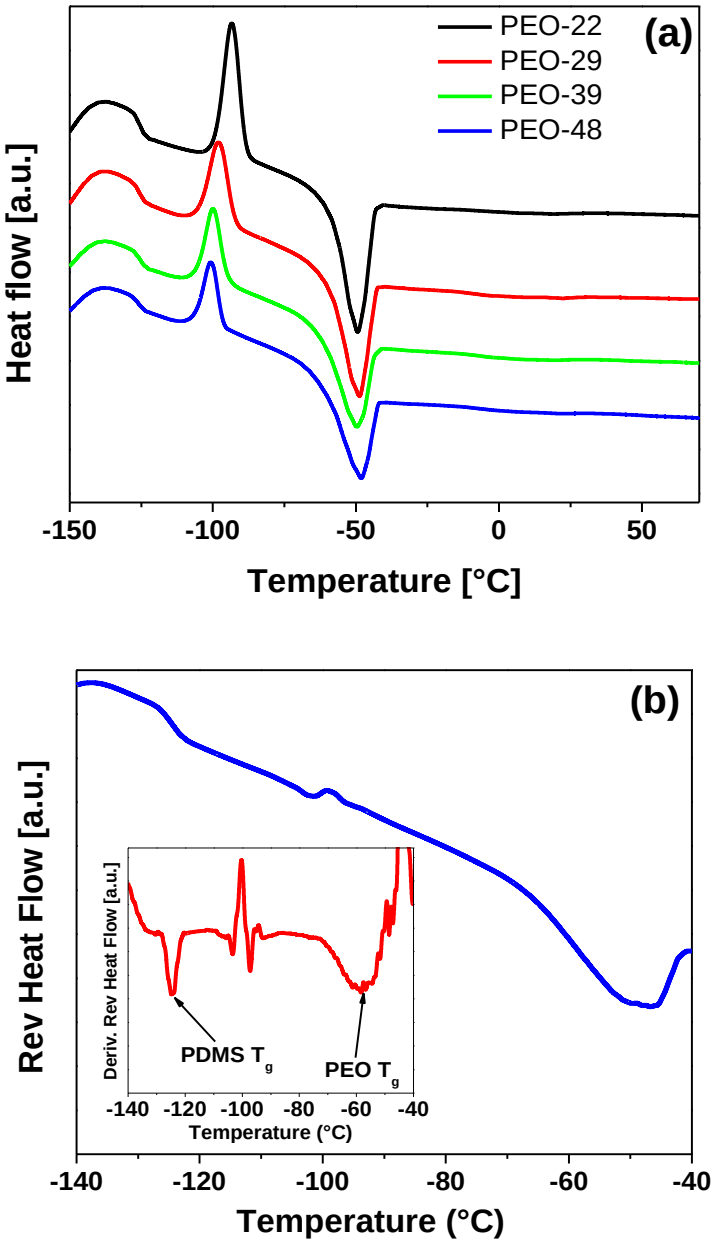

Figure 5.3. (a) DSC curves for PEO-PDMSPNB membranes. All curves have been shifted vertically to illustrate the systematic change of the peak shape and positon. (b) Reversible heat flow curve of PEO-50 membrane. Inset is the derivative of reversible heat flow change. The T_g is determined from both the transition process in reversible heat flow curves and the peak position in the derivative curves.

Table 5.2 Summary of density, membrane composition, glass transition temperature and gas transport properties for PEO-PDMSPNB samples.

Sample*	Density (g/cm^3)	$T_{g,1}$ (°C)	$T_{g,2}$ (°C)	P_0 [Barrer]		CO_2/N_2 selectivity	m×10^3 [1/atm]	
				CO_2	N_2		CO_2	N_2
XLPDMSPNB[160]	0.98	-125	-	6700	490	13.8	-	
PEO-22	0.98	-124	-53	6200 ± 70	770 ± 10	8.1 ± 0.2	18.5 ± 0.1	19.0 ± 0.3
PEO-29	1.01	-124	-54	4600 ± 60	370 ± 10	12.4 ± 0.2	9.0 ± 0.1	28.6 ± 0.5
PEO-39	1.04	-124	-57	3400 ± 20	180 ± 10	18.8 ± 0.4	20.9 ± 0.1	15.0 ± 0.8
PEO-48	1.06	-124	-58	2300 ± 30	120 ± 5	19.2 ± 0.5	-17.4 ± 0.1	-20.1 ± 1.3

*Membrane composition determined using TGA.

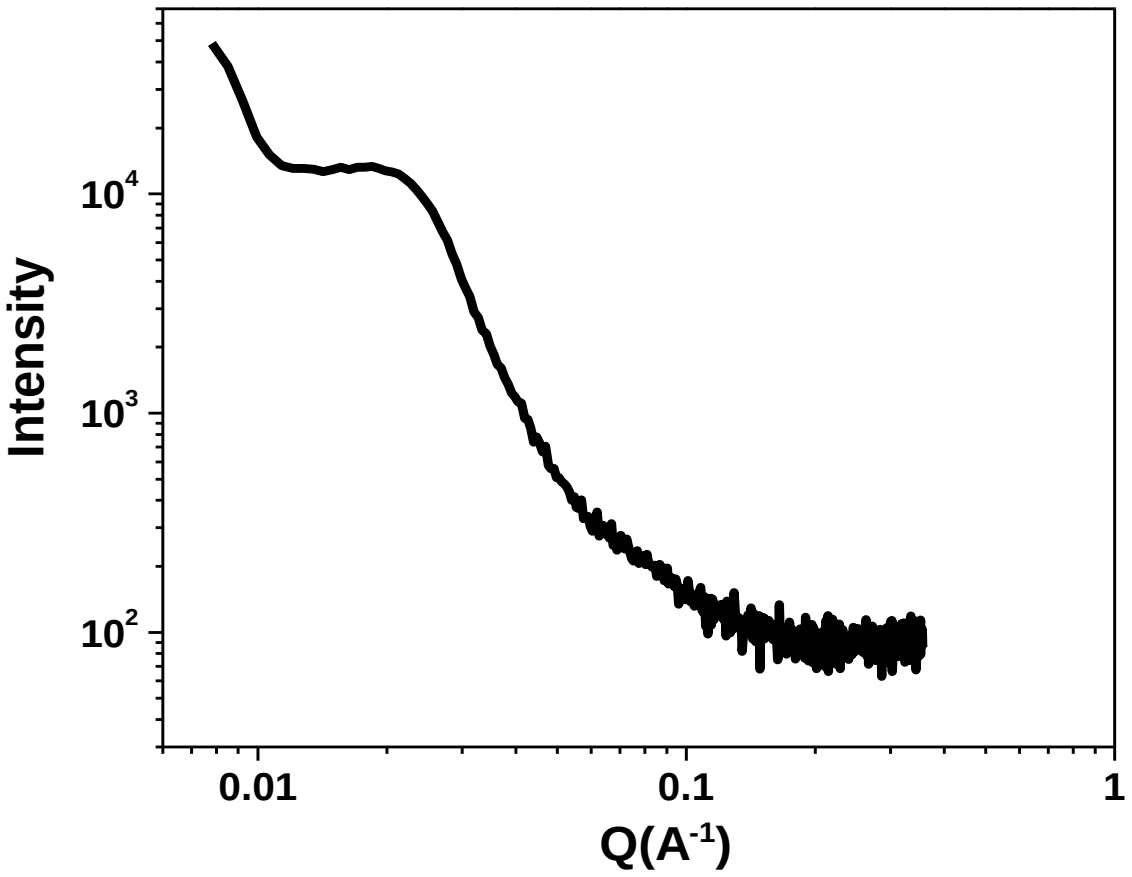

Figure 5.4 SAXS profile of the PEO-48 membrane.

The thermogravimetric analysis (TGA) results for PEO-PDMSPNB membranes are shown in Figure 5.5. The PEO-PDMSPNB copolymers show good thermal stability and exhibit a two-step decomposition, indicating that the PDMS and PEO components have different thermal stabilities. With higher PEO composition, the decomposition process shows a slight shift toward lower temperature. Based on previous studies, PDMS is typically stable until around 430 °C, while PEO is likely to be completely decomposed at this temperature.[216, 217] In this study, the PEO compositions are estimated from the weight percentage at second onset temperature (460 °C) and are summarized in Table 5.2. It is shown that the estimated PEO/PDMS composition is similar with the original feed ratio. The compositions of the PEO-PDMSPNB membranes were also investigated using X-ray photoelectron spectroscopy (XPS), [218] and representative spectra are shown in Figure 5.6. The main C-C bonding peak at 284.4 eV, the C-O peak located at 286.1 eV and small O-C=O peak observed at 288.8 eV originate from the PEONB moiety. The Si 2p 3/2 peak at 101.8 eV and Si 2p 1/2 peak at 102.3 eV represent the Si atom response in PDMS. The molar ratio of the two components was determined by the ratio of the integrated peak areas of Si and C-O peaks. As shown in Table 5.3, the comparison of PEO composition determined using TGA and XPS is presented. Although showing the same trend, the value of PEO content obtained from two measurements show some discrepancy. Taken into account that XPS is a surface-sensitive technique that probes the chemical composition at a depth of only a few nanometers from the surface, and the composition in this surface layer might differ from that in the bulk, the TGA data is used to determine the PEO content in the membranes.

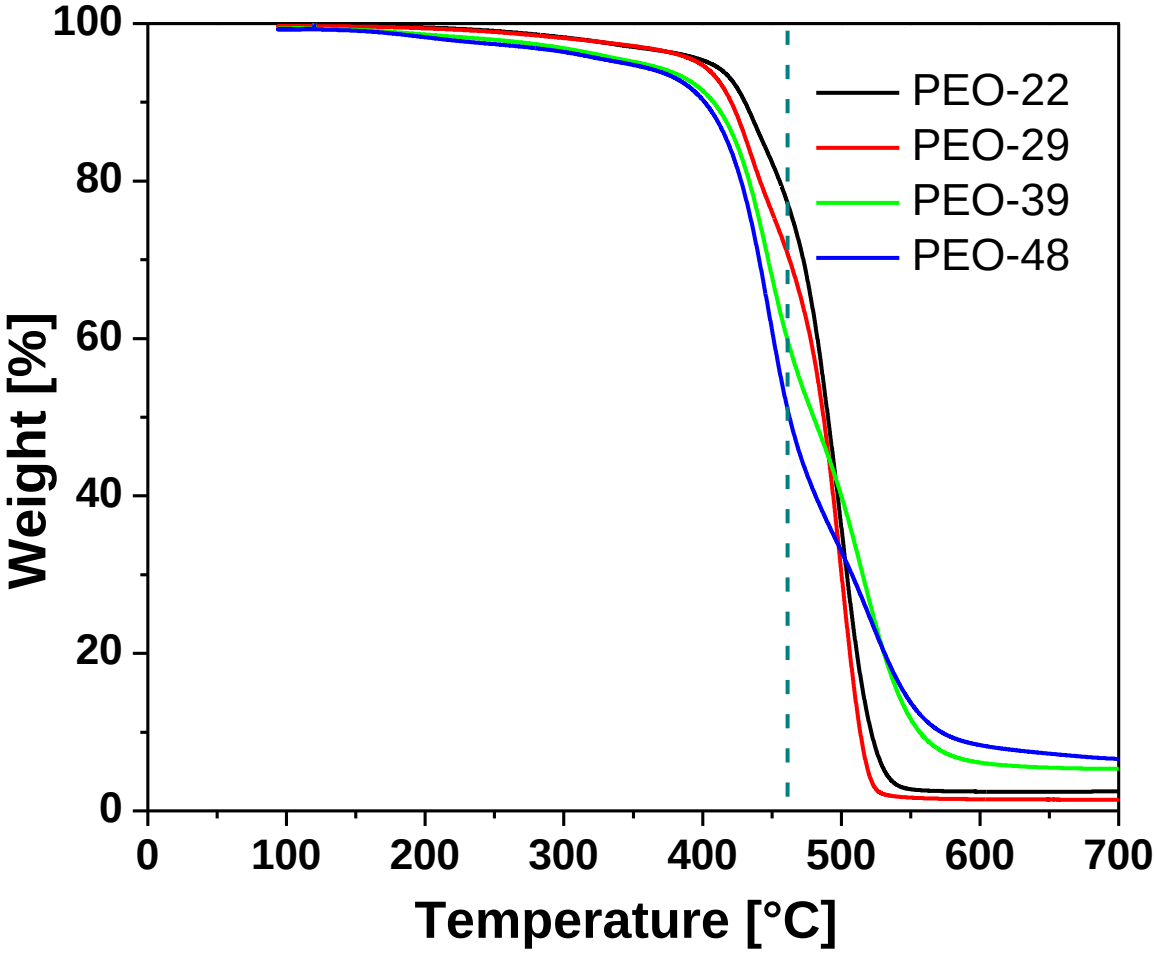

Figure 5.5 TGA curves of PEO-PDMSPNB membranes. Dashed line indicates the onset temperature of PDMS decomposition.

Figure 5.6 X-ray photoelectron spectra of PEO-PDMSPNB membranes. Fitting results for each component are shown in lines.

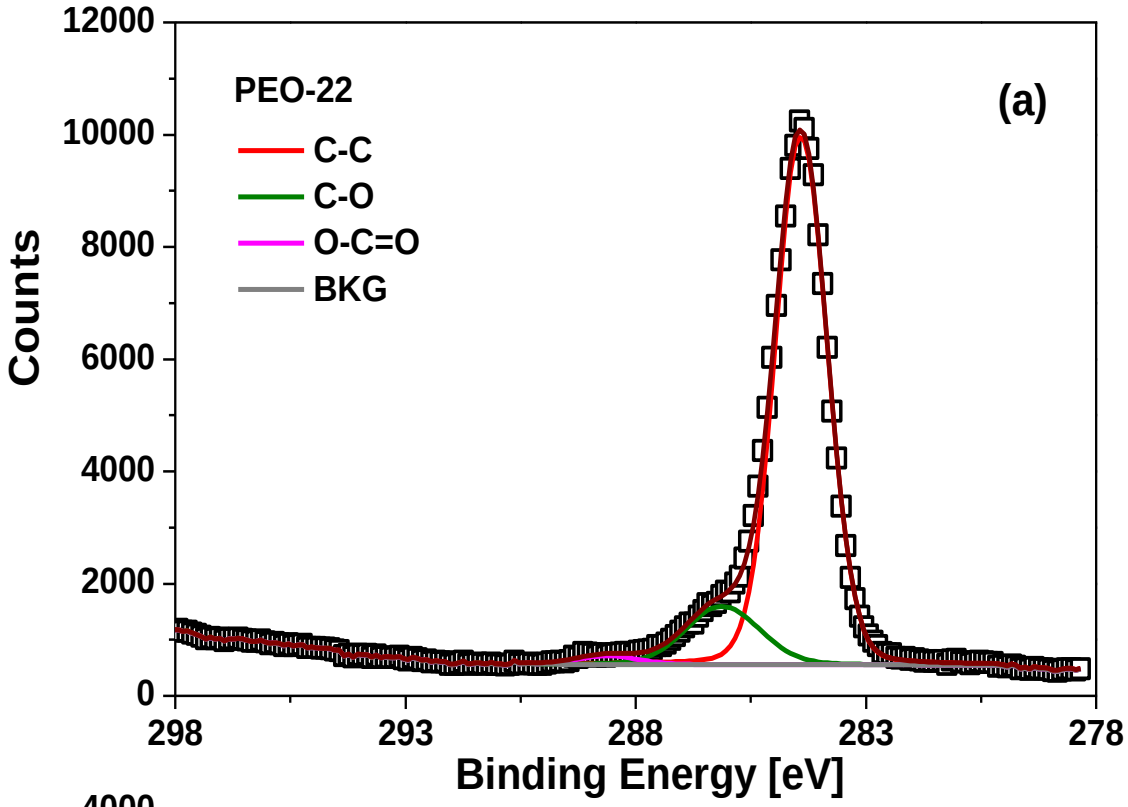

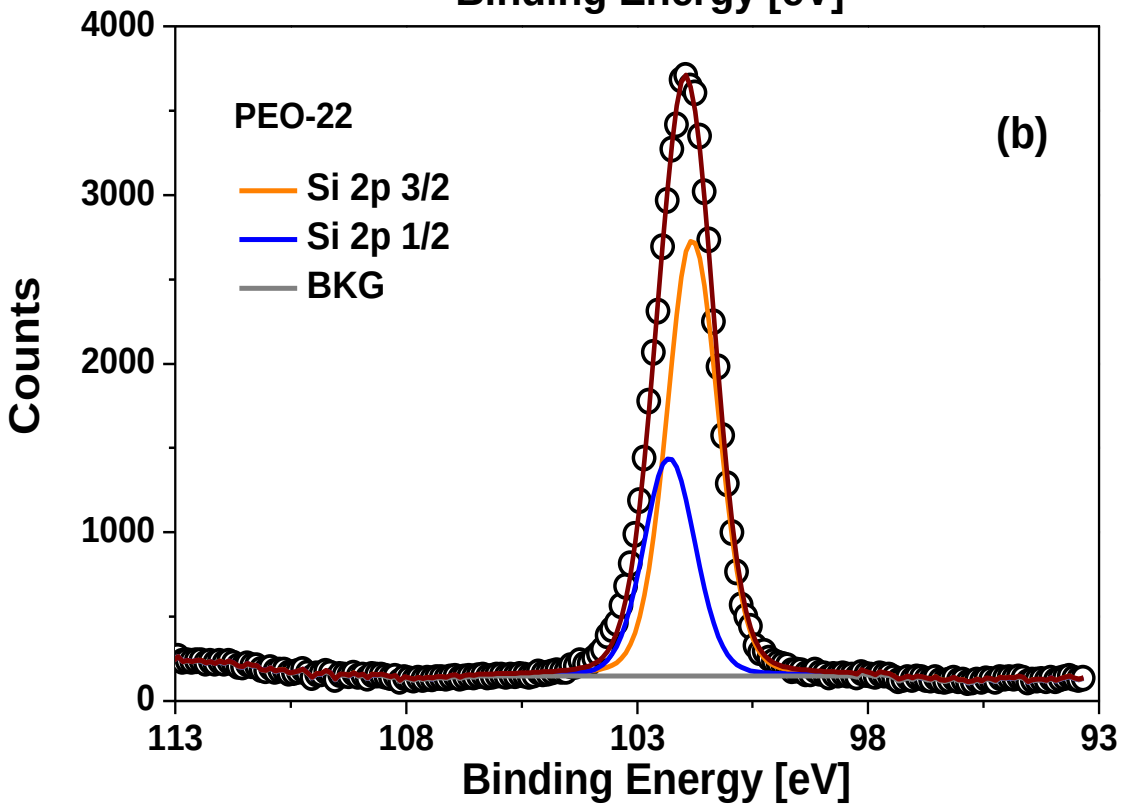

Figure 5.6 continued

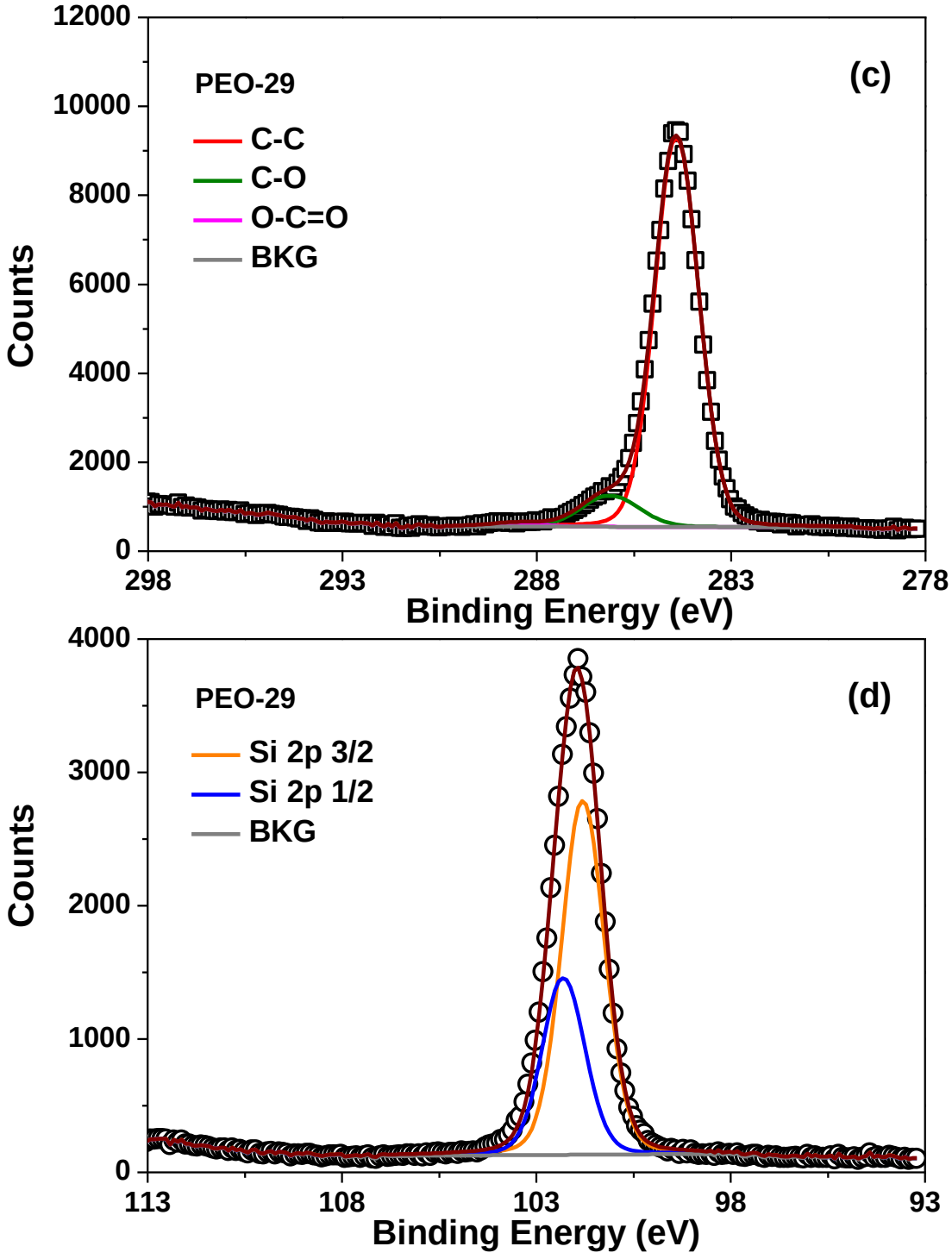

Figure 5.6 continued

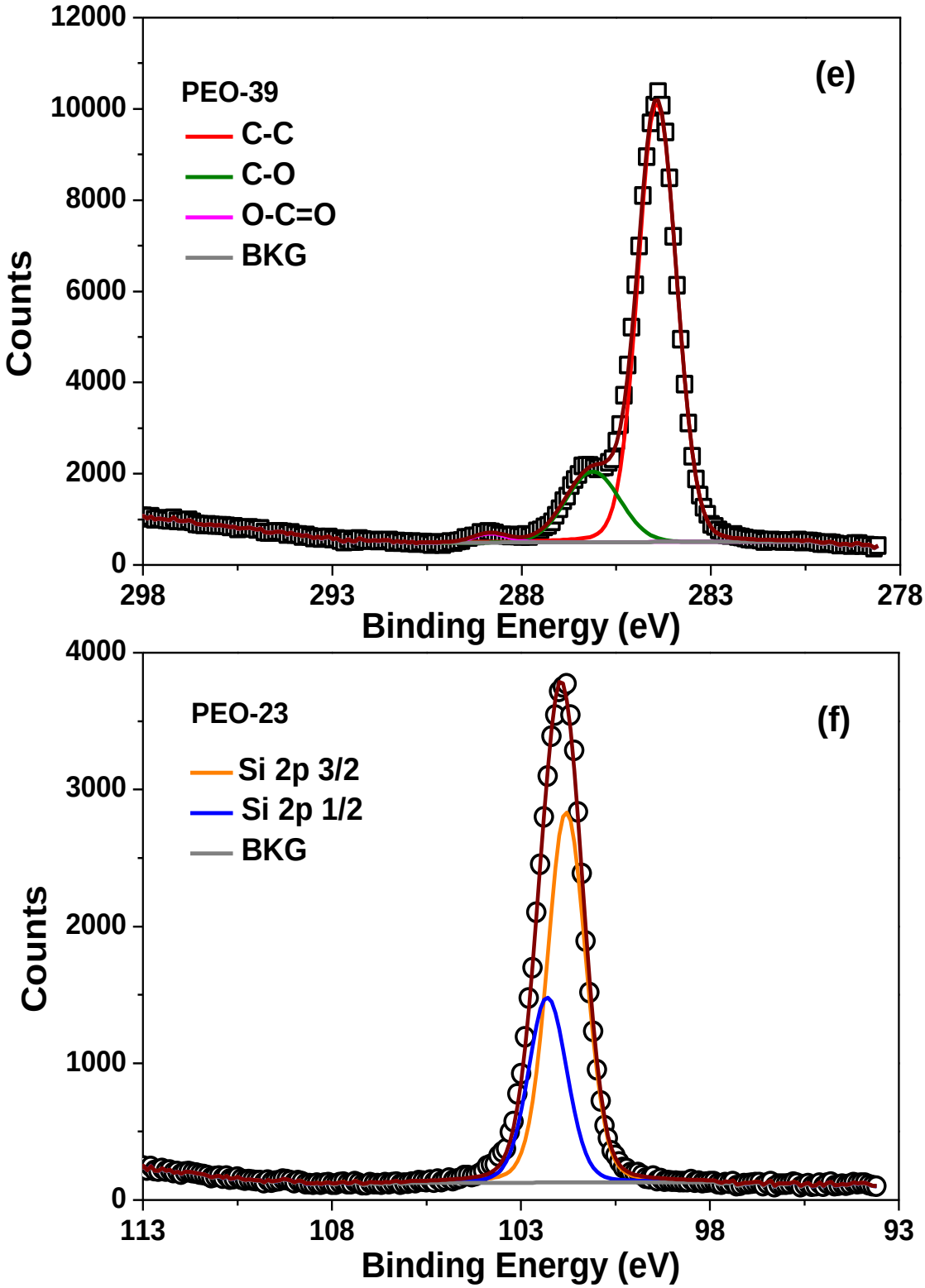

Figure 5.6 continued

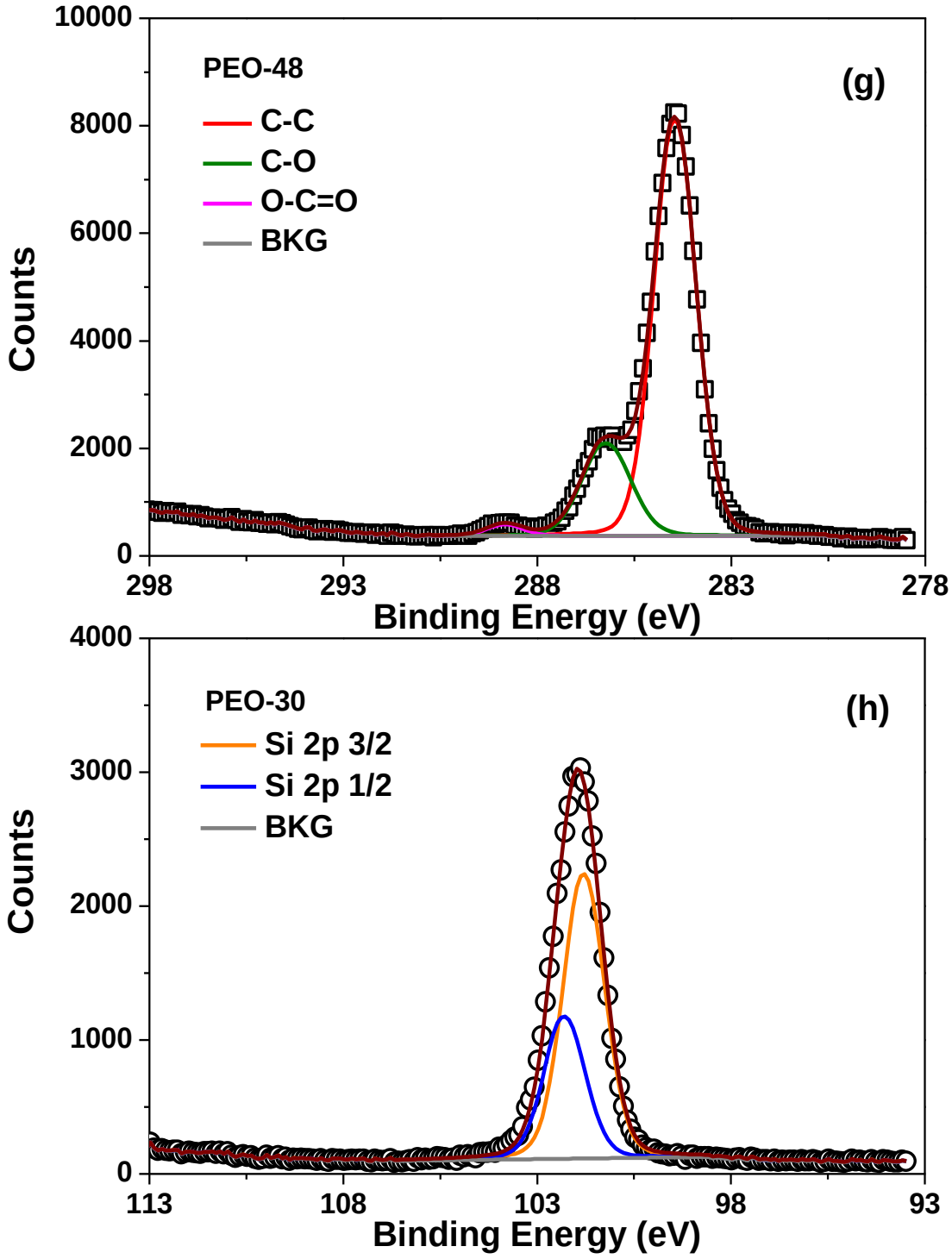

Figure 5.6 continued

Table 5.3 Comparison of PEO content obtained from TGA and XPS.

NB-PEO feed ratio (%)	Wt% residue at 460 °C	XPS composition (%)
20	22	10
30	29	14
40	39	23
50	48	30

5.3.2 Cross-link density of U-PDMS membranes

As illustrated in Scheme 5.2, the cross-linked membranes were synthesized *via* the isocyanate-amine ([NCO]-[NH_2]) reaction. A fixed molar ratio of reactive groups (isocyanate: amine = 1.05:1) was utilized. A decrease of polymer density with higher PDMS MW was observed, which was likely originated from the decrease of weight composition of the poly(hexamethylene diisocyanate) (ρ=1.12 g/cm^3) in the cross-link matrix.

To investigate the effect of PDMS MW, cross-link density of the polymer membranes was calculated *via* the following equation:[134]

$$c_x = \frac{2\rho}{3M_x} = \frac{2G'}{3RT} \quad (5.1)$$

where c_x is the moles of cross-links per unit volume, ρ is the density of cross-linked polymer, M_x is the number-average molecular weight of the polymer segments between cross-links, G' is the plateau value of real part of shear modulus, R is the gas constant, T is the temperature in Kelvin.

The plateau value of the real part of the shear modulus (*G'*) is shown in Figure 5.7 and summarized in Table 5.4. It is observed that the *G'* value generally decreases with higher PDMS MW, whereas the calculated M_x values show an increasing trend. Due to the use of a fixed isocyanate/amine ratio, low MW PDMS tends to form tighter and denser cross-link networks in the membrane. Thus, much stronger shear response is observed in low MW PDMS membranes.

5.3.3 Gas transport properties of PEO-PDMSPNB membranes

Gas permeabilities and CO_2/N_2 selectivites of the PEO-PDMSPNB membranes are shown in Figure 5.8 and summarized in Table 5.2. The gas permeability measurements are performed under different pressure: 0.2atm, 0.5atm, 1.0 atm and 1.5 atm and 2.0 atm. The gas permeability as a linear function of Δp can be written as:

$$P = P_0(1 + m\Delta p) \tag{5.2}$$

where P_0 is the permeability coefficient at Δp=0, the slope, *m*, characterizes the pressure dependence of permeability, and Δp is the pressure difference of upstream and downstream. Typically, the upstream pressure is much higher than the downstream. Thus, Δp is replaced by upstream feed pressure.

The results in Figure 5.8 demonstrate that the gas permeability showed some, but very weak dependence on feed pressure. Compared with gas permeability obtained at high pressure, the P_0 values always showed less than 5% difference. Consider the possible experimental error during the measurements, we assume that the gas permeabilities are independent on feed pressure in PEO-PDMSPNB membranes.

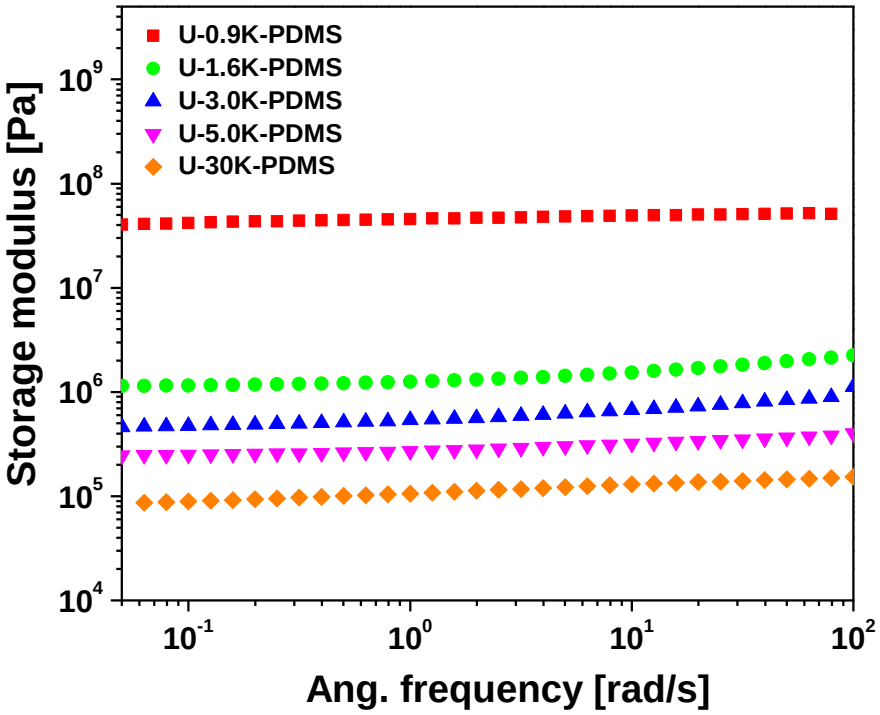

Figure 5.7 Storage modulus of the U-PDMS-NW measured from rheometer.

Table 5.4 Combined basic analysis of U-PDMS-NW derived from PDMS with different molecular weights.

Sample	Density (g/cm^3)	G' (Pa)	M_x (g/mol)	Cross-link density (mol/cm^3)
U-0.9K-PDMS	1.028	4.6×10^{7}	0.06×10^{3}	1.21×10^{-2}
U-1.6K-PDMS	1.023	1.5×10^{6}	1.60×10^{3}	4.01×10^{-4}
U-3.0K-PDMS	1.001	6.7×10^{5}	3.68×10^{3}	1.77×10^{-4}
U-5.0K-PDMS	0.996	3.2×10^{5}	7.71×10^{3}	8.50×10^{-5}
U-30K-PDMS	0.983	1.3×10^{5}	1.90×10^{4}	3.40×10^{-6}

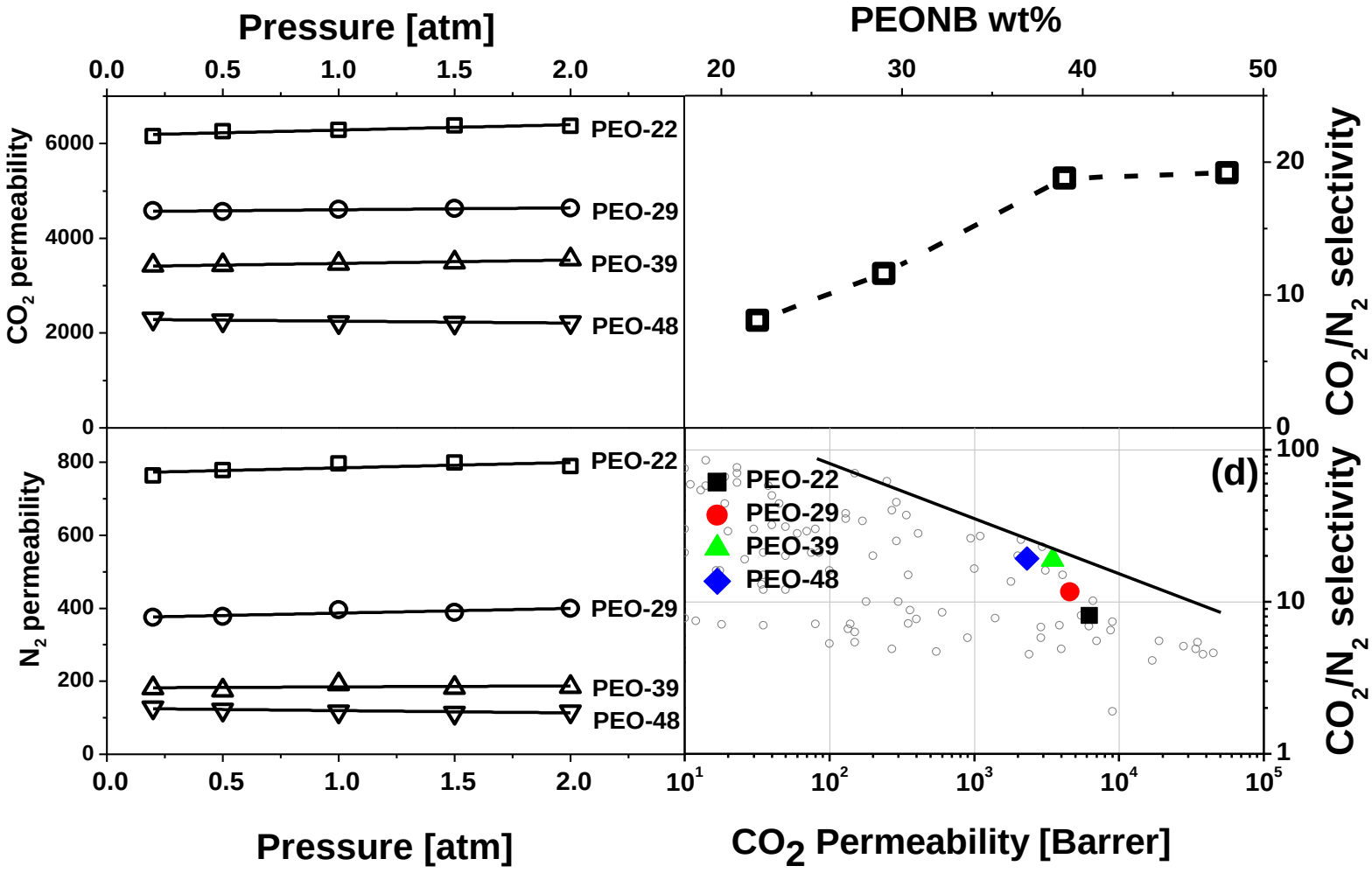

Figure 5.8 (a) CO_2 permeability, (b) N_2 permeability, and (c) CO_2/N_2 selectivity versus degree of CN group conversion (%) for the AO-PDMSPNB membranes. (d) Summary of the PEO-PDMSPNB membranes as a function of PEO content in a Robeson plot.

It can be noticed that both CO_2 and N_2 permeability follow a monotonous decreasing trend with higher PEO content in the membranes (Figure 5.8 (a) and (b)). When PEO content is low (22%), the gas permeability is still comparable to that of XLPDMSPNB.[160] After 48% PEO is incorporated, the CO_2 permeability exhibits about a 65% decrease. This drop of gas permeability is likely due to the incorporation of PEO components, which provide relatively slow CO_2 diffusion, as well as the short NB-PEO chains, which can form a more tightly cross-linked network, leading to the decrease of chain mobility/gas diffusivity. Moreover, the slight change of membrane density indicates the variation of chain packing efficiency/fractional free volume (FFV) in the membrane matrix. The higher PEO content membranes, which show slightly higher density, should possess decreased FFV, which could also contribute to the some decrease of gas diffusivity. Despite this, when compared to many previously reported PEO- containing membranes,[198, 199, 204, 205] our PEO-PDMSPNB membranes still show about one order of magnitude higher CO_2 permeability. For CO_2/N_2 selectivity, it is observed that the selectivity of PEO-22 and PEO 29 is lower than that of PDMSPNB. Due to the use of short chain NB-PEO, we have to significantly increase the cross-link density to form a free-standing film. The higher cross-link density could lead to a decrease in gas selectivity.[160] However, with the further increase of PEO content, the selectivity is enhanced. The improvement of CO_2/N_2 selectivity (Figure 5.8 (c)) relative to the XLPDMSPNB membranes reveals the great potential of PEO-PDMSPNB membranes for being applied in a practical flue gas treatment. When plotting the permeability data on a Robeson plot (Figure 5.8(d)), the highest performing sample (PEO-39) has achieved

parameters very close to the upper bound, indicating its advanced performance as compared with other purely polymeric membranes.

5.3.4 Gas transport property of U-PDMS membranes

To study the effect of PDMS MW on gas separation performance, each membrane was tested using the constant-volume variable-pressure gas flux method. All the membranes show much higher CO_2 permeability than that of N_2. The results of the permeability and gas selectivity values are summarized in Figure 5.9 and Table 5.5. It can be noticed that all gas permeabilities showed a monotonous increase with higher PDMS MW. As demonstrated in Table 5.4, compared with U-0.9K-PDMS, the cross-link density of U-30K-PDMS showed about 4 orders of magnitude decrease. It is reported in our previous work that, the denser cross-link network could significantly slow down the segmental dynamics of the PDMS matrix.[65] For rubbery polymers like PDMS, due to their low gas solubility, the gas permeability is predominantly determined by gas diffusivity (i.e. dynamics). Thus, with higher MW/lower cross-link density, the gas permeability increased. Moreover, it was reported that the intermolecular H-bonding could be formed within urethane junctions, leading to a further decrease of gas diffusivity.[20, 194, 207]

The CO_2/N_2 selectivity of U-PDMS showed a slight decrease with higher PDMS MW, while the CO_2/CH_4 selectivity remained similar. For rubbery polymers, due to their poor size-sieving capability, [88] the selectivity is typically determined by solubility selectivity. Because of the same PDMS material utilized in this study, it was within our expectation that the selectivity remained unchanged.

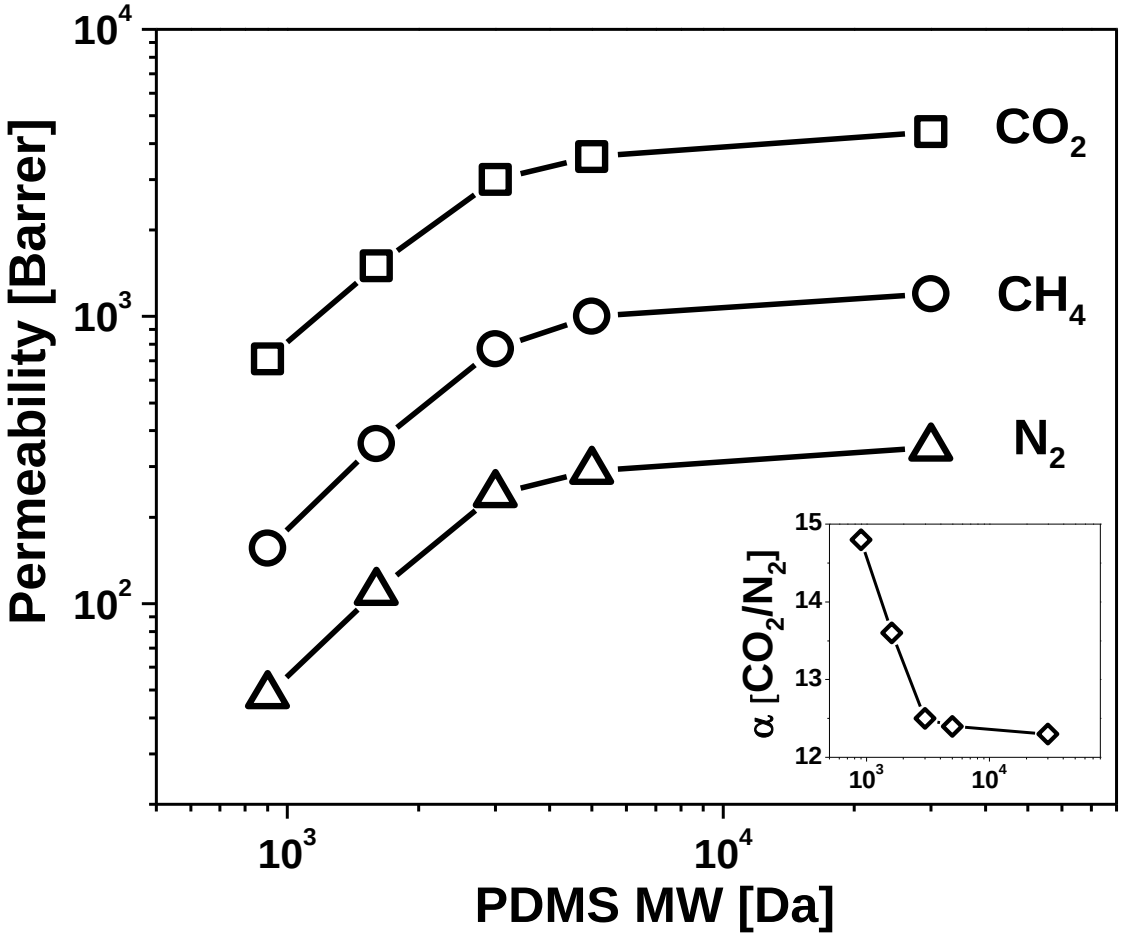

Figure 5.9 Gas permeability (CO_2, N_2 and CH_4) of the U-PDMS membranes as a function of the PDMS MW. Inset is the gas selectivity ($\alpha[PCO_2/PN_2]$) of U-PDMS.

Table 5.5 Summary of gas transport property of U-PDMS membranes.

Sample	Permeability [Barrer]			α [CO_2/N_2]	α [CO_2/CH_4]
	CO_2	N_2	CH_4		
U-0.9K-PDMS	710±40	48±12	156±12	14.8±0.3	4.6±0.3
U-1.6K-PDMS	1500±25	110±3	360±2	13.6±0.2	4.1±0.1
U-3K-PDMS	3000±50	240±5	770±15	12.5±0.1	3.9±0.1
U-5K-PDMS	3600±20	290±4	1000±20	12.4±0.1	3.6±0.1
U-30K-PDMS	4400±60	350±5	1200±50	12.3±0.2	3.6±0.2
U-PEO21-PDMS	500±10	32±1	109±3	15.6±0.2	4.6±0.2
U-PEO36-PDMS	390±5	13.1±0.7	62±2	30.0±1.6	6.3±0.2
U-PEO58-PDMS	111±1	2.7±0.1	6.9±0.1	41.4±0.6	15.9±0.2

5.3.5 Gas sorption measurements of PEO-PDMSPNB membranes

To further investigate the gas transport mechanism of PEO-PDMSPNB membranes, CO_2 sorption measurements were performed and the calculated solubility values are presented in Figure 5.10 and Table 5.6. Generally, for rubbery polymers, due to the low Langmuir sorption, the sorption behavior can be well-described by Henry's law. However, due to the existence of norbornene junctions, which serve as glassy domain in the polymer matrix, the Henry's law fitting was slightly deviated. Thus, the dual-mode model is used to fit the sorption curves.[123]

The fitting parameters are summarized in Table 5.6. For condensed rubbery films, the gas sorption capacity is low due to the low free volume. Thus, the amount of N_2 sorption is below the detection limit of the instrument and not reported here. It can be noticed that higher PEO content in the membrane leads to increased CO_2 solubility. Compared with XLPDMSPNB membranes, the incorporation of PEO moiety contributed to about 30% increase of CO_2 solubility. In Table 5.6, the k_D value generally increases with PEO incorporation, providing solid support that the incorporation of CO_2-philic PEO groups contribute to higher CO_2 dissolution into the polymer matrix. The decrease of C'_H (which reflects the sorption by FFV) parameter is likely due to the higher membrane density, which leads to the slight drop of FFV. Although the N_2 sorption cannot be measured, we expect that the decrease of C'_H value with more PEO in the polymer matrix should reduce the N_2 Langmuir sorption, and the non N_2-philic PEO moiety cannot compensate the solubility by increasing k_D value. Thus, the lower N_2 sorption should result in the enhancement of overall CO_2/N_2 solubility selectivity. However, after 39% PEO amount is

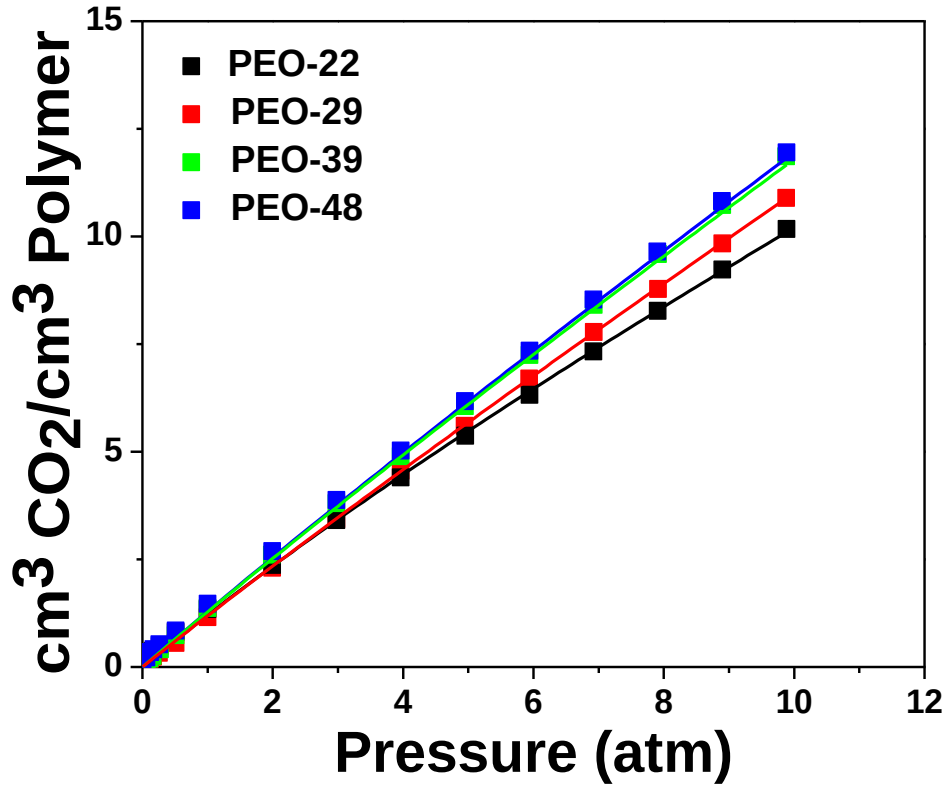

Figure 5.10 CO_2 sorption isotherms for PEO-PDMSPNB membranes. The solid curves show the fits to the dual-mode sorption model.

Table 5.6 Summary of dual-mode model parameters and CO_2 solubility for PEO-PDMSPNB membranes.

Sample code	k_D $\left[\frac{cm^3(STP)}{cm^3\ atm}\right]$	C'_H $\left[\frac{cm^3(STP)}{cm^3}\right]$	b $[atm^{-1}]$	S $\left[\frac{cm^3(STP)}{cm^3\ atm}\right]$
PEO-22	0.78	4.55	0.1	1.16
PEO-29	0.91	3.50	0.1	1.20
PEO-39	1.06	2.44	0.1	1.26
PEO-48	1.07	2.32	0.1	1.27
XLPDMSPNB[160]	-	-	-	0.9-1.0

reached, no further change of selectivity is observed with the increase of PEO content. Feng *et al* and Reijerkerk *et al* also reported the plateauing behavior of CO_2/N_2 selectivity with high PEO content in their studies.[97, 198] Based on their explanation and the gas separation performance of our membranes, we expect that when PEO composition is lower than 39%, the gas selectivity is predominantly influenced by solubility selectivity. After the PEO incorporation of 39% is reached, the CO_2 solubility saturates due to the intrinsically limited PEO sorption capability. This could be likely attributed to plasticization effect within membrane matrix, which leads to no further change of gas selectivity with more PEO content.

5.3.6 Impact of PEO functionality in U-PDMS membranes

Although showing higher permeability, the CO_2/N_2 selectivity of U-PDMS membranes (~14) are still below practical requirements. Thus, the PEO functionality is incorporated into the U-0.9K-PDMS matrix *via* the same isocyanate-amine reaction. By varying the feed ratio, membranes with PEO wt% from 21%-58% are synthesized. The gas transport property of U-PEO-PDMS membranes and Robeson plot are demonstrated in Figure 5.11 and summarized in Table 5.5. With higher PEO content, the gas permeability shows a decreasing trend, which agrees well with the PEO-PDMSPNB membranes discussed before. When PEO wt% reaches 58%, all gas permeabilities show more than 85% decrease. For N_2 and CH_4, the permeabilities demonstrate about 95% drop compared to U-0.9K-PDMS (0 wt% PEO). The major reason for permeability reduction is likely the much slower diffusivity in PEO moiety. Moreover, the incorporation of short-chain PEO could form tighter cross-link networks, therefore further reducing the gas diffusivity.

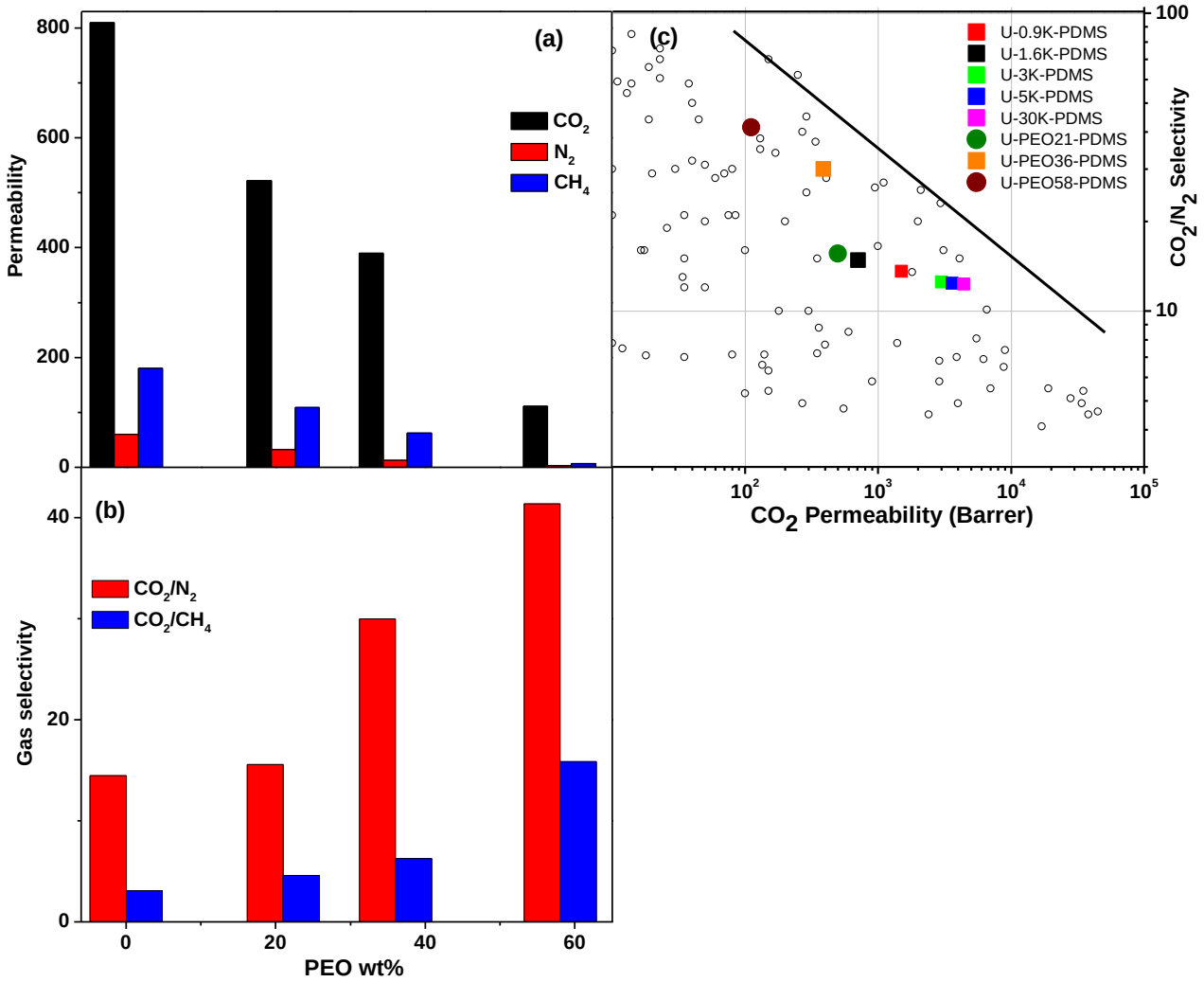

Figure 5.11 Gas transport properties of the U-PEO-PDMS membranes as a function of PEO wt%.

Despite the huge drop in gas permeability, with the incorporation of PEO functionality, both CO_2/N_2 and CO_2/CH_4 selectivity show a factor of 3 increase. As mentioned before, the CO_2-philic, polar PEO groups could enhance the polymer-CO_2 interaction, thus increasing the dissolution of CO_2 into the polymer materials and increase solubility selectivity. Compared with PEO-PDMSPNB membranes, the highest performing U-PEO58-PDMS membrane showed a factor of 2 increase of CO_2/N_2 selectivity (41 *versus* 19). This is likely due to the large increase of PEO wt% in the membrane matrix. Based on our calculation, the highest PEO content PEO-PDMSPNB membrane contains about 48 wt% of NB-PEO moiety. However, the PEO functionality only makes up about 70 wt% of NB-PEO. Thus, the actual PEO content in PEO-PDMSPNB membrane is about 34 wt%, which is much lower than that in PEO58-PDMS membrane. In both membrane matrices, the PEO moiety performs as the CO_2-interactive segments, which contributes to the enhanced CO_2/N_2 solubility selectivity. The significant difference of PEO amount leads to the large discrepancy in gas selectivity. Moreover, based on our simulation study, longer PEO chains, which offer additional ether oxygen linkages for CO_2 interaction, showed higher CO_2 binding energies than shorter chain PEO. The poly(oxyethylene bis(amine)) used for U-PDMS membranes has ~22 EO units, which is much longer than 4EO oligomer used for PEO-PDMSPNB membranes. This also in part contributed to the increase of CO_2/N_2 selectivity in U-PDMS membranes.

5.4 Conclusion

In conclusion, we have synthesized two series of PEO-containing PDMS membranes: PEO-PDMSPNB and U-PEO-PDMS. Most of synthesized membranes exhibit

significantly higher CO_2 permeability than previously reported PEO-containing membranes. The highest performing PEO-PDMSPNB membrane with 39% PEO content, exhibiting CO_2 permeability ~3400 Barrer and CO_2/N_2 selectivity ~19, has achieved performance very close to the Robeson upper bound, and its highly permeable nature could potentially benefit practical flue gas separation. The U-PEO58-PDMS membrane exhibits the CO_2/N_2 selectivity of 41, which has already met the practical requirements for flue gas treatment.

The PEO content was found to significantly influence gas separation performance, which has been attributed to controlling CO_2 solubility within the copolymer matrix. Furthermore, these results demonstrate that by careful tuning of the PEO/PDMS composition, it is possible to significantly increase CO_2/N_2 selectivity with a small loss in permeability. These findings provide strong support to practical CO_2 separation material development as well as fostering fundamental understanding of the gas separation process using polymer membranes.

CONCLUSIONS AND FUTURE WORK

Conclusions

Membrane separation is highlighted as one of the most promising approaches to mitigate the excessive CO_2 emission, due to its significant reduction of energy cost compared with many conventional separation techniques. Unfortunately, the separation performance of current membranes does not meet the practical CO_2/N_2 separation requirements. And because of the huge volume of industrial flue gas emission, membranes with high permeability are needed for practical reasons.

Currently, the separation mechanism of most polymeric membranes is based on size-sieving. However, this method is not sufficient for CO_2/N_2 separations due to the similar kinetic diameters of CO_2 (3.30 Å) and N_2 (3.64 Å). Thus, developing a new method based on a non-size sieving mechanism could offer a solution to the improvement of CO_2/N_2 separation efficiency.

In this study, we focused on the development of high-performing polymer materials, as well as fostering fundamental understanding in the gas separation field. Two polymer systems, the rubbery PDMS and glassy PTMSP, and two CO_2-philic functionalities, AO and PEO, were investigated. The main experiments performed were the gas permeation test, gas sorption test, along with a variety of polymer characterization techniques. By carefully tuning of membrane composition and detailed analysis of experimental data, we were able to demonstrate how the tuning of solubility selectivity could help enhance CO_2/N_2 separation performance.

Firstly, the lightly cross-linked PDMSPNB membranes was developed *via* the *in-situ* ROMP. The novel cross-linked PDMSPNB membranes achieved excellent CO_2 permeability with good selectivity (a factor of two improvement in CO_2 permeability and CO_2/N_2 selectivity over the well-studied conventional cross-linked PDMS), and their performance is very close to the Robeson upper bound line. The unprecedented performance by a careful design of the macromolecular architecture and cross-link mechanism has revealed the strong potential of the rubbery polymer, PDMS, for gas separation. The key factor to the improved performance was ascribed to the much faster segmental dynamics in our membranes.

In the following work, different functionalities with high CO_2 affinity were incorporated into the polymer systems. Among the various CO_2-philic groups that have been reported, we chose AO group. The effect of AO incorporation was examined in two different polymer systems: PDMS and PTMSP. The degree of amidoximation was found to significantly alter gas separation performance in both rubbery and glassy systems, which has been attributed to CO_2 binding affinity and H-bonding within the AO functionalities. The highest performing membranes (AO-12-PDMSPNB and AO-31-PTMSP) showed significantly enhanced performance relative to our earlier studied PDMSPNB and PTMSP membranes. These significant gains allowed AO-12-PDMSPNB and AO-31-PTMSP to exceed/achieve the Robeson upper bound at very high permeability (6800 Barrer and 6000 Barrer, respectively), which is critical for practical applications in treating the enormous amount of flue gases generated by power plants.

Lastly, to further investigate the effect of CO_2-philic groups on the gas separation performance, two series of PEO-containing PDMS membranes: PEO-PDMSPNB and U-PEO-PDMS, were studied. The fabricated membranes exhibit significantly higher CO_2 permeability than previously reported PEO-containing membranes. The highest performing PEO-PDMSPNB membrane with 39% PEO content, exhibiting CO_2 permeability ~3400 Barrer and CO_2/N_2 selectivity ~19, has achieved performance very close to the Robeson upper bound. The U-PEO58-PDMS membrane achieved the CO_2/N_2 selectivity of 41, which has already met the practical requirements for flue gas treatment. The PEO content was found to significantly influence gas separation performance, which has been attributed to controlling CO_2 solubility within the copolymer matrix.

Overall, our findings on these novel membranes could open up a new approach to enhance performance for gas separation and could elucidate additional factors for the gas separation mechanisms in the field. Moreover, from an industrial viewpoint, according to Merkel *et al.*'s study,[89] our membranes could offer the permeance of thousands of GPU if thin membranes could be cast and coated on the gas separation media. This should allow reduction of CO_2 capture cost to less than $20 per ton.

Future work

PEO-PDMS membranes *via* Thiol-ene click reaction

As shown in Chapter 5, PEO-PDMS membranes exhibit huge potential for practical CO_2 separation application. Thus, developing a facile and efficient route to synthesize PEO-PDMS membranes could lead to great improvement of membrane performance.

Among a variety of synthetic techniques, the thiol-ene click route was selected. The thiol-ene reaction is happened *via* the hydrothiolation of a carbon-carbon double bond. They are widely used in various cross-linking reaction due to their advanced properties, e.g. facile and fast synthetic strategies, versatility in different reaction solvents/conditions, well-defined reaction products, etc.[219-221] In our proposed experiments, a series of PEO-PDMS copolymer membranes will be synthesized *via* the thiol-ene reaction.

As shown in the following scheme, the mercaptopropyl methyl siloxane (SMS-992) is used to provide "thiol" functionality, and the cross-linked network is formed by the reaction of SMS-992 and acryloxy terminated ethyleneoxide dimethylsiloxane-ethyleneoxide copolymer (DBE-U22). By tuning the PEO-(DBE-U22) composition, we expect to observe the systematical change of thermal, mechanical and gas transport properties of the thiol-ene membranes. In our preliminary experiments, all the membranes were formed *via in-situ* thiol-ene cross-linking and the reactions were finished in 3 minutes. The copolymer membrane with 75 mol% PEO content showed CO_2 permeability ~ 960 Barrer and CO_2/N_2 selectivity of 39, which has already achieved above the Robeson upper bound. In the future study, in order to obtain the highest performing membrane, the effect of various parameters, e.g., membrane composition, synthetic procedures, initiator amount will be investigated in detail.

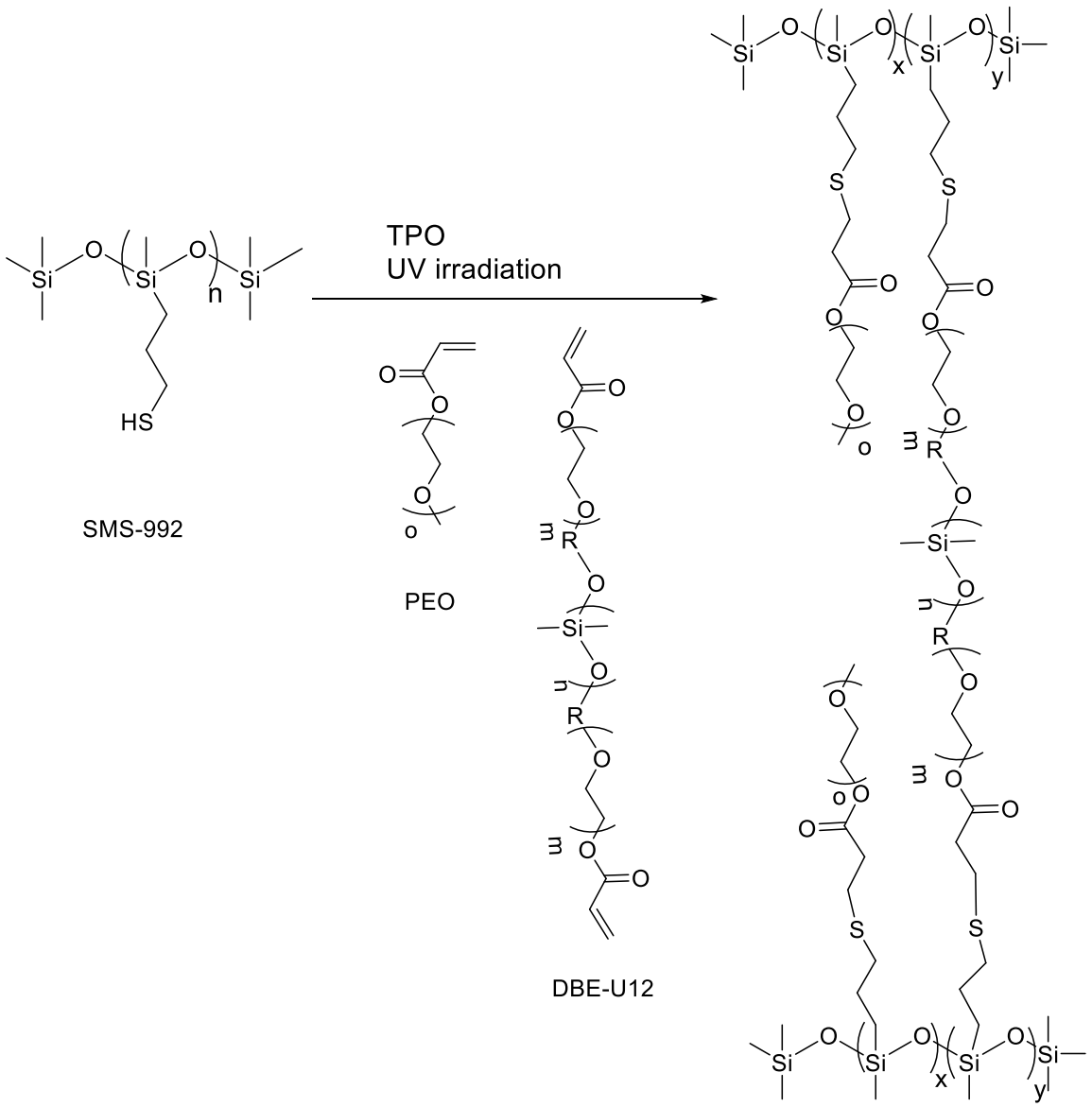

Synthetic mechanism of PEO-PDMS cross-linked membranes *via* Thiol-ene reaction.

Development of polymer-composite membranes

To overcome the trade-off relation between permeability and selectivity, a variety of fillers are added to the polymer matrix to fabricate the composite membranes. In current studies, two types of fillers, porous and nonporous fillers, are used for different purposes. The typical porous fillers include: carbon molecular sieves, zeolites, zeolite imidazole frameworks (ZIFs), metal organic frameworks (MOFs), porous organic cages (POCs) and carbon nanotubes (CNTs). Nonporous fillers include: titanium dioxide (TiO_2), silica (SiO_2), polyhedral oligomeric silsesquioxane (POSS), magnesium oxide (MgO), calixarenes and nanohydrogels (NHs).

By the addition of fillers into the polymer matrix, the gas transport property is influenced from three aspects: (1) the chain packing capability is tuned and the free volume of the polymer is changed, (2) some fillers contains CO_2-philic functionality, which could help increase CO_2 solubility in the membrane matrix, (3) some fillers are functionalized to possess CO_2-reactive carriers to facilitate the transport of CO_2 molecules.[104]

In the proposed experiments, a variety of fillers, e.g. silica nanoparticles, POSS particles, MOFs and other custom-synthesized fillers, will be added into the polymer membranes. In our preliminary studies, the incorporation of 10 wt% silica nanoparticles (Nissan Chemicals, 40nm) contributed to a factor of 2 increase of CO_2 permeability in XLPDMSPNB membranes. In the following study, the filler type, membrane composition and synthetic method will be discussed and we expect to observe a further increase of both gas permeability and selectivity in designed materials.

Incorporation of CO_2-philic Ionic liquids

By the carefully design of chemical structures, Ionic liquids (ILs) could provide a unique and desirable physicochemical properties such as low volatility, strong CO_2 interaction, and high CO_2/gas selectivity. Various ILs have been developed for gas separation applications, including imidazolium-based ILs, amino acid-based ILs, protic ILs and amine-based ILs. It was reported that the performance of ILs are influenced by different factors, e.g. viscosity, cation size, molar volume and density. Currently, poly(ionic liquid) membranes (PILMs), supported ionic liquid membranes (SILMs), poly(ionic liquid)-ionic liquid composite membranes, ion-gel membranes and polymer-ionic liquid composite membranes have been reported for the CO_2 separation purposes.[222, 223] In our proposed experiments, ILs with strong CO_2 binding energy/affinity will be blended/coated with high permeable polymers to further enhance gas selectivity. The selection of ILs, membrane composition and synthetic route will be investigated.

REFERENCES

1. Paul, D. R.; Yampol'skii, Y. P., *Polymeric gas separation membranes*. CRC press: 1993.

2. Freeman, B.; Yampolskii, Y.; Pinnau, I., *Materials science of membranes for gas and vapor separation*. John Wiley & Sons: 2006.

3. Wijmans, J.; Baker, R. The solution-diffusion model: a review. *Journal of membrane science* **1995,** 107 (1-2), 1-21.

4. Robeson, L. M. Correlation of Separation Factor Versus Permeability for Polymeric Membranes. *Journal of Membrane Science* **1991,** 62 (2), 165-185.

5. Robeson, L. M. The upper bound revisited. *Journal of Membrane Science* **2008,** 320 (1), 390-400.

6. Freeman, B. D. Basis of permeability/selectivity tradeoff relations in polymeric gas separation membranes. *Macromolecules* **1999,** 32 (2), 375-380.

7. Robeson, L.; Burgoyne, W.; Langsam, M.; Savoca, A.; Tien, C. High performance polymers for membrane separation. *Polymer* **1994,** 35 (23), 4970-4978.

8. Robeson, L. M.; Liu, Q.; Freeman, B. D.; Paul, D. R. Comparison of transport properties of rubbery and glassy polymers and the relevance to the upper bound relationship. *Journal of Membrane Science* **2015,** 476, 421-431.

9. Merkel, T. C.; Lin, H.; Wei, X.; Baker, R. Power plant post-combustion carbon dioxide capture: an opportunity for membranes. *Journal of membrane science* **2010,** 359 (1), 126-139.

10. Merkel, T. C.; Zhou, M.; Baker, R. W. Carbon dioxide capture with membranes at an IGCC power plant. *Journal of membrane science* **2012,** 389, 441-450.

11. Park, H. B.; Jung, C. H.; Lee, Y. M.; Hill, A. J.; Pas, S. J.; Mudie, S. T.; Van Wagner, E.; Freeman, B. D.; Cookson, D. J. Polymers with cavities tuned for fast selective transport of small molecules and ions. *Science* **2007,** 318 (5848), 254-258.

12. Park, H. B.; Han, S. H.; Jung, C. H.; Lee, Y. M.; Hill, A. J. Thermally rearranged (TR) polymer membranes for CO 2 separation. *Journal of Membrane Science* **2010,** 359 (1), 11-24.

13. Han, S. H.; Lee, J. E.; Lee, K.-J.; Park, H. B.; Lee, Y. M. Highly gas permeable and microporous polybenzimidazole membrane by thermal rearrangement. *Journal of Membrane Science* **2010,** 357 (1), 143-151.

14. Calle, M.; Lee, Y. M. Thermally rearranged (TR) poly (ether− benzoxazole) membranes for gas separation. *Macromolecules* **2011,** 44 (5), 1156-1165.

15. Budd, P. M.; Msayib, K. J.; Tattershall, C. E.; Ghanem, B. S.; Reynolds, K. J.; McKeown, N. B.; Fritsch, D. Gas separation membranes from polymers of intrinsic microporosity. *Journal of Membrane Science* **2005,** 251 (1), 263-269.

16. Ghanem, B. S.; McKeown, N. B.; Budd, P. M.; Al-Harbi, N. M.; Fritsch, D.; Heinrich, K.; Starannikova, L.; Tokarev, A.; Yampolskii, Y. Synthesis, characterization, and gas permeation properties of a novel group of polymers with intrinsic microporosity: PIM-polyimides. *Macromolecules* **2009,** 42 (20), 7881-7888.

17. McKeown, N. B.; Budd, P. M. Polymers of intrinsic microporosity (PIMs): organic materials for membrane separations, heterogeneous catalysis and hydrogen storage. *Chemical Society Reviews* **2006,** 35 (8), 675-683.

18. Choi, J. I.; Jung, C. H.; Han, S. H.; Park, H. B.; Lee, Y. M. Thermally rearranged (TR) poly (benzoxazole-co-pyrrolone) membranes tuned for high gas permeability and selectivity. *Journal of Membrane Science* **2010,** 349 (1), 358-368.

19. Freeman, B.; Pinnau, I. Separation of gases using solubility-selective polymers. *Trends in polymer science* **1997,** 5 (5), 167-173.

20. Lin, H.; Freeman, B. D. Materials selection guidelines for membranes that remove CO 2 from gas mixtures. *Journal of Molecular Structure* **2005,** 739 (1), 57-74.

21. Car, A.; Stropnik, C.; Yave, W.; Peinemann, K.-V. PEG modified poly (amide-b-ethylene oxide) membranes for CO 2 separation. *Journal of Membrane Science* **2008,** 307 (1), 88-95.

22. Li, Y.; Chung, T.-S. Molecular-level mixed matrix membranes comprising Pebax® and POSS for hydrogen purification via preferential CO 2 removal. *international journal of hydrogen energy* **2010,** 35 (19), 10560-10568.

23. Car, A.; Stropnik, C.; Yave, W.; Peinemann, K.-V. Pebax®/polyethylene glycol blend thin film composite membranes for CO 2 separation: performance with mixed gases. *Separation and Purification Technology* **2008,** 62 (1), 110-117.

24. Murali, R. S.; Sridhar, S.; Sankarshana, T.; Ravikumar, Y. Gas permeation behavior of Pebax-1657 nanocomposite membrane incorporated with multiwalled carbon nanotubes. *Industrial & Engineering Chemistry Research* **2010,** 49 (14), 6530-6538.

25. Yu, B.; Cong, H.; Li, Z.; Tang, J.; Zhao, X. S. Pebax-1657 nanocomposite membranes incorporated with nanoparticles/colloids/carbon nanotubes for CO2/N2 and CO2/H2 separation. *Journal of Applied Polymer Science* **2013,** 130 (4), 2867-2876.

26. Yi, C.; Wang, Z.; Li, M.; Wang, J.; Wang, S. Facilitated transport of CO2 through polyvinylamine/polyethlene glycol blend membranes. *Desalination* **2006,** 193 (1-3), 90-96.

27. Kim, T. J.; Li, B.; Hägg, M. B. Novel fixed-site–carrier polyvinylamine membrane for carbon dioxide capture. *Journal of Polymer Science Part B: Polymer Physics* **2004,** 42 (23), 4326-4336.

28. Du, N.; Park, H. B.; Robertson, G. P.; Dal-Cin, M. M.; Visser, T.; Scoles, L.; Guiver, M. D. Polymer nanosieve membranes for CO2-capture applications. *Nature materials* **2011,** 10 (5), 372-375.

29. Du, N.; Robertson, G. P.; Dal-Cin, M. M.; Scoles, L.; Guiver, M. D. Polymers of intrinsic microporosity (PIMs) substituted with methyl tetrazole. *Polymer* **2012,** 53 (20), 4367-4372.

30. Zulfiqar, S.; Karadas, F.; Park, J.; Deniz, E.; Stucky, G. D.; Jung, Y.; Atilhan, M.; Yavuz, C. T. Amidoximes: promising candidates for CO 2 capture. *Energy & Environmental Science* **2011,** 4 (11), 4528-4531.

31. Zulfiqar, S.; Awan, S.; Karadas, F.; Atilhan, M.; Yavuz, C. T.; Sarwar, M. I. Amidoxime porous polymers for CO 2 capture. *RSC Advances* **2013,** 3 (38), 17203-17213.

32. Swaidan, R.; Ghanem, B. S.; Litwiller, E.; Pinnau, I. Pure-and mixed-gas CO 2/CH 4 separation properties of PIM-1 and an amidoxime-functionalized PIM-1. *Journal of Membrane Science* **2014,** 457, 95-102.

33. Mahurin, S. M.; Gorka, J.; Nelson, K. M.; Mayes, R. T.; Dai, S. Enhanced CO 2/N 2 selectivity in amidoxime-modified porous carbon. *Carbon* **2014,** 67, 457-464.

34. Hong, T.; Chatterjee, S.; Mahurin, S. M.; Fan, F.; Tian, Z.; Jiang, D.-e.; Long, B. K.; Mays, J. W.; Sokolov, A. P.; Saito, T. Impact of tuning CO 2-philicity in polydimethylsiloxane-based membranes for carbon dioxide separation. *Journal of Membrane Science* **2017,** 530, 213-219.

35. Hodge, I. M. Physical aging in polymer glasses. *Science* **1995,** 267 (5206), 1945.

36. Pfromm, P.; Koros, W. Accelerated physical ageing of thin glassy polymer films: evidence from gas transport measurements. *Polymer* **1995,** 36 (12), 2379-2387.

37. Struik, L. C. E., *Physical aging in amorphous polymers and other materials*. Elsevier Amsterdam: 1978; Vol. 106.

38. Huang, Y.; Wang, X.; Paul, D. R. Physical aging of thin glassy polymer films: Free volume interpretation. *Journal of Membrane Science* **2006,** 277 (1), 219-229.

39. Huang, Y.; Paul, D. R. Physical aging of thin glassy polymer films monitored by gas permeability. *Polymer* **2004,** 45 (25), 8377-8393.

40. Lin, W.-H.; Chung, T.-S. Gas permeability, diffusivity, solubility, and aging characteristics of 6FDA-durene polyimide membranes. *Journal of Membrane Science* **2001,** 186 (2), 183-193.

41. Rowe, B. W.; Freeman, B. D.; Paul, D. R. Physical aging of ultrathin glassy polymer films tracked by gas permeability. *Polymer* **2009,** 50 (23), 5565-5575.

42. Nagai, K.; Nakagawa, T. Effects of aging on the gas permeability and solubility in poly (1-trimethylsilyl-1-propyne) membranes synthesized with various catalysts. *Journal of Membrane Science* **1995,** 105 (3), 261-272.

43. Kim, J.; Koros, W. J.; Paul, D. R. Effects of CO 2 exposure and physical aging on the gas permeability of thin 6FDA-based polyimide membranes: Part 2. with crosslinking. *Journal of membrane science* **2006,** 282 (1), 32-43.

44. McCaig, M.; Paul, D. Effect of UV crosslinking and physical aging on the gas permeability of thin glassy polyarylate films. *Polymer* **1999,** 40 (26), 7209-7225.

45. Langsam, M.; Robeson, L. M. Substituted propyne polymers—part II. Effects of aging on the gas permeability properties of poly [1-(trimethylsilyl) propyne] for gas separation membranes. *Polymer Engineering & Science* **1989,** 29 (1), 44-54.

46. Nagai, K.; Freeman, B. D.; Hill, A. J. Effect of physical aging of poly (1-trimethylsilyl-1-propyne) films synthesized with TaCl5 and NbCl5 on gas permeability, fractional free volume, and positron annihilation lifetime spectroscopy parameters. *Journal of Polymer Science Part B: Polymer Physics* **2000,** 38 (9), 1222-1239.

47. Cui, L.; Qiu, W.; Paul, D. R.; Koros, W. J. Physical aging of 6FDA-based polyimide membranes monitored by gas permeability. *Polymer* **2011,** 52 (15), 3374-3380.

48. Nagai, K.; Masuda, T.; Nakagawa, T.; Freeman, B. D.; Pinnau, I. Poly [1-(trimethylsilyl)-1-propyne] and related polymers: synthesis, properties and functions. *Progress in Polymer Science* **2001,** 26 (5), 721-798.

49. Dorkenoo, K. D.; Pfromm, P. H. Accelerated physical aging of thin poly [1-(trimethylsilyl)-1-propyne] films. *Macromolecules* **2000,** 33 (10), 3747-3751.

50. Yampol'Skii, Y. P.; Shishatskii, S.; Shantorovich, V.; Antipov, E.; Kuzmin, N.; Rykov, S.; Khodjaeva, V.; Plate, N. Transport characteristics and other physicochemical properties of aged poly (1-(trimethylsilyl)-1-; propyne). *Journal of applied polymer science* **1993,** 48 (11), 1935-1944.

51. Nagai, K.; Higuchi, A.; Nakagawa, T. Gas permeability and stability of poly (1-trimethylsilyl-1-propyne-co-1-phenyl-1-propyne) membranes. *Journal of Polymer Science Part B: Polymer Physics* **1995,** 33 (2), 289-298.

52. McCaig, M.; Paul, D. R. Effect of film thickness on the changes in gas permeability of a glassy polyarylate due to physical agingPart I. Experimental observations. *Polymer* **2000,** 41 (2), 629-637.

53. McCaig, M.; Paul, D. R.; Barlow, J. Effect of film thickness on the changes in gas permeability of a glassy polyarylate due to physical agingPart II. Mathematical model. *Polymer* **2000,** 41 (2), 639-648.

54. Tiwari, R. R.; Smith, Z. P.; Lin, H.; Freeman, B.; Paul, D. Gas permeation in thin films of “high free-volume” glassy perfluoropolymers: Part I. Physical aging. *Polymer* **2014,** 55 (22), 5788-5800.

55. Huang, Y.; Paul, D. R. Effect of temperature on physical aging of thin glassy polymer films. *Macromolecules* **2005,** 38 (24), 10148-10154.

56. Huang, Y.; Paul, D. Effect of molecular weight and temperature on physical aging of thin glassy poly (2, 6-dimethyl-1, 4-phenylene oxide) films. *Journal of Polymer Science Part B: Polymer Physics* **2007,** 45 (12), 1390-1398.

57. Gomes, D.; Nunes, S. P.; Peinemann, K.-V. Membranes for gas separation based on poly (1-trimethylsilyl-1-propyne)–silica nanocomposites. *Journal of Membrane Science* **2005,** 246 (1), 13-25.

58. Rangel, E. R.; Maya, E. M.; Sánchez, F.; de Abajo, J.; José, G. Gas separation properties of mixed-matrix membranes containing porous polyimides fillers. *Journal of membrane science* **2013,** 447, 403-412.

59. Lau, C. H.; Nguyen, P. T.; Hill, M. R.; Thornton, A. W.; Konstas, K.; Doherty, C. M.; Mulder, R. J.; Bourgeois, L.; Liu, A. C.; Sprouster, D. J. Ending aging in super glassy polymer membranes. *Angewandte Chemie International Edition* **2014,** 53 (21), 5322-5326.

60. Kelman, S. D.; Rowe, B. W.; Bielawski, C. W.; Pas, S. J.; Hill, A. J.; Paul, D.; Freeman, B. Crosslinking poly [1-(trimethylsilyl)-1-propyne] and its effect on physical stability. *Journal of Membrane Science* **2008,** 320 (1), 123-134.

61. Li, F. Y.; Xiao, Y.; Chung, T.-S.; Kawi, S. High-performance thermally self-cross-linked polymer of intrinsic microporosity (PIM-1) membranes for energy development. *Macromolecules* **2012,** 45 (3), 1427-1437.

62. Zhao, Y.; Zhang, X. In *Mechanical properties evolution of polydimethylsiloxane during crosslinking process*, MATERIALS RESEARCH SOCIETY SYMPOSIUM PROCEEDINGS, 2007; Warrendale, Pa.; Materials Research Society; 1999: 2007; p 75.

63. Hanson, D. An explicit polymer and node network model to compute micromechanical properties of silica-filled polydimethylsiloxane. *Polymer* **2004,** 45 (3), 1055-1062.

64. Merkel, T.; Bondar, V.; Nagai, K.; Freeman, B.; Pinnau, I. Gas sorption, diffusion, and permeation in poly (dimethylsiloxane). *Journal of Polymer Science Part B: Polymer Physics* **2000,** 38 (3), 415-434.

65. Hong, T.; Niu, Z. B.; Hu, X. X.; Gmernicki, K.; Cheng, S. W.; Fan, F.; Johnson, J. C.; Hong, E.; Mahurin, S.; Jiang, D. E.; Long, B.; Mays, J.; Sokolov, A.; Saito, T. Effect of Cross-Link Density on Carbon Dioxide Separation in Polydimethylsiloxane-Norbornene Membranes. *Chemsuschem* **2015,** 8 (21), 3524-3524.

66. Brunchi, C. E.; Filimon, A.; Cazacu, M.; Ioan, S. Properties of some poly (siloxane) s for optical applications. *High Performance Polymers* **2009,** 21 (1), 31-47.

67. Dittrich, P. S.; Manz, A. Lab-on-a-chip: microfluidics in drug discovery. *Nature Reviews Drug Discovery* **2006,** 5 (3), 210-218.

68. Bélanger, M. C.; Marois, Y. Hemocompatibility, biocompatibility, inflammatory and in vivo studies of primary reference materials low-density polyethylene and polydimethylsiloxane: A review. *Journal of Biomedical Materials Research Part A* **2001,** 58 (5), 467-477.

69. Horn, G., Silicone polymer contact lens compositions and methods of use. Google Patents: 2005.

70. Prentice, W. E.; Voight, M. L., *Techniques in musculoskeletal rehabilitation*. McGraw-Hill Prof Med/Tech: 2001.

71. Hunt, R. H.; Tytgat, G., *Helicobacter pylori: basic mechanisms to clinical cure*. Springer Science & Business Media: 2012.

72. Limited, M. s. R. o. C. *McDonald's Food Facts: Ingredients*; 2013-09-08, p 13.

73. Wendy's International, I. *Wendy's: Nutrition and ingredient information*; 2013; pp 8-9.

74. Clarson, S. J.; Semlyen, J. A., *Siloxane polymers*. Prentice Hall: 1993.

75. Lötters, J.; Olthuis, W.; Veltink, P.; Bergveld, P. The mechanical properties of the rubber elastic polymer polydimethylsiloxane for sensor applications. *Journal of Micromechanics and Microengineering* **1997,** 7 (3), 145.

76. Stern, S. A.; Shah, V. M.; Hardy, B. J. Structure-Permeability Relationships in Silicone Polymers. *J Polym Sci Pol Phys* **1987,** 25 (6), 1263-1298.

77. Shah, V. M.; Hardy, B. J.; Stern, S. A. Solubility of Carbon-Dioxide, Methane, and Propane in Silicone Polymers - Effect of Polymer Backbone Chains. *J Polym Sci Pol Phys* **1993,** 31 (3), 313-317.

78. Bélanger, M. C.; Marois, Y. Hemocompatibility, biocompatibility, inflammatory and in vivo studies of primary reference materials low-density polyethylene and polydimethylsiloxane: A review. *Journal of biomedical materials research* **2001,** 58 (5), 467-477.

79. Nakagawa, T.; Nishimura, T.; Higuchi, A. Morphology and gas permeability in copolyimides containing polydimethylsiloxane block. *Journal of Membrane Science* **2002,** 206 (1-2), 149-163.

80. Jullok, N.; Martinez, R.; Wouters, C.; Luis, P.; Sanz, M. T.; Van der Bruggen, B. A Biologically Inspired Hydrophobic Membrane for Application in Pervaporation. *Langmuir* **2013,** 29 (5), 1510-1516.

81. Jia, M. D.; Peinemann, K. V.; Behling, R. D. Preparation and Characterization of Thin-Film Zeolite Pdms Composite Membranes. *Journal of Membrane Science* **1992,** 73 (2-3), 119-128.

82. Tsujita, Y.; Yoshimura, K.; Yoshimizu, H.; Takizawa, A.; Kinoshita, T.; Furukawa, M.; Yamada, Y.; Wada, K. Structure and Gas-Permeability of Siloxane Imide Block-Copolymer Membranes .1. Effect of Siloxane Content. *Polymer* **1993,** 34 (12), 2597-2601.

83. Smaihi, M.; Schrotter, J.-C.; Lesimple, C.; Prevost, I.; Guizard, C. Gas separation properties of hybrid imide–siloxane copolymers with various silica contents. *Journal of membrane science* **1999,** 161 (1), 157-170.

84. Sadrzadeh, M.; Shahidi, K.; Mohammadi, T. Effect of operating parameters on pure and mixed gas permeation properties of a synthesized composite PDMS/PA membrane. *Journal of Membrane Science* **2009,** 342 (1-2), 327-340.

85. Berean, K.; Ou, J. Z.; Nour, M.; Latham, K.; McSweeney, C.; Paull, D.; Halim, A.; Kentish, S.; Doherty, C. M.; Hill, A. J. The effect of crosslinking temperature on the permeability of PDMS membranes: Evidence of extraordinary CO 2 and CH 4 gas permeation. *Separation and Purification Technology* **2014,** 122, 96-104.

86. Merkel, T. C.; Bondar, V. I.; Nagai, K.; Freeman, B. D.; Pinnau, I. Gas sorption, diffusion, and permeation in poly(dimethylsiloxane). *J Polym Sci Pol Phys* **2000,** 38 (3), 415-434.

87. Lin, H.; Freeman, B. D. Gas solubility, diffusivity and permeability in poly (ethylene oxide). *Journal of Membrane Science* **2004,** 239 (1), 105-117.

88. Ghosal, K.; Freeman, B. D. Gas separation using polymer membranes: an overview. *Polym Adv Technol* **1994,** 5 (11), 673–697.

89. Merkel, T. C.; Lin, H. Q.; Wei, X. T.; Baker, R. Power plant post-combustion carbon dioxide capture: An opportunity for membranes. *Journal of Membrane Science* **2010,** 359 (1-2), 126-139.

90. Esteves, A.; Brokken-Zijp, J.; Lavèn, J.; Huinink, H.; Reuvers, N.; Van, M.; De With, G. Influence of cross-linker concentration on the cross-linking of PDMS and the network structures formed. *Polymer* **2009,** 50 (16), 3955-3966.

91. Rao, H.-X.; Liu, F.-N.; Zhang, Z.-Y. Preparation and oxygen/nitrogen permeability of PDMS crosslinked membrane and PDMS/tetraethoxysilicone hybrid membrane. *Journal of Membrane Science* **2007,** 303 (1), 132-139.

92. Gong, C.; Fréchet, J. M. End functionalization of hyperbranched poly (siloxysilane): novel crosslinking agents and hyperbranched–linear star block copolymers. *Journal of Polymer Science Part A: Polymer Chemistry* **2000,** 38 (16), 2970-2978.

93. Fu, Y.-J.; Qui, H.-z.; Liao, K.-S.; Lue, S. J.; Hu, C.-C.; Lee, K.-R.; Lai, J.-Y. Effect of UV-ozone treatment on poly (dimethylsiloxane) membranes: surface characterization and gas separation performance. *Langmuir* **2009,** 26 (6), 4392-4399.

94. Firpo, G.; Angeli, E.; Repetto, L.; Valbusa, U. Permeability thickness dependence of polydimethylsiloxane (PDMS) membranes. *Journal of Membrane Science* **2015,** 481, 1-8.

95. Mensitieri, G.; Del Nobile, M.; Monetta, T.; Nicodemo, L.; Bellucci, F. The effect of film thickness on oxygen sorption and transport in dry and water-saturated Kapton® polyimide. *Journal of membrane science* **1994,** 89 (1), 131-141.

96. Kocherlakota, L. S.; Knorr, D. B.; Foster, L.; Overney, R. M. Enhanced gas transport properties and molecular mobilities in nano-constrained poly [1-(trimethylsilyl)-1-propyne] membranes. *Polymer* **2012,** 53 (12), 2394-2401.

97. Reijerkerk, S. R.; Knoef, M. H.; Nijmeijer, K.; Wessling, M. Poly (ethylene glycol) and poly (dimethyl siloxane): combining their advantages into efficient CO 2 gas separation membranes. *Journal of membrane science* **2010,** 352 (1), 126-135.

98. Park, H. B.; Kim, C. K.; Lee, Y. M. Gas separation properties of polysiloxane/polyether mixed soft segment urethane urea membranes. *Journal of membrane science* **2002,** 204 (1), 257-269.

99. Yun, C.; Nagase, Y. Synthesis of PDMS/PEO-grafted aromatic polyamides and the property as the separation membrane. *Polym. Prepr. Jpn* **2006,** 55 (1), 1583.

100. Yun, C.; Saito, Y.; Nagase, Y. Synthesis and functionality of PDMS/PEO-grafted aromatic polyamides. *Polym. Prepr. Jpn* **2006,** 55 (2), 2907.

101. Queiroz, D. P.; de Pinho, M. N. Structural characteristics and gas permeation properties of polydimethylsiloxane/poly (propylene oxide) urethane/urea bi-soft segment membranes. *Polymer* **2005,** 46 (7), 2346-2353.

102. Madhavan, K.; Reddy, B. Poly (dimethylsiloxane-urethane) membranes: effect of hard segment in urethane on gas transport properties. *Journal of membrane science* **2006,** 283 (1), 357-365.

103. Li, Y.; He, G.; Wang, S.; Yu, S.; Pan, F.; Wu, H.; Jiang, Z. Recent advances in the fabrication of advanced composite membranes. *Journal of Materials Chemistry A* **2013,** 1 (35), 10058-10077.

104. Wang, S.; Li, X.; Wu, H.; Tian, Z.; Xin, Q.; He, G.; Peng, D.; Chen, S.; Yin, Y.; Jiang, Z. Advances in high permeability polymer-based membrane materials for CO 2 separations. *Energy & Environmental Science* **2016,** 9 (6), 1863-1890.

105. Hussain, M.; Koenig, A. Mixed-Matrix Membrane for Gas Separation: Polydimethylsiloxane Filled with Zeolite. *Chemical Engineering & Technology* **2012,** 35 (3), 561-569.

106. Gurr, P. A.; Scofield, J. M.; Kim, J.; Fu, Q.; Kentish, S. E.; Qiao, G. G. Polyimide polydimethylsiloxane triblock copolymers for thin film composite gas separation membranes. *Journal of Polymer Science Part A: Polymer Chemistry* **2014,** 52 (23), 3372-3382.

107. Nour, M.; Berean, K.; Balendhran, S.; Ou, J. Z.; Du Plessis, J.; McSweeney, C.; Bhaskaran, M.; Sriram, S.; Kalantar-zadeh, K. CNT/PDMS composite membranes for H

2 and CH 4 gas separation. *International Journal of Hydrogen Energy* **2013,** 38 (25), 10494-10501.

108. Pechar, T. W.; Kim, S.; Vaughan, B.; Marand, E.; Baranauskas, V.; Riffle, J.; Jeong, H. K.; Tsapatsis, M. Preparation and characterization of a poly (imide siloxane) and zeolite L mixed matrix membrane. *Journal of membrane science* **2006,** 277 (1), 210-218.

109. Vogiatzis, K. D.; Mavrandonakis, A.; Klopper, W.; Froudakis, G. E. Ab initio Study of the Interactions between CO2 and N-Containing Organic Heterocycles. *ChemPhysChem* **2009,** 10 (2), 374-383.

110. Tian, Z.; Saito, T.; Jiang, D.-e. Ab Initio Screening of CO2-philic Groups. *The Journal of Physical Chemistry A* **2015,** 119 (16), 3848-3852.

111. Li, H.; Li, L.; Nguyen, T.; Rochelle, G. T.; Chen, J. Characterization of piperazine/2-aminomethylpropanol for carbon dioxide capture. *Energy Procedia* **2013,** 37, 340-352.

112. Chowdhury, F. A.; Okabe, H.; Shimizu, S.; Onoda, M.; Fujioka, Y. Development of novel tertiary amine absorbents for CO2 capture. *Energy Procedia* **2009,** 1 (1), 1241-1248.

113. Mason, C. R.; Maynard-Atem, L.; Al-Harbi, N. M.; Budd, P. M.; Bernardo, P.; Bazzarelli, F.; Clarizia, G.; Jansen, J. C. Polymer of intrinsic microporosity incorporating thioamide functionality: preparation and gas transport properties. *Macromolecules* **2011,** 44 (16), 6471-6479.

114. Patel, H. A.; Yavuz, C. T. Noninvasive functionalization of polymers of intrinsic microporosity for enhanced CO 2 capture. *Chemical Communications* **2012,** 48 (80), 9989-9991.

115. Le, N. L.; Wang, Y.; Chung, T.-S. Pebax/POSS mixed matrix membranes for ethanol recovery from aqueous solutions via pervaporation. *Journal of Membrane Science* **2011,** 379 (1), 174-183.

116. Rahman, M. M.; Filiz, V.; Shishatskiy, S.; Abetz, C.; Neumann, S.; Bolmer, S.; Khan, M. M.; Abetz, V. PEBAX® with PEG functionalized POSS as nanocomposite membranes for CO 2 separation. *Journal of membrane science* **2013,** 437, 286-297.

117. Wang, S.; Liu, Y.; Huang, S.; Wu, H.; Li, Y.; Tian, Z.; Jiang, Z. Pebax–PEG–MWCNT hybrid membranes with enhanced CO 2 capture properties. *Journal of Membrane Science* **2014,** 460, 62-70.

118. Chen, J. C.; Feng, X.; Penlidis, A. Gas Permeation Through Poly (Ether-b-amide)(PEBAX 2533) Block Copolymer Membranes. *Separation science and technology* **2005,** 39 (1), 149-164.

119. Kim, K.; Ingole, P. G.; Kim, J.; Lee, H. Separation performance of PEBAX/PEI hollow fiber composite membrane for SO 2/CO 2/N 2 mixed gas. *Chemical Engineering Journal* **2013,** 233, 242-250.

120. Rahman, M. M.; Shishatskiy, S.; Abetz, C.; Georgopanos, P.; Neumann, S.; Khan, M. M.; Filiz, V.; Abetz, V. Influence of temperature upon properties of tailor-made pebax® mh 1657 nanocomposite membranes for post-combustion CO 2 capture. *Journal of Membrane Science* **2014,** 469, 344-354.

121. Trong Nguyen, Q.; Sublet, J.; Langevin, D.; Chappey, C.; Marais, S.; Valleton, J. M.; Poncin-Epaillard, F. CO2 Permeation with pebax®-based membranes for global warming reduction. *Membrane Gas Separation* **2010**, 255-277.

122. Kanehashi, S.; Nagai, K. Analysis of dual-mode model parameters for gas sorption in glassy polymers. *Journal of Membrane Science* **2005,** 253 (1), 117-138.

123. Koros, W. J.; Chan, A.; Paul, D. Sorption and transport of various gases in polycarbonate. *Journal of Membrane Science* **1977,** 2, 165-190.

124. Frisch, H. Sorption and transport in glassy polymers–a review. *Polymer Engineering & Science* **1980,** 20 (1), 2-13.

125. Daynes, H. A. In *The process of diffusion through a rubber membrane*, Proceedings of the Royal Society of London A: Mathematical, Physical and Engineering Sciences, 1920; The Royal Society: 1920; pp 286-307.

126. Barrer, R.; Rideal, E. K. Permeation, diffusion and solution of gases in organic polymers. *Transactions of the Faraday Society* **1939,** 35, 628-643.

127. Rutherford, S.; Do, D. Review of time lag permeation technique as a method for characterisation of porous media and membranes. *Adsorption* **1997,** 3 (4), 283-312.

128. Strzelewicz, A.; Grzywna, Z. J. On the permeation time lag for different transport equations by Frisch method. *Journal of Membrane Science* **2008,** 322 (2), 460-465.

129. Czichos, H.; Saito, T.; Smith, L. E., *Springer handbook of metrology and testing*. Springer Science & Business Media: 2011.

130. Mahurin, S. M.; Lee, J. S.; Baker, G. A.; Luo, H.; Dai, S. Performance of nitrile-containing anions in task-specific ionic liquids for improved CO 2/N 2 separation. *Journal of Membrane Science* **2010,** 353 (1), 177-183.

131. Mahurin, S. M.; Lee, J. S.; Baker, G. A.; Luo, H. M.; Dai, S. Performance of nitrile-containing anions in task-specific ionic liquids for improved CO2/N-2 separation. *Journal of Membrane Science* **2010,** 353 (1-2), 177-183.

132. Carraher, E., Jr., *Seymour/Carraher's Polymer Chemistry, Seventh Edition.* Marcel Dekker: New York, 2000.

133. Xu, B.; Wu, J.; McKenna, G. B. Mechanical and Swelling Behaviors of End-Linked PDMS Rubber and Randomly Cross-Linked Polyisoprene. *Macromolecules* **2013,** 46 (5), 2015-2022.

134. Hiemenz, P. C.; Lodge, T. P., *Polymer Chemistry, Second Edition*. Taylor & Francis Group: New York, 2007.

135. Mulder, J., *Basic principles of membrane technology*. Springer Science & Business Media: 2012.

136. Amouroux, N.; Leger, L. Effect of dangling chains on adhesion hysteresis of silicone elastomers, probed by JKR test. *Langmuir* **2003,** 19 (4), 1396-1401.

137. Perutz, S.; Kramer, E. J.; Baney, J.; Hui, C. Y. Adhesion between hydrolyzed surfaces of poly(dimethylsiloxane) networks. *Macromolecules* **1997,** 30 (25), 7964-7969.

138. Stafie, N.; Stamatialis, D. F.; Wessling, M. Effect of PDMS cross-linking degree on the permeation performance of PAN/PDMS composite nanofiltration membranes. *Sep Purif Technol* **2005,** 45 (3), 220-231.

139. Esteves, A. C. C.; Brokken-Zijp, J.; Laven, J.; Huinink, H. P.; Reuvers, N. J. W.; Van, M. P.; de With, G. Influence of cross-linker concentration on the cross-linking of PDMS and the network structures formed. *Polymer* **2009,** 50 (16), 3955-3966.

140. Nguyen, Q. T.; Bendjama, Z.; Clement, R.; Ping, Z. H. Poly(dimethylsiloxane) crosslinked in different conditions - Part II. Pervaporation of water-ethyl acetate mixtures. *Phys Chem Chem Phys* **2000,** 2 (3), 395-400.

141. Choi, S. H.; Kim, J. H.; Lee, S. B. Sorption and permeation behaviors of a series of olefins and nitrogen through PDMS membranes. *Journal of Membrane Science* **2007,** 299 (1-2), 54-62.

142. Rao, H. X.; Liu, F. N.; Zhang, Z. Y. Preparation and oxygen/nitrogen permeability of PDMS crosslinked membrane and PDMS/tetraethoxysilicone hybrid membrane. *Journal of Membrane Science* **2007,** 303 (1-2), 132-139.

143. Lue, S. J.; Tsai, C. L.; Lee, D. T.; Mahesh, K. P. O.; Hua, M. Y.; Hu, C. C.; Jean, Y. C.; Lee, K. R.; Lai, J. Y. Sorption, diffusion, and perm-selectivity of toluene vapor/nitrogen mixtures through polydimethylsiloxane membranes with two cross-linker densities. *Journal of Membrane Science* **2010,** 349 (1-2), 321-332.

144. Tin, P. S.; Chung, T. S.; Liu, Y.; Wang, R.; Liu, S. L.; Pramoda, K. P. Effects of cross-linking modification on gas separation performance of Matrimid membranes. *Journal of Membrane Science* **2003,** 225 (1-2), 77-90.

145. Lin, H. Q.; Kai, T.; Freeman, B. D.; Kalakkunnath, S.; Kalika, D. S. The effect of cross-linking on gas permeability in cross-linked poly(ethylene glycol diacrylate). *Macromolecules* **2005,** 38 (20), 8381-8393.

146. Wind, J. D.; Staudt-Bickel, C.; Paul, D. R.; Koros, W. J. The effects of crosslinking chemistry on CO2 plasticization of polyimide gas separation membranes. *Ind Eng Chem Res* **2002,** 41 (24), 6139-6148.

147. Li, S.-Y.; Srivastava, R.; Parnas, R. S. Separation of 1-butanol by pervaporation using a novel tri-layer PDMS composite membrane. *Journal of Membrane Science* **2010,** 363 (1), 287-294.

148. Hill, A. J.; Freeman, B. D.; Jaffe, M.; Merkel, T. C.; Pinnau, I. Tailoring nanospace. *J Mol Struct* **2005,** 739 (1-3), 173-178.

149. Pethrick, R. A. Positron annihilation - A probe for nanoscale voids and free volume? *Prog Polym Sci* **1997,** 22 (1), 1-47.

150. Jean, Y.; Mallon, P.; Schrader, D. M., *Principles and applications of positron and positronium chemistry*. World Scientific: 2003.

151. Hu, X.; Koyanagi, T.; Fukuda, M.; Katoh, Y.; Wirth, B. D.; Snead, L. L. Defect evolution in single crystalline tungsten following low temperature and low dose neutron irradiation. **In progress**.

152. Saito, H.; Nagashima, Y.; Kurihara, T.; Hyodo, T. A new positron lifetime spectrometer using a fast digital oscilloscope and BaF 2 scintillators. *Nuclear Instruments and Methods in Physics Research Section A: Accelerators, Spectrometers, Detectors and Associated Equipment* **2002,** 487 (3), 612-617.

153. Hu, X.; Xu, D.; Wirth, B. D. Quantifying He-point defect interactions in Fe through coordinated experimental and modeling studies of He-ion implanted single-crystal Fe. *Journal of Nuclear Materials* **2013,** 442 (1), S649-S654.

154. Tao, S. J. Positronium Annihilation in Molecular Substances. *J Chem Phys* **1972,** 56 (11), 5499-&.

155. Eldrup, M.; Lightbody, D.; Sherwood, J. N. The Temperature-Dependence of Positron Lifetimes in Solid Pivalic Acid. *Chem Phys* **1981,** 63 (1-2), 51-58.

156. Seeger, A. Study of Defects in Crystals by Positron-Annihilation. *Appl Phys* **1974,** 4 (3), 183-199.

157. Robeson, L. M. The upper bound revisited. *J. Membr. Sci.* **2008,** 320 (1-2), 390-400.

158. Schroeder, M. J.; Roland, C. M. Segmental relaxation in end-linked poly(dimethylsiloxane) networks. *Macromolecules* **2002,** 35 (7), 2676-2681.

159. Roland, C. M. Constraints on Local Segmental Motion in Poly(Vinylethylene) Networks. *Macromolecules* **1994,** 27 (15), 4242-4247.

160. Hong, T.; Niu, Z.; Hu, X.; Gmernicki, K.; Cheng, S.; Fan, F.; Johnson, J. C.; Hong, E.; Mahurin, S.; Jiang, D. e. Effect of Cross-Link Density on Carbon Dioxide Separation in Polydimethylsiloxane-Norbornene Membranes. *ChemSusChem* **2015,** 8 (21), 3595-3604.

161. Jue, M. L.; Lively, R. P. Targeted gas separations through polymer membrane functionalization. *Reactive and Functional Polymers* **2015,** 86, 88-110.

162. Mason, C. R.; Maynard-Atem, L.; Heard, K. W.; Satilmis, B.; Budd, P. M.; Friess, K.; Lanč, M.; Bernardo, P.; Clarizia, G.; Jansen, J. C. Enhancement of CO2 affinity in a polymer of intrinsic microporosity by amine modification. *Macromolecules* **2014,** 47 (3), 1021-1029.

163. Du, N.; Robertson, G. P.; Song, J.; Pinnau, I.; Guiver, M. D. High-performance carboxylated polymers of intrinsic microporosity (PIMs) with tunable gas transport properties†. *Macromolecules* **2009,** 42 (16), 6038-6043.

164. Srinivasan, R.; Auvil, S. R.; Burban, P. M. Elucidating the Mechanism(S) of Gas-Transport in Poly[1-(Trimethylsilyl)-1-Propyne] (Ptmsp) Membranes. *J. Membr. Sci.* **1994,** 86 (1-2), 67-86.

165. Swaidan, R.; Ghanem, B. S.; Litwiller, E.; Pinnau, I. Pure- and mixed-gas CO2/CH4 separation properties of PIM-1 and an amidoxime-functionalized PIM-1. *J. Membr. Sci.* **2014,** 457, 95-102.

166. Fritsch, D.; Bengtson, G.; Carta, M.; McKeown, N. B. Synthesis and Gas Permeation Properties of Spirobischromane-Based Polymers of Intrinsic Microporosity. *Macromol. Chem. Phys.* **2011,** 212 (11), 1137-1146.

167. Du, N.; Robertson, G. P.; Song, J.; Pinnau, I.; Guiver, M. D. High-performance carboxylated polymers of intrinsic microporosity (PIMs) with tunable gas transport properties. *Macromolecules* **2009,** 42 (16), 6038-6043.

168. Du, N.; Dal-Cin, M. M.; Robertson, G. P.; Guiver, M. D. Decarboxylation-induced cross-linking of polymers of intrinsic microporosity (PIMs) for membrane gas separation. *Macromolecules* **2012,** 45 (12), 5134-5139.

169. Matteucci, S.; Kusuma, V. A.; Sanders, D.; Swinnea, S.; Freeman, B. D. Gas transport in TiO 2 nanoparticle-filled poly (1-trimethylsilyl-1-propyne). *Journal of Membrane Science* **2008,** 307 (2), 196-217.

170. Merkel, T. C.; He, Z.; Pinnau, I.; Freeman, B. D.; Meakin, P.; Hill, A. J. Effect of nanoparticles on gas sorption and transport in poly (1-trimethylsilyl-1-propyne). *Macromolecules* **2003,** 36 (18), 6844-6855.

171. Sultanov, E. Y.; Ezhov, A. A.; Shishatskiy, S. M.; Buhr, K.; Khotimskiy, V. S. Synthesis, Characterization, and Properties of Poly (1-trimethylsilyl-1-propyne)-block-poly (4-methyl-2-pentyne) Block Copolymers. *Macromolecules* **2012,** 45 (3), 1222-1229.

172. Nagase, Y.; Ishihara, K.; Matsui, K. Chemical modification of poly (substituted-acetylene): II. Pervaporation of ethanol/water mixture through poly (1-trimethylsilyl-1-propyne)/poly (dimethylsiloxane) graft copolymer membrane. *J. Polym. Sci., Part B: Polym. Phys.* **1990,** 28 (3), 377-386.

173. Bondi, A. van der Waals volumes and radii. *The Journal of physical chemistry* **1964,** 68 (3), 441-451.

174. Senthilkumar, U.; Reddy, B. Polysiloxanes with pendent bulky groups having amino-hydroxy functionality: structure–permeability correlation. *Journal of membrane science* **2007,** 292 (1), 72-79.

175. Ahlrichs, R.; Bär, M.; Häser, M.; Horn, H.; Kölmel, C. Electronic structure calculations on workstation computers: The program system turbomole. *Chemical Physics Letters* **1989,** 162 (3), 165-169.

176. Bondi, A. van der Waals volumes and radii. *J. Phys. Chem.* **1964,** 68 (3), 441-451.

177. Van Krevelen, D. W.; Te Nijenhuis, K., Properties of polymers: their correlation with chemical structure; their numerical estimation and prediction from additive group contributions. Elsevier: 2009.

178. Nizam El-Din, H.; Badawy, S.; Dessouki, A. Chelating polymer granules prepared by radiation-induced homopolymerization. I—Kinetic study of radiation polymerization process. *Journal of Applied Polymer Science* **2000,** 77 (7), 1405-1412.

179. Brown, S.; Yue, Y.; Kuo, L.-J.; Mehio, N.; Li, M.; Gill, G.; Tsouris, C.; Mayes, R. T.; Saito, T.; Dai, S. Uranium Adsorbent Fibers Prepared by Atom-Transfer Radical Polymerization (ATRP) from Poly (vinyl chloride)-co-chlorinated Poly (vinyl chloride)(PVC-co-CPVC) Fiber. *Industrial & Engineering Chemistry Research* **2016,** 55 (15), 4139-4148.

180. Zhang, X.; Ye, H.; Xiao, B.; Yan, L.; Lv, H.; Jiang, B. Sol− gel preparation of PDMS/Silica hybrid antireflective coatings with controlled thickness and durable antireflective performance. *The Journal of Physical Chemistry C* **2010,** 114 (47), 19979-19983.

181. Bodas, D.; Khan-Malek, C. Formation of more stable hydrophilic surfaces of PDMS by plasma and chemical treatments. *Microelectronic engineering* **2006,** 83 (4), 1277-1279.

182. Şahiner, N.; Pekel, N.; Güven, O. Radiation synthesis, characterization and amidoximation of N-vinyl-2-pyrrolidone/acrylonitrile interpenetrating polymer networks. *Reactive and Functional Polymers* **1999,** 39 (2), 139-146.

183. Kawai, T.; Saito, K.; Sugita, K.; Kawakami, T.; Kanno, J.-i.; Katakai, A.; Seko, N.; Sugo, T. Preparation of hydrophilic amidoxime fibers by cografting acrylonitrile and methacrylic acid from an optimized monomer composition. *Radiation Physics and Chemistry* **2000,** 59 (4), 405-411.

184. Kang, S. O.; Vukovic, S.; Custelcean, R.; Hay, B. P. Cyclic imide dioximes: Formation and hydrolytic stability. *Industrial & Engineering Chemistry Research* **2012,** 51 (19), 6619-6624.

185. Seko, N.; Katakai, A.; Tamada, M.; Sugo, T.; Yoshii, F. Fine fibrous amidoxime adsorbent synthesized by grafting and uranium adsorption–elution cyclic test with seawater. *Separation science and technology* **2004,** 39 (16), 3753-3767.

186. Brown, S.; Yue, Y.; Kuo, L.-J.; Mehio, N.; Li, M.; Gill, G. A.; Tsouris, C.; Mayes, R. T.; Saito, T.; Dai, S. Uranium adsorbent fibers prepared by ATRP from PVC-co-CPVC fiber. *Industrial & Engineering Chemistry Research* **2016**.

187. Nagai, K.; Masuda, T.; Nakagawa, T.; Freeman, B. D.; Pinnau, I. Poly[1-(trimethylsilyl)-1-propyne] and related polymers: synthesis, properties and functions. *Prog. Polym. Sci.* **2001,** 26 (5), 721-798.

188. Merkel, T.; Bondar, V.; Nagai, K.; Freeman, B. Sorption and transport of hydrocarbon and perfluorocarbon gases in poly (1-trimethylsilyl-1-propyne). *Journal of Polymer Science Part B: Polymer Physics* **2000,** 38 (2), 273-296.

189. Ichiraku, Y.; Stern, S.; Nakagawa, T. An investigation of the high gas permeability of poly (1-trimethylsilyl-1-propyne). *J. Membr. Sci.* **1987,** 34 (1), 5-18.

190. Nakagawa, T.; Fujisaki, S.; Nakano, H.; Higuchi, A. Physical modification of poly [1 (trimethylsilyl)-1-propyne] membranes for gas separation. *Journal of membrane science* **1994,** 94 (1), 183-193.

191. Nagai, K.; Nakagawa, T. Effects of Aging on the Gas-Permeability and Solubility in Poly(1-Trimethylsilyl-1-Propyne) Membranes Synthesized with Various Catalysts. *J. Membr. Sci.* **1995,** 105 (3), 261-272.

192. Nagai, K.; Mori, M.; Watanabe, T.; Nakagawa, T. Gas permeation properties of blend and copolymer membranes composed of 1-trimethylsilyl-1-propyne and 1-phenyl-1-propyne structures. *Journal of Polymer Science Part B: Polymer Physics* **1997,** 35 (1), 119-131.

193. Bruton, E. A.; Brammer, L.; Pigge, F. C.; Aakeröy, C. B.; Leinen, D. S. Hydrogen bond patterns in aromatic and aliphatic dioximes. *New journal of chemistry* **2003,** 27 (7), 1084-1094.

194. Lee, W. Selection of barrier materials from molecular structure. *Polymer Engineering & Science* **1980,** 20 (1), 65-69.

195. Liu, S. L.; Shao, L.; Chua, M. L.; Lau, C. H.; Wang, H.; Quan, S. Recent progress in the design of advanced PEO-containing membranes for CO 2 removal. *Progress in Polymer Science* **2013,** 38 (7), 1089-1120.

196. Bondar, V.; Freeman, B.; Pinnau, I. Gas sorption and characterization of poly (ether-b-amide) segmented block copolymers. *Journal of Polymer Science Part B: Polymer Physics* **1999,** 37 (17), 2463-2475.

197. Yave, W.; Car, A.; Funari, S. S.; Nunes, S. P.; Peinemann, K.-V. CO2-philic polymer membrane with extremely high separation performance. *Macromolecules* **2009,** 43 (1), 326-333.

198. Feng, S.; Ren, J.; Hua, K.; Li, H.; Ren, X.; Deng, M. Poly (amide-12-b-ethylene oxide)/polyethylene glycol blend membranes for carbon dioxide separation. *Separation and Purification Technology* **2013,** 116, 25-34.

199. Kim, S. J.; Jeon, H.; Kim, D. J.; Kim, J. H. High-performance Polymer Membranes with Multi-functional Amphiphilic Micelles for CO2 Capture. *ChemSusChem* **2015,** 8 (22), 3783-3792.

200. Lin, H.; Freeman, B. D. Gas solubility, diffusivity and permeability in poly(ethylene oxide). *Journal of Membrane Science* **2004,** 239 (1), 105-117.

201. Budd, P. M.; McKeown, N. B.; Ghanem, B. S.; Msayib, K. J.; Fritsch, D.; Starannikova, L.; Belov, N.; Sanfirova, O.; Yampolskii, Y.; Shantarovich, V. Gas permeation parameters and other physicochemical properties of a polymer of intrinsic microporosity: Polybenzodioxane PIM-1. *Journal of Membrane Science* **2008,** 325 (2), 851-860.

202. Budd, P. M.; McKeown, N. B. Highly permeable polymers for gas separation membranes. *Polymer Chemistry* **2010,** 1 (1), 63-68.

203. Ahn, J.; Chung, W.-J.; Pinnau, I.; Song, J.; Du, N.; Robertson, G. P.; Guiver, M. D. Gas transport behavior of mixed-matrix membranes composed of silica nanoparticles in a polymer of intrinsic microporosity (PIM-1). *Journal of membrane science* **2010,** 346 (2), 280-287.

204. Khosravi, T.; Omidkhah, M. Preparation of CO 2-philic polymeric membranes by blending poly (ether-b-amide-6) and PEG/PPG-containing copolymer. *RSC Advances* **2015,** 5 (17), 12849-12859.

205. Kusuma, V. A.; Freeman, B. D.; Smith, S. L.; Heilman, A. L.; Kalika, D. S. Influence of TRIS-based co-monomer on structure and gas transport properties of cross-linked poly (ethylene oxide). *Journal of Membrane Science* **2010,** 359 (1), 25-36.

206. Cordier, P.; Tournilhac, F.; Soulié-Ziakovic, C.; Leibler, L. Self-healing and thermoreversible rubber from supramolecular assembly. *Nature* **2008,** 451 (7181), 977-980.

207. Engel, J. M.; Chen, J.; Liu, C.; Bullen, D. Polyurethane rubber all-polymer artificial hair cell sensor. *Journal of Microelectromechanical Systems* **2006,** 15 (4), 729-736.

208. Abdelghany, A.; Abdelrazek, E.; Badr, S.; Morsi, M. Effect of gamma-irradiation on (PEO/PVP)/Au nanocomposite: Materials for electrochemical and optical applications. *Materials & Design* **2016,** 97, 532-543.

209. Chapi, S.; Raghu, S.; Devendrappa, H. Enhanced electrochemical, structural, optical, thermal stability and ionic conductivity of (PEO/PVP) polymer blend electrolyte for electrochemical applications. *Ionics* **2015**, 1-12.

210. Kumar, K.; Ravi, M.; Pavani, Y.; Bhavani, S.; Sharma, A.; VVR, N. R. Electrical conduction mechanism in NaCl complexed PEO/PVP polymer blend electrolytes. *Journal of Non-Crystalline Solids* **2012,** 358 (23), 3205-3211.

211. Ochsner, M.; Dusseiller, M. R.; Grandin, H. M.; Luna-Morris, S.; Textor, M.; Vogel, V.; Smith, M. L. Micro-well arrays for 3D shape control and high resolution analysis of single cells. *Lab on a Chip* **2007,** 7 (8), 1074-1077.

212. Choi, K. M.; Rogers, J. A. A photocurable poly (dimethylsiloxane) chemistry designed for soft lithographic molding and printing in the nanometer regime. *Journal of the American Chemical Society* **2003,** 125 (14), 4060-4061.

213. He, X.; Widmaier, J.; Herz, J.; Meyer, G. Polydimethylsiloxane/poly (methyl methacrylate) interpenetrating polymer networks: 2. Synthesis and properties. *Polymer* **1992,** 33 (4), 866-871.

214. Srividhya, M.; Reddy, B. Synthesis and characterization of polyimide containing PEG/PDMS amphiphilic conetworks by hydrosilylation: Correlation between structure and properties. *Journal of Polymer Science Part A: Polymer Chemistry* **2007,** 45 (9), 1707-1726.

215. Simon, F. T.; Rutherford Jr, J. Crystallization and melting behavior of polyethylene oxide copolymers. *Journal of Applied Physics* **1964,** 35 (1), 82-86.

216. Grainger, D. W.; Okano, T.; Kim, S. W.; Castner, D. G.; Ratner, B. D.; Briggs, D.; Sung, Y. Poly (dimethylsiloxane)-poly (ethylene oxide)-heparin block copolymers III: Surface and bulk compositional differences. *Journal of biomedical materials research* **1990,** 24 (5), 547-571.

217. Çakmak, G.; Küçükyavuz, Z.; Küçükyavuz, S.; Çakmak, H. Mechanical, electrical and thermal properties of carbon fiber reinforced poly

(dimethylsiloxane)/polypyrrole composites. *Composites Part A: Applied Science and Manufacturing* **2004,** 35 (4), 417-421.

218. Voylov, D. N.; Holt, A. P.; Doughty, B.; Bocharova, V.; Meyer III, H. M.; Cheng, S.; Martin, H.; Dadmun, M.; Kisliuk, A.; Sokolov, A. P. Unraveling the Molecular Weight Dependence of Interfacial Interactions in Poly (2-vinylpyridine)/Silica Nanocomposites. *ACS Macro Letters* **2017,** 6, 68-72.

219. Hoyle, C. E.; Bowman, C. N. Thiol–ene click chemistry. *Angewandte Chemie International Edition* **2010,** 49 (9), 1540-1573.

220. Lowe, A. B. Thiol-ene "click" reactions and recent applications in polymer and materials synthesis. *Polymer Chemistry* **2010,** 1 (1), 17-36.

221. Kade, M. J.; Burke, D. J.; Hawker, C. J. The power of thiol-ene chemistry. *Journal of Polymer Science Part A: Polymer Chemistry* **2010,** 48 (4), 743-750.

222. Bara, J. E.; Camper, D. E.; Gin, D. L.; Noble, R. D. Room-temperature ionic liquids and composite materials: platform technologies for CO2 capture. *Accounts of Chemical Research* **2009,** 43 (1), 152-159.

223. Dai, Z.; Noble, R. D.; Gin, D. L.; Zhang, X.; Deng, L. Combination of ionic liquids with membrane technology: A new approach for CO 2 separation. *Journal of Membrane Science* **2016,** 497, 1-20.

VITA

Tao Hong was born in Hangzhou, Zhejiang, China in 1990. He graduated from Hangzhou Foreign Language School in 2008 and entered Hunan University at the same year. He received his B.S. degree in Chemistry in June 2012 and came to the University of Tennessee-Knoxville in the pursuit of Ph.D. degree in polymer chemistry. He joined Prof. Alexei P. Sokolov's group in December 2012 with a research focus on dynamics of soft matter. He started the research project on the development of CO_2 separation membranes in June 2014. By August 2017, he has authored or coauthored eight peer-reviewed publications and one US patent. One of his first author papers was highlighted on the front cover of *ChemSucChem*. He presented his research work in various conferences including ACS National Meeting, National Graduate Research Polymer Conference and Southeast Polymer Forum. He was invited to talk in ACS "Excellence in Graduate Polymer Research" symposium (2017) and was honored Graduate Student Senate Travel Award (2016 and 2017) from the University of Tennessee.